Quantum Dots - Interactions at the Nano-bio Interface

By
Kevin Neibert

Department of Pharmacology and Therapeutics
Faculty of Medicine
McGill University, Montreal

April 2014

A thesis submitted to McGill University in partial fulfillment of the requirements of the degree of Doctor of Philosophy (PhD)

Dedicated to my friends and family,
whose love and wisdom have made this journey possible

Abstract

Nanotechnology is an area of research that lies at the interface of physics, chemistry, engineering and biotechnology. The last decade has seen nanotechnology become a household term, as nano-scale products, known as nanoparticles, have become diverse in nature and form. Despite their immense promise, the widespread application of nanoparticles is currently limited due to their questionable biocompatibility and unclear consequences on cells and other biological components. We have selected fluorescent nanocrystals, called quantum dots (QDs), to investigate the interactions between nanoparticles and the biological environment, due to their superior optical properties. In the present studies, the mechanisms underlying the adaptive cell response to QDs were examined in multiple model cell lines. We observed significant morphological and functional changes at the cellular and subcellular levels following long term exposure to uncapped QDs. We showed that QD-induced toxicity included the production of reactive oxygen and nitrogen species as well as disruption of mitochondrial function. In addition, we found a novel role for transcription factor EB (TFEB), a master regulator of lysosome biogenesis in the successful cellular adaptation process. We showed that modifications to the QD surface can significantly decrease its toxicity, and in some cases, render the QDs non-toxic. Understanding the mechanisms of cellular adaptation to QDs is a first step for the establishment of protocols to evaluate the safety of other nanomaterials.

We then investigated the effects of QD surface properties and how they contribute to particle uptake by using QDs with the same core, but with different surface functionalization. We demonstrated that QD surface charge plays an important role in internalization in two different human cell lines. In addition, we provided evidence for the involvement of several overlapping modes of uptake and export from the cell. Finally, we systematically investigated the effects of QD surface properties on particle stability in biological media. We found that serum proteins were differently adsorbed to the particle surface, and this played a key role in determining the primary mode of internalization.

Taken together, the results from this work contribute to the development of nano-scale materials in two main ways:

1) by presenting *in vitro* measures as the first step in the evaluation of nanomaterial safety.
2) by demonstrating how surface charge and ligand properties drive specific modes of internalization

The findings presented herein promote understanding of the intricacies at the nano-bio interface and provide guiding principles for sensible nanoparticle design, with careful consideration for size, shape and surface charge.

Résumé

La nanotechnologie se trouve à l'interface de la physique, de la chimie, de l'ingénierie et de la biotechnologie. Au cours de la dernière décennie, les produits de taille nanométrique, appelées nanoparticules, sont devenus de nature et forme de plus en plus diversifiée menant à un grand essor de la nanotechnologie. Malgré leur immense potentiel, l'application généralisée des nanoparticules est actuellement limitée en raison du manque d'information sur leur biocompatibilité et leurs conséquences néfastes sur les cellules et autres composants biologiques. Nous avons sélectionné des nanocristaux fluorescents de propriétés optiques supérieures, appelés points quantiques (QD), afin d'étudier les interactions entre les nanoparticules et l'environnement biologique. Dans cette étude, les mécanismes sous-jacents de la réponse adaptative des cellules lors de l'exposition à des points quantiques ont été examinés dans plusieurs lignées cellulaires. Nous avons observé des changements morphologiques et fonctionnels importants aux niveaux cellulaire et subcellulaire suite à une exposition de long terme à des points quantiques non-revêtu de coque. Nous avons démontré que la toxicité induite par ces QD implique la production d'espèces réactives de l'oxygène et de l'azote ainsi que des perturbations de la fonction mitochondriale. Nous avons également découvert un nouveau rôle pour transcription factor EB (TFEB), un régulateur clé de la biogenèse des lysosomes, dans la réussite du processus d'adaptation cellulaire. Nous avons montré que la présence d'une coque recouvrant les QD ainsi que des modifications à leur surface peuvent diminuer significativement leur toxicité, et dans certains cas, les rendre non-toxiques. La compréhension des mécanismes d'adaptation cellulaire en réaction aux points quantiques est essentielle au développement de procédés évaluant la sécurité d'autres nanomatériaux.

Nous avons par la suite étudié l'effet des propriétés de surface des QD et comment elles contribuent à l'absorption des particules. Nous avons utilisé des points quantiques de même noyau mais ayant des modifications de surface distinctes. Nous avons démontré que la charge de surface des QD joue un rôle important dans leur internalisation cellulaire dans deux lignés de cellules humaines différentes. De plus, nous avons montré que plusieurs modes d'importation et d'exportation de la cellule étaient impliqués dans ce processus. Enfin, nous avons étudié systématiquement les effets des propriétés de surface des QD sur la stabilité des

particules dans les milieux biologiques. Nous avons découvert que les protéines du sérum sont différemment adsorbées à la surface des particules ce qui joue un rôle déterminant dans le mode d'intériorisation principal.

En conclusion, ces résultats aident au développement de matériaux d'échelle nanométrique de deux façons:

1) en promouvant les modèles in vitro comme une première étape dans l'évaluation de la sécurité des nanomatériaux.
2) en démontrant un lien entre la charge de surface ainsi que les propriétés des ligands et les modes spécifiques d'internalisation cellulaire.

Les résultats présentés ici contribuent à la compréhension de la complexité de l'interface nano-bio et fournissent des principes directeurs pour la conception minutieuse de nanoparticules, avec une attention particulière pour la taille, la forme et la charge de surface.

Table of Contents

List of Figures and Tables

FIGURES

TABLES

List of Abbreviations

AF4	asymmetrical flow field-flow fractionation
ANOVA	analysis of variance
BSA	bovine serum albumin
BSO	l-buthionine sulfoximine
CA	cysteamine
CAT	catalase
Cd^{2+}	cadmium ion
CdS	cadmium sulfide
CdSe	cadmium selenide
CdSeTe	cadmium selenium telluride
CdTe	cadmium telluride
CNS	central nervous system
CPZ	chlorpromazine
CYS	l-cysteine
CytoD	cytochalasin D
Dg	gyration diameter
Dh	hydrodynamic diameters
DHE	dihydroethidium
DHLA	dihydrolipoic acid
DLS	dynamic light scattering
DMEM	dulbecco's modified eagle medium
DMSO	dimethyl sulfoxide
DNA	deoxyribonucleic acid
EDTA	ethylenediaminetetraacetic acid
Em	emission wavelength
Ex	excitation wavelength
FAA	flame atomic absorption
FACS	fluorescence-activated cell sorting

FBS	fetal bovine serum
FLIM	fluorescence-lifetime imaging microscopy
FRET	fluorescence resonance energy transfer
FSC	forward scatter
GPx	glutathione peroxidase
GR	glutathione reductase
GSH	glutathione (reduced state)
GSSG	glutathione disulfide (oxidized state)
Hrs	hours
IV	intravenous
LA	α-lipoic acid
LAMP1	lysosomal-associated membrane protein 1
MALS	multi-angle light scattering
MBCD	methyl β-cyclodextrin
mCBI	monochlorobimane
MFI	mean fluorescence intensity
Min	minute
MPA	mercaptopropionic acid
MPS	mononuclear phagocyte system
MTT	[3-(4,5-dimethyl thiazol-2-yl)-2,5-diphenyl] tetrazolium bromide
NAC	N-acetylcysteine
NaCl	sodium chloride
NADPH	reduced nicotinamide adenine dinucleotide phosphate
NIR	near-infrared
Nrf2	nuclear factor (erythroid-derived 2)-like 2
NTA	nanoparticle tracking analysis
PBS	phosphate buffered saline
PEG	polyethylene glycol
PGP	p glycoprotein
ppm	parts per million

QD	quantum dot
QELS	quasi-elastic light scattering
RFI	relative fluorescence intensity
Rh	hydrodynamic radius
RNS	reactive nitrogen species
ROS	reactive oxygen species
RT	room temperature
SEM	standard error of the mean
siRNA	small interfering RNA
SOD-1	superoxide dismutase
SSC	side scatter
TEM	transmission electron microscopy
TFEB	transcription factor EB
THA	threo-β-hydroxyaspartate
UV	ultraviolet
X-AG	sodium dependent cysteine transporter
ZnS	zinc sulfide

Statement of Contributions

The following dissertation conforms to the guidelines for a manuscript-based thesis as outlined by the Graduate and Postdoctoral Studies Office (GPSO) of McGill University. A collection of three (3) original, co-authored manuscripts are presented herein, for which the contributions of each of those co-authors have been outlined below.

1. Mechanisms of Cellular Adaptation to Quantum Dots - the Role of Glutathione and Transcription Factor EB.
Neibert K, Maysinger D. Nanotoxicology. 2012, 6(3), 249-262

The study was conceived by D Maysinger and K Neibert. K Neibert carried out all the experiments, collected and analyzed the data. The first draft of the manuscript was prepared by K Neibert. The manuscript was revised and edited by D Maysinger.

The authors would like to acknowledge H. Vali and members of the Facility for Electron Microscopy Research (FEMR) for assisting with electron microscopy, Alexandre Moquin for the preparation and characterization of the CdTe QDs, Anja Kretzshmar for help with preliminary TFEB translocation experiments and Jasmina Lovrić for the western blotting.

2. Short Ligands Affect Modes of QD Uptake and Elimination in Human Cells.
Al-Hajaj N*, Moquin A*, Neibert K*, Soliman G, Winnik F, Maysinger D.
ACS Nano. 2011, 5(6), 4909-4918

The authorship is shared between the first 3 authors. The study was conceived by D Maysinger and F Winnik. K Neibert carried out the experimental design, data collection and data analysis for the biological experiments (imaging, uptake and export determinations). N Al-Hajaj helped K Neibert with the export experiments. The QDs were prepared and characterized by A Moquin and G Soliman under the supervision of F Winnik. The first draft

of the manuscript was prepared by K Neibert, Al-Hajaj N and A Moquin. The manuscript was revised and edited by D Maysinger and F Winnik.

The authors would like to acknowledge the Natural Sciences and Engineering Research Council of Canada (NSERC) and the Canadian Institutes of Health Research (CIHR) for their financial support.

3. Impact of biological media on quantum dot aggregation and cell recognition of nanocrystals.
Moquin A*, Neibert K*, Maysinger D, Winnik F. (*to be submitted*)

The authorship is shared between the first 2 authors. The study was conceived by D Maysinger and F Winnik. K Neibert and A Moquin equally shared the experimental design, data collection and data analysis. K Neibert performed all biological experiments (imaging and uptake determination), while A Moquin prepared and characterized the QDs. The first draft of the manuscript was prepared by K Neibert and A Moquin. The manuscript was revised and edited by D Maysinger and F Winnik.

The authors would like to acknowledge the Natural Sciences and Engineering Research Council of Canada (NSERC, Discovery grant to FMW), the World Premier International Research Center Initiative (WPI), MEXT Japan (FMW) and the Canadian Institutes of Health Research (CIHR, DM).

*These authors contributed equally

Contributions to Original Knowledge

1. Mechanisms of Cellular Adaptation to Quantum Dots - the Role of Glutathione and Transcription Factor EB.
Neibert K, Maysinger D. Nanotoxicology. 2012, 6(3), 249-262

This work was the first to investigate the role of glutathione in cellular adaptation to quantum dots by identifying differences in the antioxidant capacity of individual cells within the total cell population. We demonstrated that cells under basal conditions have varied distributions of intracellular glutathione, which reflects their adaptive capacity to quantum dot induced stress. Exposure to toxic quantum dots shifted the distribution of the intracellular glutathione subpopulations towards cells containing higher levels of intracellular glutathione, which was dependent on *de novo* glutathione synthesis. In addition, we were the first to implicate transcription factor EB, a master regulator of lysosomal biogenesis, as an important mediator of cellular adaptation to quantum dots through modulation of LAMP1 expression. Our findings emphasize the role of endogenous antioxidant defense mechanisms in cellular adaptation to nanoparticles.

2. Short Ligands Affect Modes of QD Uptake and Elimination in Human Cells.
Al-Hajaj N*, Moquin A*, Neibert K*, Soliman G, Winnik F, Maysinger D. ACS Nano. 2011, 5(6), 4909-4918

This work was among the first to systematically investigate effect of surface properties, specifically surface charge of small ligands on quantum dot uptake. We prepared quantum dots with conserved size and core composition, but varied surface modification. The data showed that QDs were differentially taken up by human kidney and liver cells depending on their surface charge. Pharmacological inhibition of several uptake mechanisms revealed that QDs were internalized through multiple modes but to a different extent. In addition, we implicated a novel role for the X-AG cysteine transporter and p-glycoprotein transporters in quantum dot uptake and elimination, respectively. Our findings emphasize the role of nanoparticle surface properties in dictating interactions with biological systems.

3. Impact of biological media on quantum dot aggregation and cell recognition of nanocrystals.

Moquin A*, Neibert K*, Maysinger D, Winnik F. 2014, (*to be submitted*)

This work was the first to systematically investigate the effect of the biological microenvironment on nanoparticle stability and cellular uptake. We used asymmetrical flow field-flow fractionation (AF4), a novel characterization technique that fractionally separates nanoparticles based on their size, to accurately characterize nanoparticles following incubation with increasingly complex biological systems. Using quantum dots with conserved size and core composition, but varied surface functionalization, we showed differential evolution of particle aggregates in cell culture medium. We showed that quantum dot aggregation status drives the primary mode cellular internalization. Our findings emphasize the importance of nanoparticle surface properties on aggregation status and demonstrate how particle stability influences interactions at the plasma membrane. In addition, we highlight a sensible strategy for nanoparticle characterization in complex biological media.

Publications

Relating the chemical and biological identity of quantum dots in N9 microglia cells through asymmetrical flow field-flow fractionation analyses.
Moquin A*, Neibert K*, Maysinger D, Winnik F. 2014, (*to be submitted*)

Quantum dots for imaging neural cells in vitro and in vivo.
Choi A, Neibert K, Maysinger D. Methods in Molecular Biology. 2013, (in press)

"Click" Dendrimers as Anti-inflammatory Agents: With Insights into Their Binding from Molecular Modeling Studies.
Neibert K*, Gosein V*, Sharma A, Khan M, Whitehead A, Maysinger D, Kakkar A. Molecular Pharmaceutics. 2013, 10(6), 2502-2508

Wound-Healing with Mechanically Robust and Biodegradable Hydrogel Fibers Loaded with Silver Nanoparticles.
Neibert K, Gopishetty V, Grigoryev A, Tokarev I, Al-Hajaj N, Vorstenbosch J, Philip A, Minko S, Maysinger D. Advanced Healthcare Materials. 2012, 1(5), 621-630

Mechanisms of Cellular Adaptation to Quantum Dots--the Role of Glutathione and Transcription Factor EB.
Neibert K, Maysinger D. Nanotoxicology. 2012, 6(3), 249-262

Facile Construction of Multifunctional Nanocarriers Using Sequential Click Chemistry for Applications in Biology.
Sharma A, Neibert K, Sharma R, Maysinger D, Kakkar A. Macromolecules. 2012, 44(3), 521-529

Short Ligands Affect Modes of QD Uptake and Elimination in Human Cells.
Al-Hajaj N*, Moquin A*, Neibert K*, Soliman G, Winnik F, Maysinger D. ACS Nano. 2011, 5(6), 4909-4918

Probing and Preventing Quantum Dot-Induced Cytotoxicity with Multimodal Alpha-Lipoic Acid in Multiple Dimensions of the Peripheral Nervous System.
Jain M, Choi A, Neibert K, Maysinger D. Nanomedicine (Lond). 2009, 4(3), 277-290

*These authors contributed equally

Acknowledgments

I would like to express my most sincere gratitude to my supervisor, **Dr. Dusica Maysinger** for her guidance over the last 7 years. Your genuine enthusiasm and passion for science is truly inspiring. Thank you for giving me the opportunity to pursue my research interests (wherever they took me), for always being supportive of my endeavours (academic and otherwise) and above all, your uncompromising understanding and dedication to our "nano-family".

Many thanks to members of my thesis advisory committee, **Dr. Guillermina Almazan**, **Dr. Anne McKinney** and **Dr. Daniel Bernard** for expressing a sincere interest in my work and for their constructive feedback throughout the years. Thank you for the constructive feedback and for keeping me on track.

I would like to sincerely thank **Dr. Daniel Bernard, Dr. Terry Hébert** and **Dr. Derek Bowie** their continued support, encouragement and invaluable advice over the years.

A very special thank you goes to my fellow "orange room" colleagues: **Dr. Angela Choi, Dr. Sebastien Boridy** and **Dr. Armen Khatchadourian.** Thank you for teaching me how to be a graduate student, for your constant encouragements, insightful discussions, lasting friendships and all the laughs along the way. I wish you all continued success in your future endeavours.

I also would like to thank both current and past lab members: Alex Moquin, Noura Al-Hajaj, Diana Mejia, Cedric Doucet, Andrew Lake, Mirela Matokanovic, Jerome Fortin, Patricia Brown, Mark Aurousseau, Dr. Varin Gosein, Dr. Ashok Kakkar, Dr. Ghareb Soliman, Dr. Eliza Hutter, Dr. Jack Diamond and Dr. Michael Holmes for their assistance, friendship and scientific insight throughout my studies. Special thanks to Dr. Jack Diamond for revision of the thesis.

Great appreciation goes to the indispensable departmental administrative staff: Hélène Duplessis, Tina Tremblay, Chantal Grignon and David Kalant. Thank you very much for your help throughout the years. Special thanks to the Dr. Gerhard Multhaup for his kind words and leadership. The department has been very good to me and I wish you all the best.

Thank you to the Facility of Medicine and Department of Pharmacology and Therapeutics for the financial support over the years in the form of travel awards and student fellowships.

My deepest gratitude goes to my family: to my parents, **Daniel** and **Mary-Beth**, and dearest brother **Eric**, thank you for your unconditional love, your unwavering support and encouragement to follow my passion. Thank you for believing in me.

Last but not least, a special thank you to **Allie Aitken**. Thank you for always offering a sympathetic ear, for putting up with me during the many long days and late nights of writing and for bringing a smile to my face exactly when I needed it most.

Chapter 1. General Introduction

1.1. Statement of the purpose of the investigation

Nanotechnology is a rapidly developing field involving the manipulation of matter at the molecular scale (1-100 nm). Nanomaterials have unique physical and chemical properties with respect to their bulk scale counterparts. These unique properties can be exploited for a number of potential applications in semiconductor physics, microfabrication, electronics, energy production, textiles, cosmetics and the biomedical industry. In particular, the application of nanoparticles in medicine, termed nanomedicine, has recently generated tremendous interest. The growing trend in Nanomedicine is reflected by substantial financial investments from the biomedical industry and the increasing global production of medically relevant nanomaterials, quickly approaching 100,000 tons per year (Hendren, Mesnard et al. 2011).

Nanotechnology is rapidly becoming an inescapable part of our everyday life and despite its transformative potential, there is still much that remains unclear. Currently, limited information is available on the biological, environmental and health risks associated with long-term and widespread use of nanomaterials. The uncertainty is primarily due to the complex biophysical interactions that take place at the boundary between the nanomaterial and the biological milieu. This dynamic interface, termed the *nano-bio interface*, is still poorly understood, limiting our understanding of the effects exerted by nanomaterials in biological systems. Interactions at the nano-bio interface are governed by the properties of the nanomaterials (size, shape, charge, etc.) and the properties of the microenvironment (protein composition, osmolarity, pH, temperature, etc.). At the start of this thesis work, systematic studies characterizing the effects of various nanomaterial properties on their biological fate (*in vitro* and *in vivo*) were lacking. This thesis aims to address some of these unanswered questions. We will first examine the adaptive cellular response to nanomaterial exposure using one representative nanoparticle type that is used for imaging applications: highly fluorescent nanocrystals. We will subsequently use nanocrystals as a model to characterize nanoparticle-cell interactions at the nano-bio interface, focusing on mechanisms of cellular internalization. Lastly, we will systematically explore the role played by the biological milieu in modulating nanoparticle stability and determine how it affects cell recognition.

1.2. Nanomedicine

Nanomedicine is the discipline that uses nano-sized tools for the diagnosis, prevention and treatment of disease and to gain insight into the complexity of disease pathology (Webster 2006). Cells, proteins, membranes, DNA and other biological complexes are comparable in size with nanomaterials, making them particularly well suited to interact with biological systems for experimental or medicinal purposes. Nanomaterials also tend to have a high surface-area-to-volume ratio, providing a greater contact area and chemical reactivity per unit density. This means that nanomaterials can interact dynamically with biological agents, providing a number of notable advantages over comparable bulk scale materials.

1.2.1. Applications

Broadly speaking, there are four key medical applications for nanomaterials in nanomedicine:

1. molecular imaging
2. drug delivery
3. diagnostics
4. therapeutic intervention

According to a recent study conducted by the Food and Drug Administration (FDA), new applications submitted for drugs that contain nanomaterials primarily target cancer (38%), chronic pain (10%) and the treatment of infections (10%) (Erickson 2012). The census covered applications for nanoparticle treatments containing at least one pharmaceutical compound, totaling more than 150 applications to date. About 25 different nanotherapeutics have already been FDA-approved and are available for clinical use (Table 1.1). A much larger number of nanomaterials are currently undergoing preclinical evaluation in private and public research laboratories around the world (Ventola 2012).

Table 1.1. List of FDA approved nanoparticle based therapeutics

Product/brand name	Active ingredient	FDA Approved Indication(s)	Delivery Route
Doxil	PEGylated doxorubicin (Adriamycin)HLC liposomes	Metastatic ovarian cancer and AIDS-related Kaposi's sarcoma	IV
Abraxane	Paclitaxel (taxol) bound albumin nanoparticles (~130 nm)	Metastatic breast cancer patients who have failed combination therapy	IV
AmBisome	Amphotericin B liposomes (~45-80 nm)	Fungal infections	IV
Myocet	Liposome-encapsulated doxorubicin-citrate complex	Cardio-protective formulation of doxorubicin used in late stage metastatic breast cancer	IV
Pegasys	PEGylated interferon alfa-2a	Chronic hepatitis C virus infection	Subcutaneous
Macugen	Pegylated anti-VEGF aptamer	Neovascular age-related macular degeneration	Intravitreal
Copaxone	Glatiramer acetate (coplymer of L-glutamic acid, L-alanine, L-tyrosine and L-lysine)	Relapsing remitting multiple sclerosis	Subcutaneous
Oncaspar	PEGylated asparginase	Leukemia	Subcutaneous
Elestrin	Estradiol gel (0.06%) incorporating calcium phosphate nanoparticles	Treatment of moderate to severe hot flashes in menopausal women	Transdermal
VivaGel	Dendrimer gel	Vaginal microbicide for the revention of HIV and genital herpes	Topical
DepoCyt	Sustained release cytarabine liposomes	Lymphomatous meningitis	IV
DaunoXome	Encapsulated-daunorubicin citrate liposomes	Advanced HIV-related Kaposi's sarcoma	IV
Eligard	Leuprolide acetate and PLGH polymer formulation	Multiple sclerosis	IV
Somavert	PEGylated human growth hormone receptor antagonist	Acromegaly	IV

References: (Moghimi, Hunter et al. 2001, Gelperina, Kisich et al. 2005, Nie, Xing et al. 2007, Torchilin 2007, Kamaly, Xiao et al. 2012)

Prominent and clinically relevant examples are liposomes and polymeric nanoparticles, nanocarriers primarily used for the encapsulation of an active compound (drug, peptide, siRNA, etc.) to promote stability and delivery to the site of action. Many bioactive compounds are hydrophobic and have low water solubility, making translation into the clinic difficult. Liposomes and amphiphilic copolymers can readily encapsulate hydrophobic drugs into protected areas of the nanocarrier, away from the surrounding aqueous medium. In addition, the nanocarrier surface can be modified to accommodate specific targeting ligands and promote interaction with the target cells. With nanocarriers, many molecules that were abandoned in clinical trials because of their poor pharmacokinetics could be successfully repurposed (Gupta, Sung et al. 2013).

1.2.2. Multimodal nanoparticles

Due to the modular nature of nanoparticle engineering, it is possible to design nanoparticles with multiple functional components. For example, one could design a fluorescent nanoparticle with photothermal ablation activity, combined with a bioactive sensor to detect changes in target tissues. This is an example of a popular class of multimodal nanoparticles called theranostics. Nanoparticles can be designed with three functional components providing imaging, therapeutic and diagnostic modalities. The first shows that a particle has successful reached the target area. The second performs a therapeutic action. The third detects a biomarker that measures the response to the treatment. Designed in this way, therapies can be carefully monitored and adjusted to maximize safety and effectiveness.

1.3. Quantum dot: semiconductor nanocrystals

Quantum dots are highly attractive tools for molecular imaging applications. As with other nano-scale materials, QDs have unique physical and chemical properties specifically related to their size and composition. QD are self-assembled fluorescent nanocrystals. They consist of a colloidal metallic core, capping shell and surface coating (Figure 1.1). The inorganic core is typically composed of semiconductor metals from groups II/VI (e.g. cadmium telluride, cadmium selenide) or III/V (e.g. indium phosphate, indium

Figure 1.1. Quantum dot structure

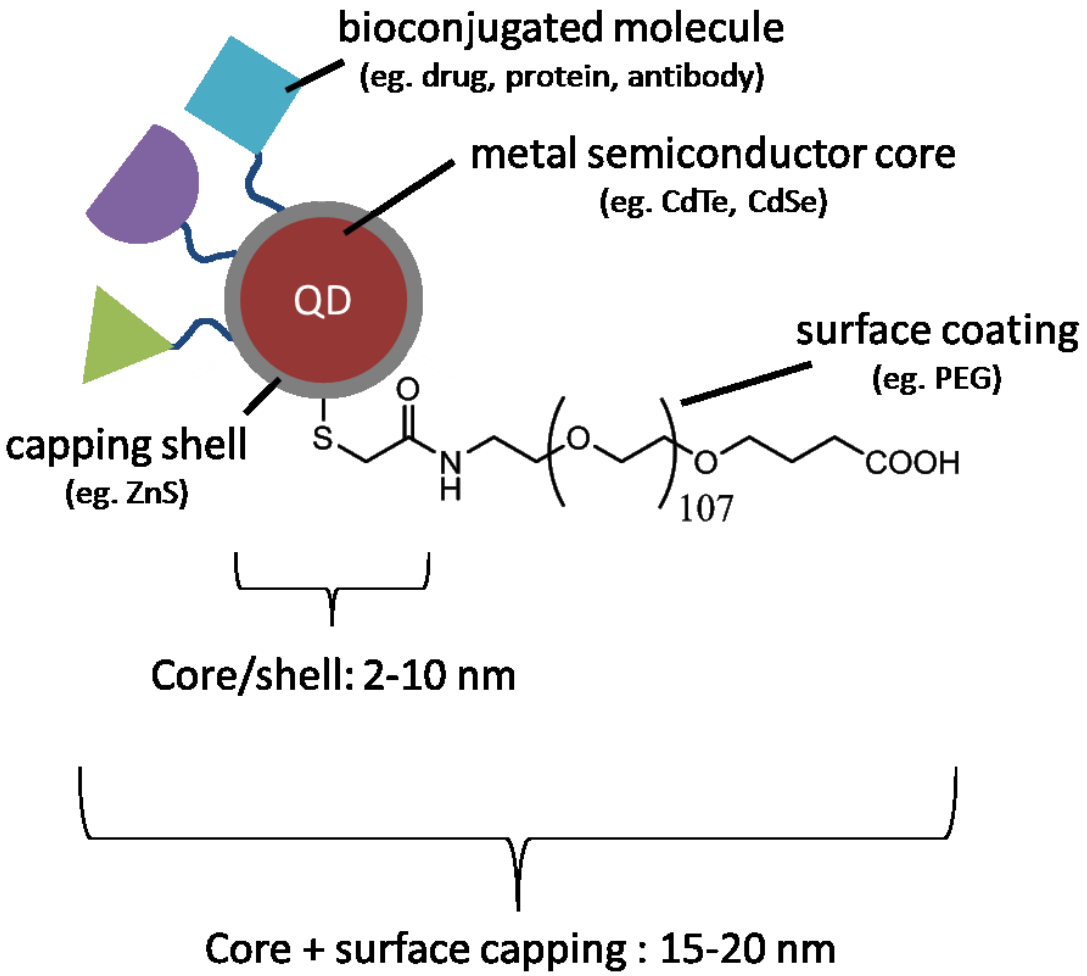

arsenide) of the periodic table. Due to the quantum mechanical behaviour of the metal semiconductor core, QDs absorb and emit light of discrete wavelengths depending on their size. Following excitation, small QDs (core ~2 nm) emit light in the ultraviolet spectrum, while larger QDs (core ~10 nm) emit in the near infrared spectrum (Medintz, Uyeda et al. 2005). Therefore, the QD emission spectrum can be tailored by controlling the size of the core during synthesis. A further advantage is the fact that QDs can be excited by a broad spectrum of wavelengths while emitting a narrow spectrum of light (Medintz, Uyeda et al. 2005, Michalet, Pinaud et al. 2005). Therefore, QDs of different sizes can be used simultaneously, providing multiplexing capabilities by avoiding signal overlap (Chan, Maxwell et al. 2002). In contrast, traditional organic fluorophores typically absorb light at a very narrow range of wavelengths and emit light with broad emission spectra.

QDs cores are commonly capped with a single or double layer zinc sulphide (ZnS) shell to improve stability in aqueous media (Reiss, Protiere et al. 2009). The ZnS shell is chemically inert and provides scaffolding for the attachment of additional layers (organic polymers or biomolecules) which can further improve the stability, biocompatibility or targeting of quantum dots. Bioconjugation of small ligands to the QD surface, such as targeting or therapeutic agents, does not completely quench their fluorescence, which is often the case for organic fluorophores (Breus, Heyes et al. 2007). The influence of the capping shell on the optical properties of QDs has been studied in detail (Dorfs and Eychmüller 2006, Rao, Müller et al. 2006, Grabolle, Ziegler et al. 2008, Smith and Nie 2009). A large body of work has focused on modifying nanoparticle surfaces (Jaiswal, Mattoussi et al. 2003, Hoshino, Fujioka et al. 2004, Susumu, Uyeda et al. 2007, Anderson and Chan 2008). Recent studies show that QDs with zwitterionic surfaces or modified with synthetic polymers such as polyethylene glycol (PEG) are highly stable and do not induce toxic responses in a number of cell types and even in animals (Choi, Liu et al. 2007, Ryman-Rasmussen, Riviere et al. 2007, Susumu, Uyeda et al. 2007). PEGylation, a process whereby polyethylene glycol (PEG) chains are conjugated to other molecules, is a common post-synthesis step performed to avoid recognition by immune surveillance mechanisms *in vivo*, such as the Mononuclear Phagocyte System (MPS). The PEG chains occupy the surface space and the immediate area surrounding the nanoparticle, significantly reducing the adsorption of serum proteins to the

nanoparticle surface. Interestingly, it seems that low amounts of PEGylation (or smaller PEG chains) leave the MPS detection intact, whereas high rates of PEGylation reduce MPS detection, suggesting that MPS detection is dependent on the adsorption of relatively large serum proteins (Walkey, Olsen et al. 2012).

QDs are also highly photostable due to their inorganic composition (Chan and Nie 1998, Jaiswal, Mattoussi et al. 2003). QDs do not photobleach even after intense and prolonged illumination, thereby permitting long-term and repeated imaging. As such, QDs are a highly valuable tool for the tracking of molecules in a biological setting, commonly referred to as single particle tracking (SPT). Fluorescent dye molecules, on the other hand, are very sensitive to light and rapidly undergo degradation and irreversible chemical modification following exposure. QDs are approximately 20 times brighter and over 100 times more photostable than traditional dyes (James and Gambhir 2012). These properties make QDs excellent candidates for *in vitro* and *in vivo* imaging applications.

1.3.1. QD Surface Conjugation

The most widely used methods for QD synthesis produce particles that are only soluble in harsh organic solvents (Murray, Norris et al. 1993). In order for QDs to be applicable for most biological applications, they must be rendered soluble in the aqueous phase. One of the most common approaches is to conjugate short ligands to the surface through thiol linkages (Figure 1.2.). These molecules can be very simple such as mercaptopropionic acid (MPA) which we employed to solubilize QDs in Chapters 2 and 3. These small molecules provide a net surface charge which is essential to maintain the QDs suspended in the aqueous phase. The stability is based on the electrostatic repulsion effect between ligands. Other short ligands such as dihydrolipoic acid (DHLA), which is attached to the QD via *two* thiol bonds, is stronger and the more difficult to detach. DHLA is an excellent surface ligand because lipoic acid is known for its anti-inflammatory and antioxidant properties. We have previously shown that such modifications can protect against the harmful effects of certain cytotoxic nanocrystals either by thiol conjugation or pre-treatment of the cells (Jain, Choi et al. 2009, Neibert and Maysinger 2012).

Figure 1.2. Quantum dots with different surface conjugations

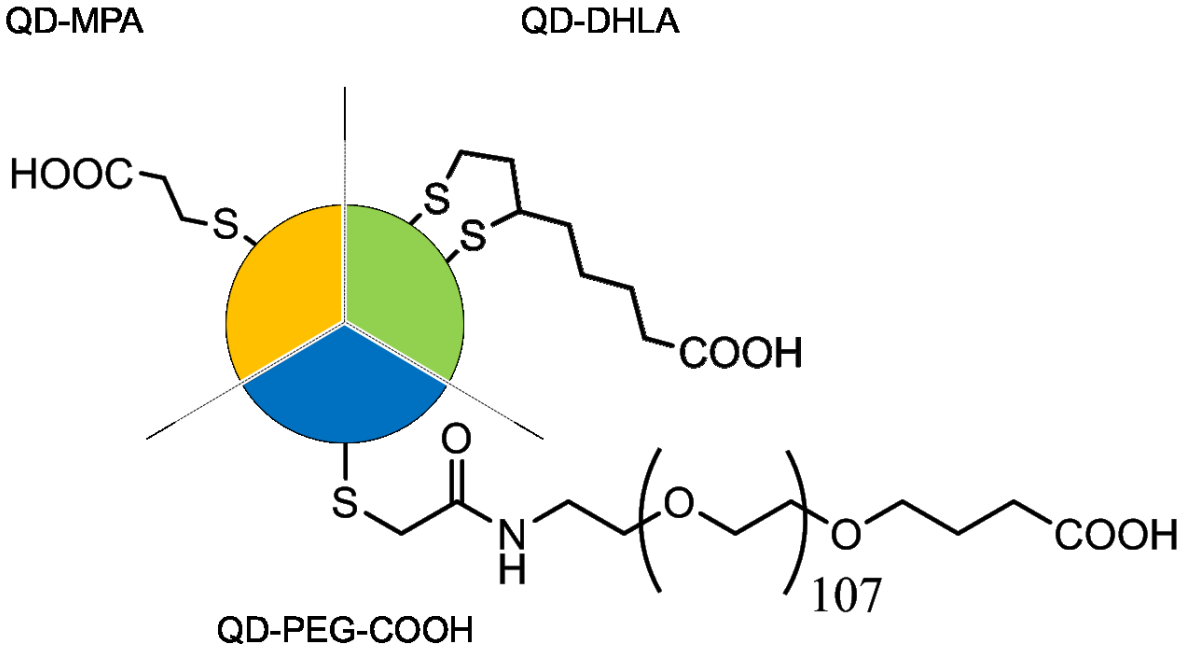

1.4. Interactions at the nano-bio interface

To achieve sensible design in nanomedicine, it is important to consider how nanoparticles will interact with components of the biological microenvironment (Walkey and Chan 2012). Nanomaterials are subject to complex molecular interactions including binding to salts, organic molecules and proteins when applied to *in vitro* and *in vivo* systems. In addition, these molecular interactions result in an altered chemical exterior of the nanoparticle. The resulting nanoparticle-biological complex depends on the local conditions of the relevant environment and changes the overall molecular signature of the nanoparticle. The biological identity of the particle, which may be vastly different from its synthetic identity, affects how cells like macrophages of the MPS perceive and interact with the nanoparticle. Included in the factors that exert an influence at the interface between the nanoparticle-medium and the biological substrate are the binding of surface ligands, hydrophobicity/charge interactions, free energy and conformational changes, oxidation injury, and particle wrapping by the surface membrane (Walkey, Olsen et al. 2012).

A number of dynamic physiochemical interactions between nanomaterial surfaces and biological surfaces occur at the nano-bio interface (Nel, Madler et al. 2009). Broadly, this interface includes three interactive components: i) the nanoparticle surface, ii) the nanoparticle-medium interface and iii) the interface between the nanoparticle-medium and biological substrates. The nanoparticle surface is defined by its material properties. Shape, size, charge, radius of curvature, chemical composition, porosity, surface functionalization, surface ligand arrangement and hydrophobicity all have important effects on the behaviour of nanoparticles (Nel, Madler et al. 2009). At the nanoparticle-medium interface complex interactions occur between nanoparticles and the liquid they are suspended in. Some aspects of the interface are determined by properties of the medium, such as ionic strength, pH, temperature, and the presence of organic molecules or detergents. Others are determined by the interaction between the nanoparticles and the medium such as solubility, surface restructuring/free energy minimization and adsorption to organic molecules and detergents (Maiorano, Sabella et al. 2010). The interface between the nanoparticle-medium and the biological substrate consists of many factors, such as binding of surface ligands,

hydrophobicity/charge interactions, free energy and conformational changes, oxidation injury, and particle wrapping by the surface membrane (Walkey and Chan 2012). The combined effect of all these interactions will subsequently play a critical role in determining biological activity, in particular in mediating cell internalization

1.5. Internalization

The interactions at the plasma membrane of phospholipids, cholesterol and a multitude of membrane proteins, determine how extracellular materials are recognized by the cell. Once appropriately identified, extracellular materials can be actively taken up by the cell. The specific route of uptake depends on the cell type and the nature of what is to be internalized. For small molecules, ions and gases, exchange is carried out passively by diffusion through the cellular membrane and membrane channels. For larger molecules, the cell uses specific modes of internalization, requiring substantial energy expenditure. The internalization of macromolecules and nanoparticles fits within this category.

1.5.1. Active transport

Active transport is the movement of molecules across a membrane in an energy dependent manner. This typically involves the internalization of extracellular materials necessary for the proper functioning of the cell. Active transport requires specialized cellular machinery such as ion channels, transmembrane pumps or vesicles formed by the invagination of the plasma membrane. Endocytosis, a type of active transport, allows the controlled internalization of large cargo into the intracellular space (Figure 1.3.). Extracellular cargo interacts with proteins and receptors at the cellular membrane and can be endocytosed by one of the following mechanisms depending on cargo properties and cell type.

Figure 1.3. Endocytosis - Gateway to the cell

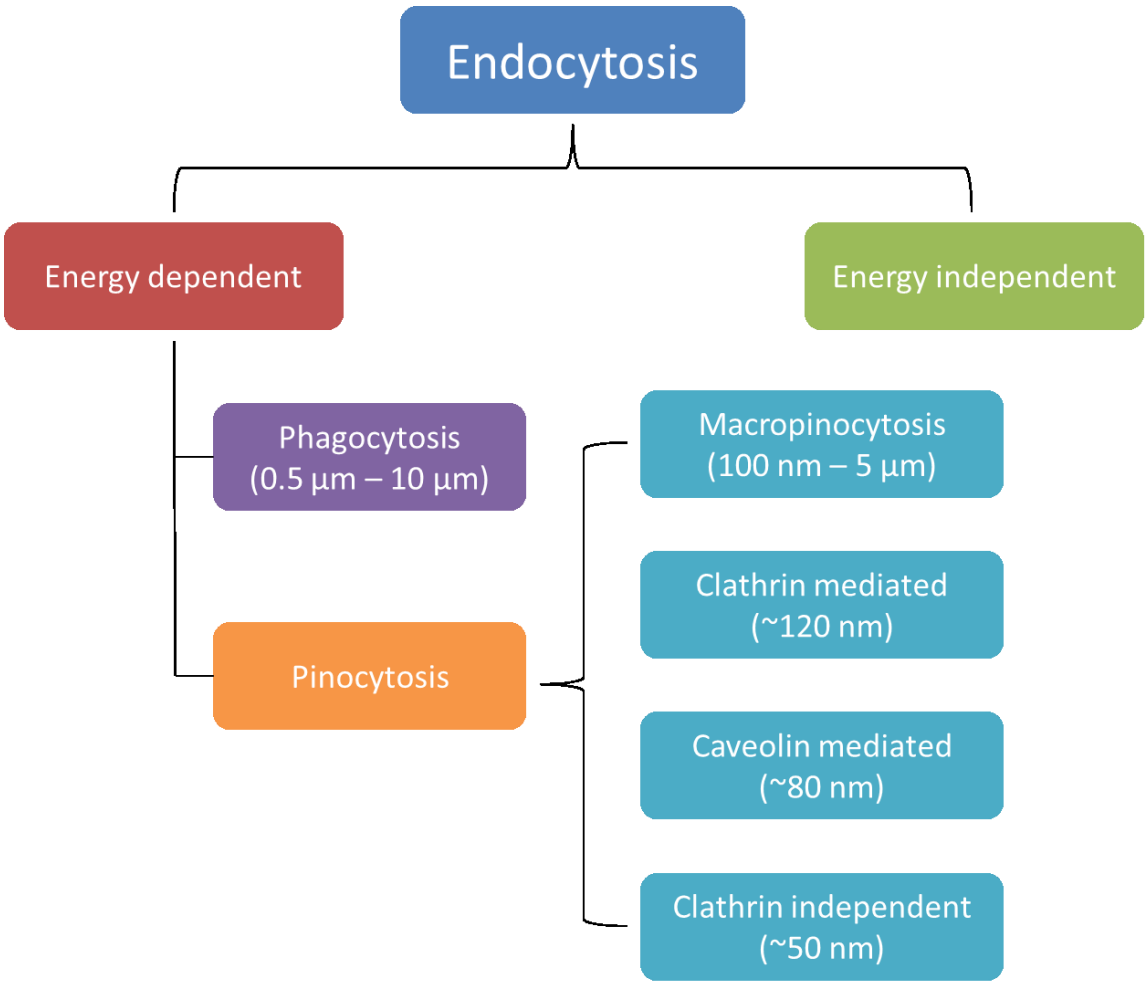

1.5.2. Clathrin mediated uptake (CME)

Clathrin dependent uptake is mediated by the formation of small plasma membrane invaginations (100-200 nm in diameter). Below this limit, the size of the invagination will depend on the size of the cargo to be internalized. Invaginations are formed by elastic deformation of the plasma membrane through interaction with the cytosolic protein clathrin and associated scaffolding proteins such as AP-2 and Eps15 (Ehrlich, Boll et al. 2004). Clathrin-coated vesicles (CCVs) are found in virtually all cell types and form domains of the plasma membrane termed clathrin-coated pits. Several studies have suggested that nanoparticles are primarily internalized through clathrin-independent mechanisms (Zhang and Monteiro-Riviere 2009, Verma and Stellacci 2010).

1.5.3. Caveolae mediated uptake

Caveolae exist at the surface of many different cell types and are considered the most common type of non-clathrin-coated plasma membrane invagination. Caveolae appear as small (50-80 nm in diameter) flask-shape pits embedded into the plasma membrane. This type of uptake is used to transport albumin and for the internalization of insulin receptors. Caveolae are ubiquitous and can make up to a third of the total plasma membrane area. They are most abundant in smooth muscle, fibroblasts, adipocytes, and endothelial cells (Parton and Simons 2007). For endothelial cells, caveolae mediated uptake is the primary mode of entry for nanoparticles into cells (Contreras, Xie et al. 2010). The maximum size of the caveolin covered vesicles restricts access to larger particles. This mode of internalization is frequently involved in the uptake of positively charged nanoparticles and can lead to cytotoxicity via disruption of the plasma membrane (Xia, Kovochich et al. 2008).

1.5.4. Receptor mediated uptake

This type of endocytosis involves the binding of a ligand to its corresponding receptor at the plasma membrane. Once the ligand is bound, the receptor and cargo are internalized through membrane invagination, typically via clathrin-dependent uptake. The best understood

examples are the low density lipoprotein (LDL) receptor, the transferrin receptor and certain hormone receptors such as the epidermal growth factor receptor (EGFR). In some cases, the receptor is recycled back to the plasma membrane. Receptor-mediated endocytosis may also participate in the internalization of non-functionalized nanoparticles through non-specific adsorption of serum proteins to the surface of the nanoparticles which can be recognized by scavenger receptors, primarily scavenger receptor A (Franca, Aggarwal et al. 2011, Vacha, Martinez-Veracoechea et al. 2011). As we will discuss in Chapter 4, serum proteins can adsorb strongly to the nanoparticle surface and this in turn has a dramatic effect on the mode and extent of uptake (Cedervall, Lynch et al. 2007, Lundqvist, Stigler et al. 2008, Casals, Pfaller et al. 2010, Maiorano, Sabella et al. 2010, Walczyk, Bombelli et al. 2010, Lundqvist, Stigler et al. 2011)

1.5.5. Macropinocytosis

Macropinocytosis involves the uptake of small particles into the cell, initially through the formation of an invagination at the plasma membrane which is then pinched off and suspended within small endocytotic vesicles. This mode of internalization is used primarily for the absorption of extracellular fluids. Pinocytotic vesicles subsequently fuse with lysosomes to hydrolyze the contents of the endosomes. This is a non-specific mode of uptake, which is recognizable by the pleating of the plasma membrane, called membrane ruffling, controlled by the intracellular actin network. Macropinocytosis can internalize materials ranging from 200 - 5000 nm. This mode has also been observed for the internalization of nanoparticles covered with positively charged ligands (Zhao, Zhao et al. 2011).

1.5.6. Phagocytosis

Phagocytosis involves the vesicular internalization of large solid particles such as bacteria and cellular debris. It is distinct from other forms of endocytosis due to the size range of materials which can be internalized. Phagocytosis plays a major role in the immune system, by removing pathogens and other xenobiotics. The internalization by phagocytosis is

non-specific and allows the absorption of foreign objects as large solid particles (> 750 nm). Phagocytosis is regulated by the p38 mitogen-activated protein kinase (MAPK), which can be activated in response to stress, such as exposing the cells to cytokines, UV radiation, heat or oxidative stress (Doyle, O'Connell et al. 2004). We will discuss in Chapter 3 and 4 how phagocytosis plays an important role in the internalization of large nanoparticle aggregates.

1.6. Nanoparticle properties

The bioactivity of a nanoparticle is defined by its material properties. Particle composition, shape, size, charge, radius of curvature, chemical composition, porosity, surface functionalization, surface ligand arrangement, hydrophobicity and others, all have important implications on the behaviour of nanoparticles in a biological system.

1.6.1. Surface charge

The charge distribution on the nanoparticle surface is an important factor in how it is perceived by the cell. Principally, the charge distribution will determine the hydrophobic/hydrophilic properties of the nanoparticle. Hydrophobic particles interact more readily with surface membranes, but they also tend to cluster and become absorbed by the MPS when administered *in vivo*. While the interaction between the negatively charged surface of nanoparticles and the membrane surface is unfavourable, internalization can still occur (Verma and Stellacci 2010). Cytotoxicity tends to be higher with positively charged nanoparticles due to the disruption of the plasma membrane. Negative nanoparticles show a lower rate of endocytosis while positive nanoparticles can be rapidly internalized by clathrin-mediated endocytosis (Zhao, Zhao et al. 2011).

1.6.2. Size

Particles above 15-50 nm readily interact with the plasma member and can become wrapped by surface membranes, facilitating uptake by endocytosis. Below a critical size (~15

nm), plasma membrane wrapping is much less effective (Nel, Madler et al. 2009). This can be advantageous if the functionality of a nanoparticle depends on endocytosis at the target area, but it also means that they will be more readily taken up and cleared by macrophages of the MPS. The internalization rate depends on the size of the particles, in part because of the time needed for coating the plasma membrane (Gao, Shi et al. 2005) . To achieve effective uptake, small nanoparticles must first concentrate at the cell surface (Jiang, Rocker et al. 2010). Nanoparticles must be packed together sufficiently to reduce the free energy necessary for membrane wrapping (Chithrani, Ghazani et al. 2006, Zhang and Monteiro-Riviere 2009). Even among very small nanoparticles, there can be particle agglomeration, whereby groups of nanoparticles and other molecules adhere together into a larger complex in the extracellular environment. This effectively creates larger nanoparticle clusters, which interact more strongly at the cell membrane (Zhang and Monteiro-Riviere 2009). Therefore, larger nanoparticles are taken up more quickly, while there is minimal internalization for smaller nanoparticles. These effects will be investigated in more detail in Chapter 4. Additionally, aggregates of nanoparticles lose some of the nano-scale activity they exhibit as individual particles (Hotze, Bottero et al. 2010).

Depending on the method of synthesis, nanoparticles in suspension are not always completely uniform in size (monodisperse). Often nanoparticle sizes are varied, forming populations of differently sized particles. If proper nanoparticle characterization is not performed, size is simply reported as the average of the population. Therefore it is possible that the same type of nanoparticle can simultaneously be internalized via multiple modes of uptake. The size will also determine the surface density of ligands which, in turn, can affect the mode of uptake. The smaller the particle, the greater the curvature and its capacity for ligands to pack closely together (Hill, Millstone et al. 2009). Consequently, the monodispersity of nanoparticle preparations should be taken into account when interpreting internalization data from studies.

1.6.3. Shape

Particle geometry plays an important role in directing the mode of internalization and the biological consequences of uptake. Several studies on geometry and morphology of particles have been done in micro-sized particles, but little is known about nanoparticles, save for a few recent studies (Champion and Mitragotri 2006, Mitragotri and Lahann 2009, Herd, Daum et al. 2013). For instance, rod-shaped particles are more efficiently internalized than spherical-shaped particles of similar size (>100 nm) (Gratton, Ropp et al. 2008). The favouring of rods over spheres is due to a greater receptor contact with the long axis, requiring minimal receptor binding along the short axis. However, the opposite is true for particles with diameters less than 100 nm (Chithrani, Ghazani et al. 2006, Qiu, Liu et al. 2010). Nanoparticle geometry may also be exploited to direct nanoparticles subcellular localization. For example, nanorods tend to accumulate in compartments around the nucleus while spherical nanoparticles of a similar size, are more diffused in the cytosol (Yoo, Doshi et al. 2010). In addition, specific cellular signaling pathways become activated in response to nanoparticles with varied geometries, resulting in shape dependent cellular phenotypes (Hutter, Boridy et al. 2010, Herd, Daum et al. 2013).

1.7. Tools to study endocytosis of nanoparticles

Endocytosis of nanoparticles is a highly complex and dynamic process. In recent years, several tools have been developed to better understand the cellular mechanisms involved in uptake. These include siRNA delivery, transfected cell lines and small molecule inhibitors (Zhang and Monteiro-Riviere 2009). Pharmacological inhibitors are often used to investigate mechanisms of endocytosis due to their commercial availability and ease of use. This strategy makes the assumption that the selected inhibitors have specific effects on only one type of endocytosis. However, this is not always the case as summarized in Table 1.2.. Several compounds believed to be specific have been later found to have off target effects. Due to these limitations, it is necessary to combine several different chemical compounds and employ complementary methods for assessing uptake when investigating the mechanisms of endocytosis (Iversen, Skotland et al. 2011).

Table 1.2. Toolbox of pharmacological inhibitors used to study endocytosis

Agent	Mechanism of action	Mode affected	Pitfalls
Chlorpromazine	Inhibits Rho GTPase	CME	Not efficient in all cell lines
Wortmannin	Inhibits phosphatidylinositol 3-kinase	Macropinocytosis and compensatory RhoA mediated endocytosis	
Cytochalasin D	Inhibits actin polymerization	Macropinocytosis and may affect several other endocytic mechanisms	Not efficient in all adherent cell types
Dynasore	Inhibits dynamin function	Several	
Genistein	Inhibitor of several tyrosine kinases	Inhibits caveolae pinching	Affects several processes
Filipin	Interacts with cholesterol	A number of clathrin-independent and cholesterol-dependent mechanisms	Unstable and toxic
Methyl-β-cyclodextrin	Cholesterol depletion from plasma membrane by extracting cholesterol	Macropinocytosis and both CME and CIE giving rise to small vesicles	Should be checked for possible leakage of K+
Nocodazole	Interferes with the polymerization of microtubules	CME and receptor mediated endocytosis	
Nystatin	Interacts with cholesterol	A number of clathrin-independent and cholesterol-dependent mechanisms	Toxic
SB-203580	Inhibits p38	Phagocytosis	
Y-27632	Inhibits Rho associated kinase (ROCK) and formation of actin stress fibers	Macropinocytosis	

References: (Rodal, Skretting et al. 1999, Zhang and Monteiro-Riviere 2009, Iversen, Skotland et al. 2011)

1.8. Rationale for thesis

Given the growing annual production of nanomaterials for industrial and medical applications, human exposure is practically unavoidable. The recent focus on nanotoxicology and exposure risks is spurred by an increased public interest and awareness in nanotechnology. Evaluation of nanoparticle toxicity is a serious concern as many nanomaterials are currently present, knowingly or unknowingly, in everyday commercial products such as electronics, cosmetics and clothing.

Unlike small molecule therapeutics with very well-defined chemical properties (size, shape, molecular weight, etc.), nanomaterials are much more difficult to characterize, especially in the context of the biological microenvironment (Crist, Grossman et al. 2013). To date, there is still no clear consensus or guidelines for the manufacturing and characterization of materials at the nano-scale. Researchers often use nanomaterials obtained commercially without performing their own analysis, while others rely on in-house synthesis. There are often significant discrepancies between what is advertised by the manufacturer and what is supplied, leading to inconsistencies in the literature (Crist, Grossman et al. 2013). At the advent of this thesis work, very little was known with regards to the potential hazards of nanomaterials and how they might interact with the biological environment. It is becoming increasingly clear that nanoparticle properties such as composition, size, shape, surface charge, purity and stability dramatically affect the biological environment, and *vice versa* (Verma and Stellacci 2010). These parameters play an important role in the biodistribution and activity of nanomaterials, defining their toxicity profile (Gaumet, Vargas et al. 2008, Jiang, Oberdörster et al. 2009). Therefore it is of the utmost importance to properly characterize nanoparticles, especially those destined for human applications.

The goal of this thesis work is to characterize nanoparticle-cell interactions and better understand their biological implications. This knowledge is essential to develop appropriately designed nanomaterials with improved biocompatibility for future use as tools in nanomedicine.

The specific objectives of this thesis were:

1. to elucidate the mechanisms underlying the adaptive cellular response to quantum dots;
2. to investigate modified quantum dot surfaces with small ligands and to study the nanoparticle-cell interactions at the nano-bio interface;
3. to explore the effect of the biological microenvironment on particle stability and cellular fate.

Connecting text

Systematic investigations into the biological consequences of the nano-bio interface remain unclear. In Chapter 2, we described the experiments carried out to uncover the underlying mechanisms of the adaptive cell response to uncapped CdTe quantum dots. These studies complemented our initial investigations of QD-dependent toxicity and the potential role of glutathione in cellular adaption (Jain, Choi et al. 2009).

In this chapter, we identified wide variations in the endogenous antioxidant potential within the total cell population. Individual cells could be divided into subpopulations by measuring intracellular glutathione concentrations using live cell fluorescence microscopy. Our findings showed that cellular exposure to toxic CdTe QDs brings about a dynamic redistribution of intracellular glutathione by selectively killing cells with low GSH concentrations and sparing those with medium to high GSH concentrations. These adaptation effects were detected in PC12 cells, where QD toxicity and the associated cellular pathways have been well characterized (Holder, Ellis et al. 2009). Further investigation of these interactions is required to better understand how different morphological, physical and chemical properties of nanoparticles direct cellular fate.

Chapter 2. Mechanisms of Cellular Adaptation to Quantum Dots--the Role of Glutathione and Transcription Factor EB

Neibert K, Maysinger D.

Nanotoxicology. 2012, 6(3), 249-262

2.1. Abstract

Cellular adaptation is the dynamic response of a cell to adverse changes in its intra/extra cellular environment. The aims of this study were to investigate the role of 1) the glutathione antioxidant system and 2) the transcription factor EB (TFEB), a newly revealed master regulator of lysosome biogenesis, in cellular adaptation to nanoparticle-induced oxidative stress. Intracellular concentrations of glutathione species and activation of TFEB were assessed in rat pheochromocytoma (PC12) cells following treatment with uncapped CdTe quantum dots (QDs), using biochemical, live cell fluorescence and immunocytochemical techniques. Exposure to toxic concentrations of QDs resulted in a significant enhancement of intracellular glutathione concentrations, a redistribution of glutathione species and a progressive translocation and activation of TFEB. These changes were associated with an enlargement of the cellular lysosomal compartment. Together, these processes appear to have an adaptive character, and thereby participate in the adaptive cellular response to toxic nanoparticles.

2.1.1 Key words

Adaptation, glutathione, quantum dots, transcription factor EB (TFEB)

2.2. Introduction

Nanoparticles are continuously being developed for a diverse range of applications in the rapidly growing field of nanomedicine, primarily as imaging, diagnostic and therapeutic tools. However, many of the interactions between nanoparticles and biological systems, as well as related mechanisms of nanoparticle-induced toxicity, remain unclear (Maysinger 2007, Mei, Susumu et al. 2009, Nel, Madler et al. 2009). The cellular response to nanoparticle exposure has been shown to be dependent on physicochemical properties such as size, shape, core composition, surface coating, ligand arrangement and charge (Idowu, Lamprecht et al. 2008, Jiang, Kim et al. 2008).

Capped quantum dots (QDs) are highly florescent and photostable nanoparticles, making them suitable candidates for *in vivo* imaging and for highly sensitive *ex vivo* diagnostic assays (Hermanson 2008). The capping of QDs with a zinc sulfide (ZnS) shell increases core stability and allows further modification of surface chemistry, providing the potential for diverse site-directed targeting and enhanced biocompatibility. First generation uncapped or "naked" cadmium telluride (CdTe) and cadmium selenide (CdSe) QDs are cytotoxic in several cell systems (Choi, Cho et al. 2007, Maysinger 2007, Hermanson 2008). QD-induced cell death involves the release of free cadmium ions from the QD core, formation of reactive oxygen species and nitrogen species (ROS/RNS), and the disruption of redox homeostasis (Choi, Cho et al. 2007). Exposure to both artificial and biological nanoparticles can lead to the disruption of cellular redox status and activation of compensatory mechanisms. However, when exposed to toxic nanomaterials for a short time or in low nanomolar concentrations, cells can successfully adapt by engaging antioxidant defenses and lipid re-distribution processes (Khatchadourian and Maysinger 2009, Nel, Madler et al. 2009). Specific mechanisms that mediate these adaptive cellular processes remain unclear.

Throughout evolution, eukaryotic cells have developed several overlapping defense mechanisms which are activated in response to varying degrees of oxidative stress (Zhu, Posati et al. 2012). The generation of oxidative stress involves the uncompensated accumulation of both ROS and RNS leading to the formation of harmful adducts with cellular proteins, lipids and DNA (Jefferis and Kumararatne 1990). ROS/RNS molecules function as both oxidants and signaling molecules through alterations in cellular redox homeostasis and the targeting of redox sensitive cysteine residues (D'Autreaux and Toledano 2007). Cell specific responses to oxidative stress have been shown to be dependent on subtle inter-population variations in cell size, adenosine triphosphate (ATP) concentration and plasma membrane composition (Casals, Pfaller et al. 2010). The capacity of cells to adapt to changes in cellular homeostasis may also depend on its endogenous antioxidant status which is determined by the content of antioxidant enzymes such as superoxide dismutase (SOD) and catalase (CAT) as well as small molecular antioxidant molecules such as ascorbic acid, tocopherol, thioredoxin and glutathione (Cedervall, Lynch et al. 2007).

Glutathione is considered to be a key regulator of the cellular redox homeostasis due to its low redox potential (-240 mV at pH 7.0), high intracellular abundance (1-13 mM) and ubiquitous expression in eukaryotic cells. Reduced glutathione (GSH) reacts primarily with H_2O_2 resulting in the formation of oxidized glutathione (GSSG) and H_20. *De novo* synthesis of glutathione by gamma-glutamylcysteine synthetase (GCL), the rate limiting step, can be enhanced by increasing the intracellular cysteine pool via the addition of thiol-containing antioxidant molecules such as N-acetylcysteine (NAC) and lipoic acid (LA) (Ruffmann and Wendel 1991, Lundqvist, Stigler et al. 2008). Healthy, unstressed cells maintain a high intracellular GSH/GSSG ratio to ensure the availability of GSH. As cells become increasingly stressed, the GSH/GSSG ratio decreases which results in the transcriptional activation of the antioxidant response element (ARE) by the NF-E2-related factor 2 (Nrf2) transcription factor, and expression of antioxidant genes such as CAT, SOD and GCL (Lundqvist, Stigler et al. 2011). Nrf2 translocation to the nucleus is tightly controlled by stress responsive mitogen activated protein kinases (MAPKs) following disruption of cellular redox homeostasis (Maiorano, Sabella et al. 2010). Indeed, activation of Nrf2 in response to GSH depletion is believed to be an important determinant of cellular fate (Kah, Chen et al. 2012). Dynamic changes in the lysosomal compartment following oxidative stress are also believed to play a role in the cellular adaptation process (Khatchadourian and Maysinger 2009).

The coordinated transcriptional behaviour of lysosomal genes was recently revealed to be dependent on transcription factors of the microphthalamia-transcription factor E (MiT/TFE) subfamily of basic helix-loop-helix leucine zippers (bHLHZIP). Overexpression of one member of this family, transcription factor EB (TFEB), was shown to significantly increase the expression of lysosomal genes and enhance the activity of lysosomal enzymes by directly binding to the CLEAR (coordinated lysosomal expression and regulation) element (Wang, Zhang et al. 2012). The protein product of one of these genes, lysosomal-associated membrane protein 1 (LAMP1), plays a key role in lysosome biogenesis, stability and function (Nel, Madler et al. 2009). Recent studies have shown that most QDs tend to accumulate in lysosomal compartments and may themselves induce lysosome formation (Behrendt, Sandros

et al. 2009, Khatchadourian and Maysinger 2009, Przybytkowski, Behrendt et al. 2009). Our hypothesis is that activation of TFEB drives many of the observed changes in the cellular lysosomal compartment in response to QD-induced oxidative stress. Understanding the mechanisms involved in the adaptation process may lead to the development of strategies that enhance intrinsic cellular defenses for the purpose of limiting and/or circumventing nanoparticle-induced toxicity.

2.3. Methods

2.3.1 Cell Culture and Media

Undifferentiated rat pheochromocytoma cells (PC12) acquired from ATCC (CRL-1721) were cultured in RPMI 1640 media (Gibco) containing 5% fetal bovine serum (Gibco), 1% penicillin–streptomycin (Gibco) and free of phenol-red. Cells were cultured in T75 cell culture flasks (Sarstedt) and maintained at 37°C, 5% CO_2 in a humidified atmosphere. The seeding density was 40,000 cells per well in 96 well plates (Sarstedt), 400,000 cells per will in 6 well plates (Sarstedt), and 10,000 cells per well in 8 well chambers slides (Lab-Tek), where indicated. Following seeding, PC12 cells were grown for 24 hours to attain confluency prior to cell treatments.

2.3.2. Cell treatments

Cells were washed twice with PBS (Gibco) before and after all cell treatments. Cell treatments were added in serum free medium and incubated at 37°C for the times indicated. In experiments involving lipoic acid (200 μM; Sigma), cells were pretreated in serum containing media for 24 hours. In experiments involving L-buthionine-sulfoximine (50 μM; Sigma), cells were pretreated in serum containing media for 4 hours.

2.3.3. Nanoparticle preparation and characterization

Poly(caprolactone)-b-poly(ethylene oxide) nanoparticles were synthesized and characterized according to previous studies (Savic, Luo et al. 2003). Gold nanoparticle containing micelles were prepared as described in detail (Sidorov, Bronstein et al. 2004, Soo, Sidorov et al. 2007). CdSe/ZnS, CdSe/ZnS/PEG and uncapped CdTe nanoparticles were synthesized and characterized as per the method described previously (Lundqvist, Stigler et al. 2008), and characterization was performed as described in our previous studies (Cho, Maysinger et al. 2007, Choi, Cho et al. 2007, Lundqvist, Stigler et al. 2011). A summary of nanoparticle composition, size, surface coating and concentrations used, is provided in table 1.

2.3.4. Flame atomic absorption

The cadmium content of CdTe and CdSe/ZnS QDs (4, 20 and 40 nM) was measured using a Perkin-Elmer 3030 atomic absorption spectrometer. The instrument was operated in background correction mode. Detection of cadmium in 3 mL sample aliquots was carried out at room temperature using a hollow cathode lamp cadmium lamp (UNICAM) at a wavelength of 228.8 nm (4 mA current, 48 energy). The calibration fits were obtained using standard solutions of cadmium (SCP Science) ranging from 0-15 mg/L.

2.3.5. Alamar Blue Assay

To assess relative metabolic activity, cells were seeded in 96 well plates and incubated with 10 µL Alamar Blue (Invitrogen) diluted with 90 µL serum free media (10% vol/vol) per well for 1 hour at 37°C following exposure to nanoparticles (4, 20, 40 and 250 nM; 24 hours). Mean fluorescent intensity was measured with a FLUOROstar Optima fluorimeter (BGM, Labtech) with filters were set to Ex/Em = 544/590 nm and employed 3x3 matrix well scanning.

2.3.6. GSH, GSSH and total glutathione assay

Reduced glutathione (GSH), oxidized glutathione (GSSG) and total glutathione (tGSH) concentrations were determined biochemically (Calbiochem Kit) based on the Tietze method which measures the reaction of DTNB (5,5'-dithio-*bis*-2-nitrobenzoic acid) with the sulfhydryl group of GSH to produce yellow colored 5-thio-2-nitrobenzoic acid (TNB) (Walkey, Olsen et al. 2012). Cells were seeded in 6 well plates and exposed to nanoparticles (4, 20, 40, 250 nM; 24 hours). Following treatment, cells were detached with 0.05% trypsin/EDTA (Gibco) for 5 minutes at 37 °C, spun down at 3000 rpm for 5 minutes and resuspended in 1 mL of fresh serum free media. Sample aliquots (90 μL) were added to trypan blue (Gibco) (10 μL) and viable cells were counted with a hemocytometer (Fisher). The remaining cells were pelleted down, resuspended in assay buffer (1 mL), lysed by freeze/thaw (5 minutes at -80°C and 5 minutes at 37°C), spun down at 10,000 rpm for 10 minutes and incubated with DTNB (0.5 mM) for 30 minutes at room temperature. The absorbance of TNB (412 nm) was measured in sample aliquots (100 μL) with a bench-top microplate reader (BIORAD).

2.3.7. Intracellular glutathione imaging

GSH reacts specifically with monochlorobimane (mCBI; Cayman), a non-fluorescent membrane permeable dye, to form a fluorescent adduct (mCBI-GSH). Cells were seeded in 96 well plates and exposed to CdTe QDs (20, 40 nM; 24 hours) then incubated with mCBI (50 μM) for 1 hour at 37^0C. Dye containing media was aspirated and cells were washed with PBS. Fresh serum free media was added prior to live cell imaging. Fluorescence images were acquired with a Leica DFC350FX monochrome digital camera connected to a Leica DMI4000B inverted fluorescence microscope. The fluorescent intensity of the mCBI-GSH adduct was quantified and individual cells were classified as containing high, med or low levels of intracellular glutathione (tGSH) following image analysis using ImageJ (low < 1000 a.u.; medium 1000 < 2000 a.u. and high > 2000 a.u.). The number of cells in each subpopulation was normalized by the total number of cells per frame. At least 9 individual pictures were used per condition for quantification. Additionally, the fluorescent intensity of the mCBI-GSH adduct was measured with a FLUOROstar Optima fluorimeter (BGM, Labtech). Filters were set to Ex/Em = 380/460 nm and employed 3x3 matrix well scanning.

2.3.8. Detection of reactive oxygen species (ROS)

ROS generation was measured using dihydroethidium (DHE; Molecular Probes). Cells were seeded in 6 well plates and treated with CdTe QDs (20 nM; 4 hours) then incubated with DHE (10 μM) in the dark for 30 minutes. The conversion of DHE into highly fluorescent ethidium bromide was measured spectrofluoremetrically with a FLUOROstar Optima fluorimeter (BGM, Labtech) with filters set to Ex/Em = 544/612 nm and employed 3x3 matrix well scanning.

2.3.9. Detection of reactive nitrogen species (RNS)

RNS generation was assessed by measuring 3-nitrotyrosine (3NT), a product of tyrosine nitration. Cells were seeded in 8 well chamber slides and treated with CdTe QDs (20 nM; 24 hours) then fixed with 4% paraformaldehyde (BDH laboratory), permeabilized with 0.1% Triton-X 100 (Amersham) and subsequently blocked with 10% goat serum (GS; Sigma). Immunostaining was performed using primary 3NT antibody (Millipore) diluted 1:1000 in GS and incubated overnight at 4°C. The next day, cells were washed with PBS and incubated Alexa 594 goat anti-rabbit IgG –conjugated secondary antibody (Molecular probes) diluted 1:1000 in 10% GS for 1 hour at room temperature. Cells were washed with PBS and then counterstained with 10 μM Hoechst 33258 (Invitrogen) for 60 min. Stained coverslips were mounted onto microscope slides (Super Frost) using aqua poly mount (Polyscience). Fluorescence images were acquired with a Leica DFC350FX monochrome digital camera connected to a Leica DMI4000B inverted fluorescence microscope.

2.3.10. Western blotting

Cells were seeded in 6 well plates and treated with CdTe QDs (20 nM; 24 hours) and washed twice with ice-cold PBS, lysed in Nonident P-40 buffer [50 mM Tris-HCl (pH 8.0), 1.37 mM NaCl, 1% (vol/vol) Nonidet P-40, 10% (vol/vol) glycerol, 0.1 mM sodium orthovanadate, complete protease inhibitor cocktail tablet (Roche)] and subjected to standard

protein separation using 12% SDS-PAGE minigels. Membranes were blocked with nonfat dry milk. Blocked membranes were then probed with primary antibodies. Anti-phospho-JNK (Promega) was used at a 1:5000 dilution. Anti-JNK1 (Santa Cruz Biotechnology) was used at a dilution of 1:1000. Anti-phospho-p38 was used at a dilution of 1:5000 (Promega). Anti-p38 was used at a dilution of 1:1000 (Santa Cruz Biotechnology). Anti-actin was used at a 1:1000 dilution (Chemicon). Horseradish peroxidase-labeled antibodies (1:4000, Amersham) were used as secondary antibodies. Immunoblots were developed using the enhanced chemiluminescence system (Amersham) and X-OMAT film (Kodak).

2.3.11 Transmission electron microscopy (TEM)

Cells were seeded in 8 well EM chamber slides (Lab-Tek) and treated with CdTe QDs (20 nM, 24 hours). Following treatment, cells were fixed with 2.5% gluteraldehyde in 0.1 M sodium cacodylate buffer and post-fixed with 1% osmium tetroxide (OsO_4) in a 1.5% potassium ferrocyanide (KFeCN) solution. Thin sections (0.1 μm) were prepared using an Ultracut-E ultramicrotome (Leica Microsystems), and digital images were taken with a Gatan 792 Bioscan 1k x 1k Wide Angle Multiscan CCD camera (JEM-2000 FX).

2.3.12 LysoTracker DND-26 Staining

The total lysosomal content of live PC12 cells was measured using LysoTracker DND-26 (Invitrogen). Cells were seeded in 8 well chamber slides and treated with rapamycin (Sigma; 200 nM) and CdTe QDs (20 nM) for 1, 6 and 24 hours, then incubated with Hoechst 33258 (10 μM) for 60 min and LysoTracker Green DND-26 (500 nM) for 2 min. Fluorescence images were acquired with a Leica DFC350FX monochrome digital camera connected to a Leica DMI4000B inverted fluorescence microscope. Total lysosomal content was then quantified using ImageJ imaging software.

2.3.13 Assessment of TFEB translocation

Cells were seeded in 8 well chamber slides and treated with rapamycin (200 nM) and CdTe QDs (20 nM) for 1, 6 and 24 hours. Following treatment, immunostaining was performed using primary TFEB antibody (Millipore) diluted 1:1000 in GS and incubated overnight at 4°C. Fluorescence images were acquired with a Leica DFC350FX monochrome digital camera connected to a Leica DMI4000B inverted fluorescence microscope. TFEB translocation was then quantified using ImageJ imaging software.

2.3.14. Statistical analysis

Statistical significance was analyzed using SYSTAT 10 (SPSS) and determined by analysis of variance (ANOVA) followed by post hoc Dunnett's test or by independent t-test (where specified). Differences were considered significant where *p <0.05, **p <0.01 and ***p <0.001.

2.4. Results

2.4.1 Changes in intracellular glutathione species in cells exposed to toxic nanoparticles

To investigate the adaptive cellular response to nanoparticle-induced stress, we first assessed PC12 cell viability following equimolar exposure (0-250 nM) to a diverse range of nanoparticles with varied composition and size (Table 2.1.). Poly(ε-caprolactone)−poly(ethylene oxide) (PCL-b-PEO) block copolymer micelles are water-soluble biocompatible nanocontainers used as a drug delivery system (DDS) for hydrophobic drugs (Savic, Luo et al. 2003). Poly(4-vinylpyridine)-*block*-poly(ethylene oxide) (P4VP21-*b*-PEO45) micelles containing gold nanoparticles (GNPs) were developed to enhance the visualization of micelles in subcellular compartments, including lysosomes (Soo, Sidorov et al. 2007). Several types of QDs were selected for this study including: uncapped (poorly stable) CdTe QDs, capped (stable) CdSe/ZnS QDs and poly ethylene glycol (PEG) conjugated (highly stable) CdSe/ZnS/PEG QDs (Choi, Cho et al. 2007, Linse, Cabaleiro-Lago et al. 2007, Walkey, Olsen et al. 2012, Salvati, Pitek et al. 2013). Uncapped QDs readily leak core components (cadmium and tellurium) and are more prone to aggregation (Kah, Chen et al. 2012). The cadmium content of uncapped CdTe QDs and capped CdSe/ZnS

QDs was determined using flame atomic absorption (FAA). CdTe QDs samples contained 5x more cadmium than CdSe/ZnS QDs at equimolar concentrations (Figure S2.1.). These results show a significant shedding of cadmium from the core of the uncapped QDs. The aggregation status of CdTe QDs was determined using dynamic light scattering (DLS). Results from these analyses show that CdTe QDs formed large aggregates (Figure S2.2). QDs capped with a ZnS shell and PEG have enhanced biological stability and plasma half-life as well as reduced immunogenicity and tendency to form aggregates (Prapainop, Witter et al. 2012). Only exposure to uncapped CdTe QDs resulted in a concentration dependent reduction in cell viability (20 nM: 64.6 ± 7.1, $p < 0.001$; 40 nM: 30.1 ± 9.7, $p < 0.001$; 250 nM: 7.7 ± 4.3, $p < 0.001$), as compared to PCL-b-PEO, $P4VP_{21}$-b-PEO_{45}-GNP, CdSe/ZnS and CdSe/ZnS/PEG nanoparticles (<250 nM). It is clear that the stability of the QD greatly influences its capacity to cause cellular perturbations.

To investigate the role of glutathione in the adaptive cell response to selected QDs (Table 2.1.), the concentrations of intracellular glutathione species were assessed biochemically using the Tietze method (Arvizo, Giri et al. 2012). Cells were exposed to nontoxic doses of CdSe/ZnS and CdTe QDs for 24 hour (250 nM and 4 nM respectively). Exposure to nontoxic CdSe/ZnS QDs did not elicit a significant change in intracellular glutathione species with respect to the control (Figure 2.1A), nor did low nanomolar concentrations of CdTe QDs (Figure 2.1B). However, total intracellular glutathione (tGSH) and GSSG concentrations increased progressively in response to increasing concentrations of CdTe QDs, indicated by diamond and triangle symbols respectively (tGSH - 20 nM: 3.7 ± 0.1 nmoles/10^6 cells, $p < 0.001$; 40 nM: 5.6 ± 0.3 nmoles/10^6 cells, $p < 0.001$ and GSSG - 20 nM: 1.34 ± 0.1, $p < 0.001$; 40 nM: 3.6 ± 0.03 nmoles/10^6 cells, $p < 0.001$; Figure 2.1B).

Having observed global upregulation of intracellular glutathione concentrations in cell lysates, tGSH concentrations were then measured at the level of individual cells using monochlorobimane (mCBI) following exposure to CdTe QDs. mCBI penetrates the cell membrane and reacts specifically with GSH to form a fluorescent adduct (mCBI-GSH) which is readily detected by fluorescent microscopy and spectrofluorimetry (Sathishkumar, Gao et al. 2010, Walkey, Olsen et al. 2012). Fluorescent images of live cells containing the mCBI-

GSH adduct were acquired following 24 hour exposure to CdTe QDs (Figure 2.2A). Individual cells were then classified as having high, medium or low levels of tGSH based on mean area grey calculations following image analysis using ImageJ software (Supplemental Information; Figure 2.2B). Under control conditions, the majority of cells contained low tGSH (92 ± 4.0%). A smaller proportion of cells (7.6 ± 3.2%) had medium levels and very few cells were observed to contain high tGSH (1.2 ± 2.2%). The tGSH subpopulation distribution was markedly different following exposure to CdTe QDs. The majority of cells exposed to CdTe QDs contained moderate tGSH levels (20 nM: 68 ± 2.1%, $p < 0.001$; 40 nM: 89 ± 5.3%, $p < 0.001$) while a smaller population exhibited high fluorescence (20 nM: 25 ± 2.6%, $p < 0.001$; 40 nM: 5.4 ± 2.3%, $p < 0.05$). There was a significant decrease in the number of cells within the low population following CdTe QDs treatment with respect to the control and a reciprocal increase in medium and high tGSH subpopulations ($p < 0.001$). Following treatment with lipoic acid, there was a significant increase in the number of both medium (66 ± 5.1%, $p < 0.001$) and high (9.4 ± 2.1%, $p < 0.01$) glutathione containing cells. Following exposure to increasing concentrations of CdTe QDs, there was no significant difference in the magnitude of the tGSH changes observed from both the biochemical assay and the spectrofluorometric determination of mCBI-GSH (Figure S2.3.).

2.4.2. The adaptive cellular response to toxic CdTe QDs involves glutathione synthesis

To examine the contribution of glutathione synthesis to the adaptive cell response, we pretreated PC12 cells with both a pharmacological inhibitor and inducer of glutathione synthesis, L-buthionine sulfoximine (BSO) and lipoic acid respectively. Pretreatment with lipoic acid for 24 hours enhanced intracellular glutathione concentrations and significantly reduced CdTe QD induced-toxicity (87 ± 2.1%, $p < 0.001$ compared to the control; Figure 2.2C). Cells were independently pretreated with 50 μM BSO, a selective inhibitor of glutathione synthesis (GCL), for 4 hours, then concomitantly with CdTe QDs for 24 hours. There was a significant decrease in cell viability (16 ± 0.3 %, $p < 0.001$) following BSO exposure, compared to CdTe QD treatment alone (64 ± 2.0 %).

2.4.3. QD-induced formation of ROS/RNS and activation of MAPKs

Next we examined the involvement of specific ROS or RNS in CdTe QD-induced oxidative stress, and the involvement of stress response signaling. DHE was used to measure superoxide formation in PC12 cells treated with 20 nM CdTe QDs for 4 hours (Figure 2.3A). We observed a significant increase in superoxide formation with respect to control in cells exposed to CdTe QDs (27 ± 3.5%, $p < 0.01$). To evaluate the effects of CdTe QDs on RNS generation, we treated PC12 cells with 20 nM CdTe QDs for 24 hours and assessed nitrosative stress using antibodies against 3-nitrotyrosine (3NT) (Figure 2.3B). 3NT is a product of tyrosine nitration mediated by reactive nitrogen species such as peroxynitrite anion and nitrogen dioxide. 3NT levels normalized to cell number were significantly increased in cells exposed to 20 nM CdTe QDs (355 ± 86 %, $p < 0.01$) (Figure 2.3C). Indeed, CdTe QDs are potent inducers of both ROS and RNS.

The JNK and p38 pathways are activated following exposure to different sources of cellular stress, including oxidative stress, environmental stress and toxic insults (Prapainop, Witter et al. 2012). Early transient activation usually mediates cell survival while prolonged activation is implicated mostly in cell differentiation and apoptosis (Rothen-Rutishauser, Schurch et al. 2006, Wang, Bai et al. 2012). We examined phosphorylation status of stress activated MAPK members JNK and p38 in PC12 cells exposed to 20 nM CdTe QDs (Figure 2.3D). Quantification of immunoreactive bands from western blots is shown, indicating significant increase in the extent of phosphorylation for JNK, and p38 compared with untreated (serum free) control cells in the presence of CdTe QDs. The JNK and p38 pathways were both significantly activated following 4 hour treatment with CdTe QDs and the activation persisted up to 24 hours (6 fold increase, $p<0.01$ and 4 fold increase, $p<0.05$ respectively). The intensity of JNK phosphorylation decreased after 24 hours from the maximal activation at the 4 hour time point. In contrast, activation of p38 in CdTe QD treated cells persisted with the same or even higher intensity at 24 hours.

2.4.4. Exposure to toxic CdTe QDs induces morphological changes in cellular organelles and the activation of TFEB

We examined the mitochondrial and lysosomal status of PC12 cells following exposure of CdTe QDs using electron and fluorescence microscopy (Figure 2.4A). Electron micrographs provided evidence for marked morphological changes of mitochondria including deformation, swelling, loss of cristae (black arrows) and the appearance of numerous vacuoles (white arrows). The increased volume of the cellular vacuolar compartment was confirmed in live cells and analyzed using LysoTracker DND-26, a marker of acidic organelles including lysosomes (Figure 2.4B). There was an apparent time dependent expansion in the total volume of the cellular lysosomal compartment following exposure to CdTe QDs. Total LysoTracker DND-26 fluorescence intensity progressively increased over time, reaching the maximum following 24 hour exposure to 20 nM CdTe QDs (3.27 ± 0.4 fold, $p<0.005$) (Figure 2.4C). Serum containing media was used for control as serum withdrawal is a potent inducer of autophagy and lysosomal biogenesis (Goodman, McCusker et al. 2004). Treatment with rapamycin (200 nM), another well characterized inducer of autophagy, significantly increased the fluorescence intensity of acidic compartment measured by lysosomal marker LysoTracker DND-26 (3.01 ± 0.4 fold, $p<0.001$) (Chithrani, Ghazani et al. 2006, Iversen, Skotland et al. 2011).

To directly assess the involvement of TFEB activation in the cellular adaptation process, we performed immunocytochemistry to assess lysosome associated membrane protein LAMP1 expression, an indicator of TFEB activation [52]. Treatment with rapamycin and CdTe QDs resulted in a significant increase in LAMP1 fluorescence intensity (200 nM rapamycin: 3.23 ± 0.6 fold, $p<0.001$; 20 nM CdTe: 5.41 ± 0.7 fold, $p<0.001$) compared to control (Figure 2.5B). TFEB activation in response to CdTe QD exposure was then evaluated by measuring the degree of translocation from the cytosol to the nucleus, where TFEB directs lysosomal biogenesis and function [40]. TFEB migrated from a primarily cytosolic localization to a perinuclear localization following 6 hour exposure to 20 nM CdTe (Figure 2.5C). Quantification of the subcellular localization of TFEB from immunofluorescence micrographs revealed a significant time dependent increase in the nuclear/cytosolic TFEB following exposure to CdTe QDs for 1 hour and 24 hours (56.2 ± 3.1%, $p<0.001$; 74.9 ± 4.2% $p<0.001$ respectively) compared to control (Figure 2.5D).

2.5. Discussion

Eukaryotic cells have acquired a series of compensatory protective mechanisms to adapt to oxidative stress throughout evolution (Dickinson, Moellering et al. 2003). We investigated two potential cellular adaptation processes and observed significant intracellular changes in both systems following exposure to toxic concentrations of CdTe QDs. We provide evidence for the involvement of the glutathione antioxidant system in the cell-specific response to QD-induced oxidative stress and propose that TFEB is a key mediator of the underlying adaptive changes observed in the cellular lysosomal compartment.

In nature, cells are exposed to a wide range of noxious stimuli some of which include biological and artificial nano-sized particles. Once endogenous cellular antioxidants are depleted, electrophiles and peroxidized lipids lead to the disruption of redox homeostasis. ROS/RNS can function as signaling molecules through modification of redox sensitive cysteine sulfhydryls which antagonize the inhibition of nuclear-factor-E2-related-factor (Nrf2) by Keap1 (Howes, Mayor et al. 2010). This results in the nuclear translocation of Nrf2 and expressions of phase II enzymes (including SOD, CAT and GCL). Nrf2 activation may occur via direct phosphorylation of Ser40 by redox sensitive protein kinases (MAPK, PKC, etc.) or via oxidation of specific cysteine residues on Nrf2 regulator proteins (Cys151, Cys 273 and Cys288 on CUL3) (D'Autreaux and Toledano 2007, Li and Kong 2009). Activation of MAPKs cascades in response to oxidative stress is well documented; however the specific molecular mechanisms of Nrf2 activation remain unclear (Piccirillo, Filomeni et al. 2009). One potential mechanism is the phosphorylation of Cul3, a Nrf2 binding protein by MAPKs (Chithrani, Ghazani et al. 2006). JNK and p38 have been specifically implicated in Nrf2 activation as their inhibition has abolished the adaptive response to GSH depletion (Andreadi, Howells et al. 2006, Cedervall, Lynch et al. 2007). We found that JNK and p38 were activated early and intensely after treatment with uncapped CdTe QDs. We propose that QD-induced oxidative stress leads to activation of MAPK kinases, translocation of Nrf2 and activation of tier 2 defenses, facilitating the enhancement of *de novo* glutathione, and cellular adaptation.

Glutathione is especially important with respect to QD toxicity as it serves in the first line of defense, due to the formation of highly stable glutathione-cadmium complexes. The cadmium center of these complexes can assume several different coordination geometries with the glutathione molecule, rendering glutathione a highly effective cadmium chelator (Lundqvist, Stigler et al. 2008, Treuel and Nienhaus 2012). However, CdTe QD toxicity does not result from the simple addition of cadmium and tellurium components, but rather depends on the unique physicochemical properties of the nanocrystal structure as a sum greater than its parts (Lacerda, Park et al. 2010). Undifferentiated rat pheochromocytoma cells (PC 12) are an attractive model to study the adaptive cellular response to oxidative stress, because they are well characterized and the signal transduction pathways have been previously described in detail (Kaplan 1998, Chithrani, Ghazani et al. 2006, Zhao, Zhao et al. 2011).

PC 12 cells with low basal tGSH appear to be more sensitive to CdTe QD exposure than those with medium or high tGSH, suggesting that cell survival is due, in part, to increased total glutathione levels. This proposition is supported by the fact that exposure to toxic concentrations of CdTe QDs resulted in a 14 fold decrease in the fraction of cells containing low tGSH and a reciprocal 14 fold decrease in the fraction of cell contacting medium/large tGSH concentrations. We believe that the dramatic shift in the distribution of glutathione subpopulations represents a cell specific adaptation response. The largest increase in the proportion of cells containing high tGSH was measured following exposure to 20 nM CdTe QDs, as opposed to 40 nM CdTe QD. This difference may be due to excessive CdTe QD-induced oxidative damage at higher QD concentrations that limit the capacity of the cell to synthesize more GSH. Nontoxic CdSe/ZnS QDs did not result in an enhancement of tGSH concentrations whatsoever, or a disruption of the GSH/GSSG ratio, suggesting a specific role for glutathione in the adaptation process to toxic QDs. Taken together, cellular exposure to toxic QDs brings about a dynamic redistribution of intracellular glutathione by selectively 1) killing cells with low GSH concentrations, and 2) sparing those with medium to high GSH concentrations by enhancing GSH synthesis in the spared population. Our findings agree with recent work investigating QD toxicity in undifferentiated PC12 cells (Jiang, Kim et al. 2008). Differentiated PC12 cells are much more sensitive to QD exposure, with significant ROS

generation, degeneration of neurite-like processes and cell death occurring at low nanomolar concentrations (0.5-1 nM) (Verma and Stellacci 2010).

The generation of oxidative stress has been shown to adversely affect the morphology and function of cellular organelles (Lewinski, Colvin et al. 2008). Highly metabolically active organelles, such as mitochondria, are particularly sensitive to changes in redox homeostasis (Herd, Daum et al. 2013). Mitochondria depend on cytosolic synthesis and trafficking of glutathione which strongly sensitizes the mitochondria to cellular GSH depletion (Hu, Dong et al. 2008). Extensive mitochondria membrane damage, observed in TEM microphotographs, has been associated with inefficient ATP production, enhanced formation of ROS and the release of pro-apoptotic factors (Hoshino, Fujioka et al. 2004). In healthy cells, dysfunctional mitochondria are efficiently engulfed by vesicles and trafficked to acidified lysosomes resulting in the controlled degradation and clearance of damaged cellular components (autophagy). Electron and fluorescence microscopy analysis confirmed the presence of enhanced vacuolization and expansion of the lysosomal compartment in PC12 cells exposed to CdTe QDs, respectively.

Oxidative stress-resistant cells have been shown to contain increased levels of cholesterol precursors (lathosterol and lenosterol) and cholesterol which accumulates in lysosomes as well as increased cellular sphingomyosin (Gerion, Pinaud et al. 2001). Lysosome-associated membrane protein 1 (LAMP1), observed to be upregulated in response to toxic concentration of CdTe QDs, has also found to be enriched in stress-resistant cells presumably by stabilizing the integrity of the lysosomal membrane and protecting it from oxidation (Zhao, Zhao et al. 2011). Additionally, heat shock protein 70 (HSP 70) has been shown to prevent cell death by inhibiting permeabilization of lysosome membranes (Verma, Uzun et al. 2008). Indeed, exposure to CdTe QDs results in the enhanced expression of HSP 70 in primary fish hepatocytes (Dobrovolskaia and McNeil 2007). As such, cellular adaptation processes serve to mitigate ROS/RNS species, thus preserving the function of the lysosome, linking autophagy with antioxidant based adaptation mechanisms (Figure 2.6.). It has been suggested that the induction of autophagy may be the direct result of interactions between nanoparticles and the endosome/lysosome or alternatively, nanoparticles may be

recognized as an endosomal pathogens and targeted to the autophagy pathway for degradation (Walkey, Olsen et al. 2012). The accumulation of damaged proteins and organelles (particularly mitochondria) following nanoparticle-induced oxidative stress may also account for the observed induction of autophagy.

Our results implicate TFEB as a mediator of the adaptive response to uncapped CdTe QDs, a proposal supported by: i) significantly increased fluorescence of lysosomal marker Lysotracker DND 26, ii) upregulation of LAMP1 expression, and iii) progressive translocation of TFEB to the nucleus. We believe that the functional outcome of TFEB activation involves the clearance of damaged cellular organelles, particularly mitochondria. Future studies are required to provide direct evidence for the functional dependence of TFEB activation. The precise function and composition of lysosomes following nanoparticle induced oxidative stress should be further investigated by time course microscopy in cells expressing lysosome-specific proteins (LAMP1/2, Rab7 and CD63) tagged with green fluorescent protein (GFP) family members and proteomic analysis in the presence and absence of TFEB siRNA. Detailed studies employing these approaches may reveal novel lysosome/nanoparticle interactions and elucidate their role in the adaptive cell response to various biological and synthetic nano-sized particles. Investigations of these interactions are required to better understand how different morphological, physical and chemical properties of nanoparticles direct cellular fate.

Table 2.1. Cytotoxicity of selected nanoparticles

Cellular viability was assessed in cells exposed to nanoparticles (4, 20, 40 and 250 nM; 24 hours). Data are presented as means ± SEM of three individual experiments of triplicates. Significance was tested with independent t-tests (with Bonferroni correction) and indicated by ***p < 0.001. *a* indicates no significant reduction in viability at all concentrations tested.

Nano sized particle	**Size (nm)**	**Surface Coating**	**Concentration (nM)**	**Cell viability (%)**
PCL-b-PEO	25	PEO	250[a]	97.6 ± 5.1
GNP-micelles	24	PEO	250[a]	96.1 ± 9.0
CdTe QD	4	Cysteamine	250 40 20 4	7.7 ± 4.3 *** 30.1 ± 9.7 *** 64.6 ± 7.1 *** 90.1 ± 15.3
CdSe/ZnS	10	Cysteamine	250[a]	95.3 ± 4.4
CdSe/ZnS/PEG	25-30	PEG	250[a]	95.7 ± 3.9

Figure 2.1. Exposure to toxic concentrations of CdTe QDs enhances total intracellular glutathione content

A) GSH, GSSG and tGSH concentrations were determined in cells exposed to CdSe/ZnS and CdTe QDs (250 and 4 nM respectively; 24 hours). Data are presented as means ± SEM of three individual experiments of triplicates. B) GSH, GSSG and tGSH concentrations were determined in cells exposed to CdTe QDs (0, 4, 20 and 40 nM; 24 hours). Data are presented as means ± SEM of three individual experiments of triplicates. Statistically significant differences from control were tested with Dunnett's test and indicated by *** $p < 0.001$. Statistically significant differences between 20 and 40 nM CdTe exposure were tested with independent t-test and are indicated by ### $p<0.001$.

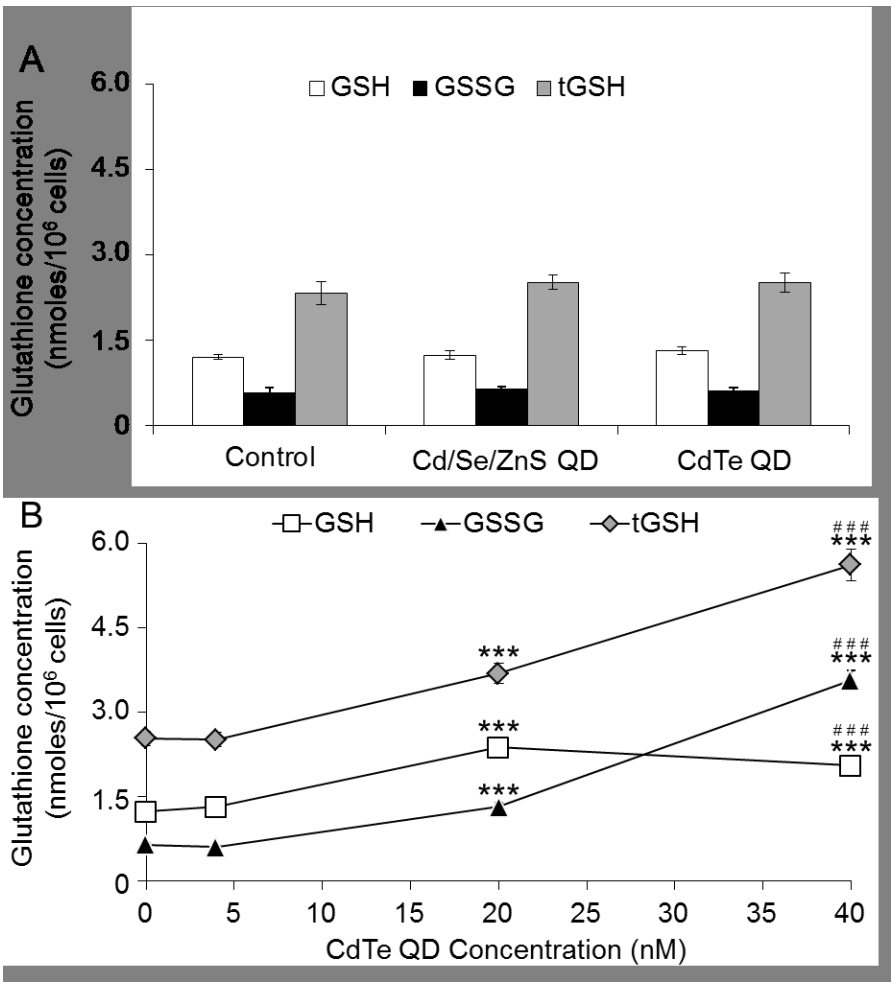

Figure 2.2. The adaptive cellular response to CdTe QDs involves redistribution of glutathione species and *de novo* glutathione synthesis

A) Intracellular glutathione was assessed with mCBI (50 μM; 1 hour) in cells exposed to CdTe QDs or lipoic acid (20, 40 nM and 200 μM respectively; 24 hours). Representative cells are shown, indicating L (low), M (medium) and H (high) total intracellular glutathione. Representative pictures are from at least 3 independent experiments of triplicates. Scale bars represent 60 μm. B) The relative number of cells containing low, medium or high tGSH concentrations of intracellular glutathione was quantified from fluorescent microscopy pictures. Data are presented as means ± SEM of at least 9 individual pictures per condition. Statistically significant differences from the control were tested with Dunnett's test and indicated by * $p < 0.05$, ** $p < 0.01$, *** $p < 0.001$. C) Cellular viability was assessed in cells exposed to CdTe QDs (20 nM; 24 hours), following pretreatment with BSO or lipoic acid (BSO: 50 μM, 4 hours; LA: 200 μM, 24 hours). Data are presented as means ± SEM of three individual experiments of triplicates. Significance was tested with independent t-tests and indicated by *** $p < 0.001$.

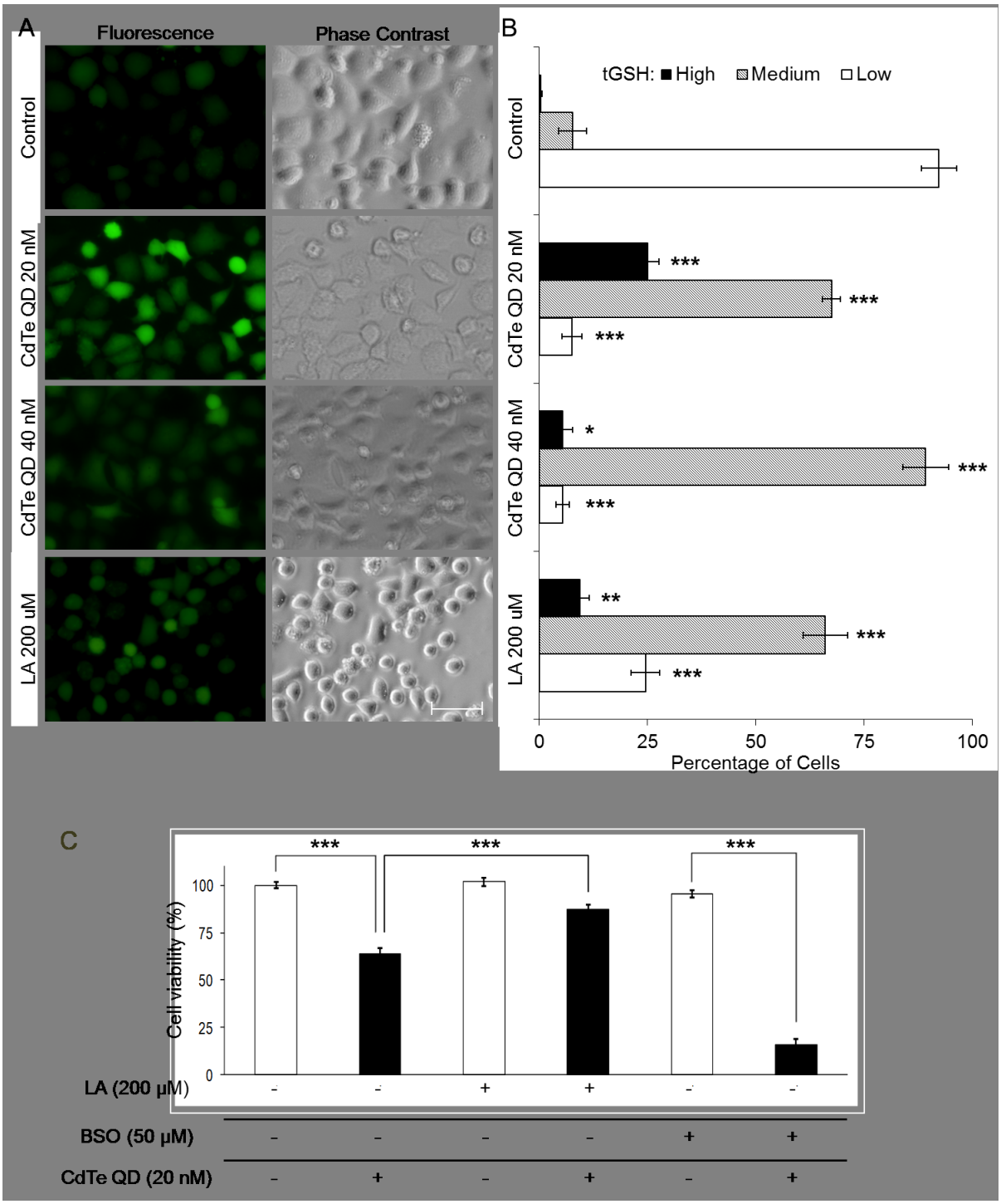
A
Fluorescence
Phase Contrast
Control
CdTe QD 20 nM
CdTe QD 40 nM
LA 200 uM
B
tGSH: High Medium Low
Control
CdTe QD 20 nM
CdTe QD 40 nM
LA 200 uM
***
***
***
*
***
***
**
***
***
0
25
50
75
100
Percentage of Cells
C
***
***
***
Cell viability (%)
100
75
50
25
0
LA (200 μM)
BSO (50 μM)
CdTe QD (20 nM)

Figure 2.3. Exposure to CdTe QDs results in the formation of ROS/RNS and activation of MAPKs

A) The formation of ROS was assessed with DHE (10 μM; 30 minutes) in cells treated with CdTe QDs (20 nM; 4 hours). Data are presented as means ± SEM of three individual experiments of triplicates. Significance was tested with independent t-test and indicated by * $p < 0.05$. B) Nitrosylated proteins (indicated in red) were labeled using a primary anti-3NT antibody in cells treated with CdTe QDs (20 nM; 4 hours). Nuclei (indicated in blue) were labeled with Hoechst (10 μM, 30 minutes). Representative pictures are from at least 3 independent experiments of triplicates. Scale bars represent 80 μm. C) 3-NT fluorescence intensity was quantified from representative pictures (n=9). Data are presented as means ± SEM of three individual experiments of triplicates. Significance was tested with independent t-test are indicated by *** $p < 0.001$. D) Western blot and densitometric values for the phosphorylation of JNK, p38 and cleaved caspase 3 in cells treated with CdTe QDs (20 nM, 1, 4; 24 hours). Data are presented as means ± SEM of three individual experiments of triplicates. Statistically significant differences were tested with independent t-tests and are indicated by * $p < 0.05$, ** $p < 0.01$, *** $p < 0.001$

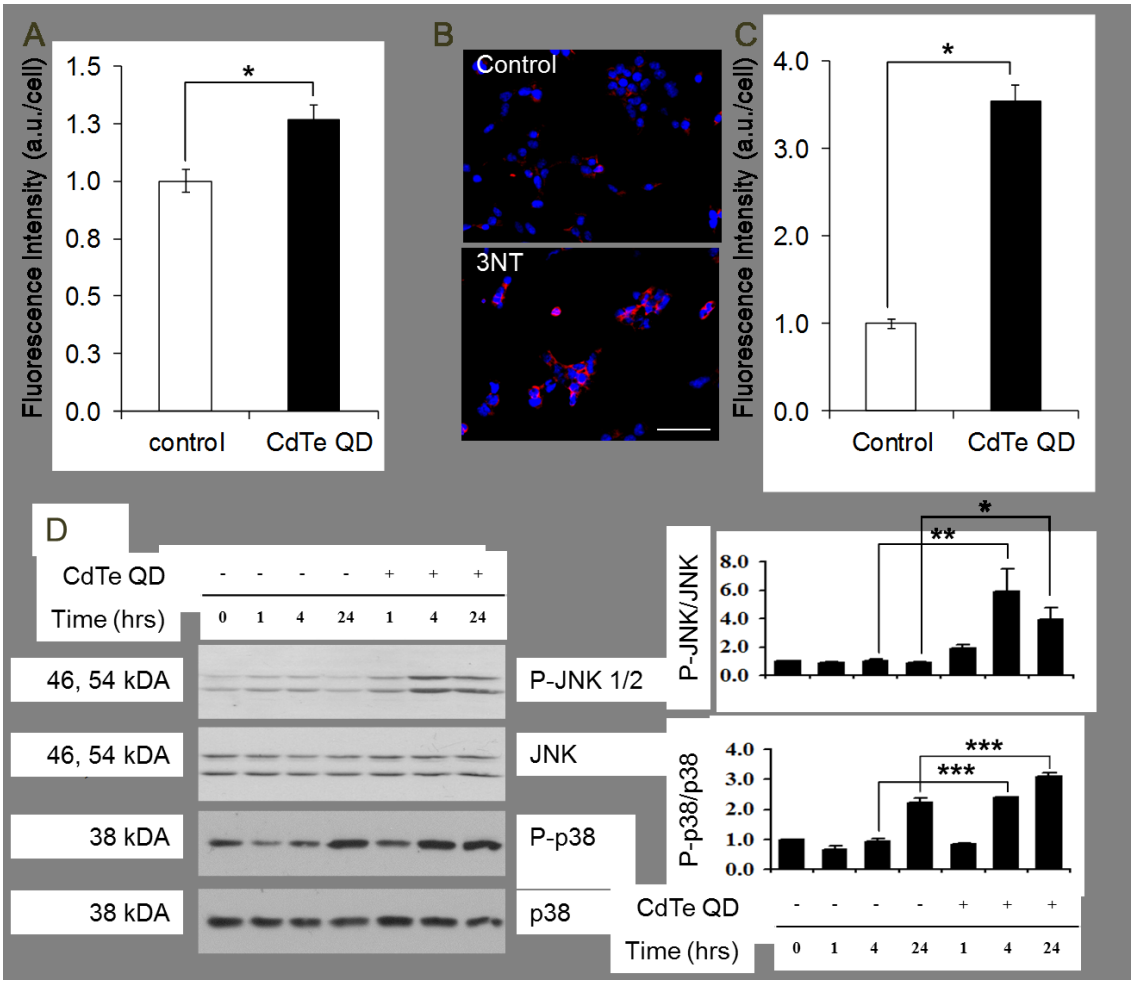
A
Fluorescence Intensity (a.u./cell)
1.5
1.3
1.0
0.8
0.5
0.3
0.0
*
control
CdTe QD
B
Control
3NT
C
Fluorescence Intensity (a.u./cell)
4.0
3.0
2.0
1.0
0.0
*
Control
CdTe QD
D
CdTe QD
- - - - + + +
Time (hrs)
0 1 4 24 1 4 24
46, 54 kDA
P-JNK 1/2
46, 54 kDA
JNK
38 kDA
P-p38
38 kDA
p38
P-JNK/JNK
8.0
6.0
4.0
2.0
0.0
*
**
P-p38/p38
4.0
3.0
2.0
1.0
0.0
***
***
CdTe QD
- - - - + + +
Time (hrs)
0 1 4 24 1 4 24

Figure 2.4. Exposure to CdTe QDs results in dynamic changes in the status of cellular organelles

A) Electron micrographs showing cells with normal nuclear membrane and mitochondria morphology (controls). Cells treated with CdTe QDs (20 nM; 24 hours) show abnormal mitochondria (black arrows) and increased presence of vacuoles and autophagosomes (white arrows). Representative pictures are from at least 3 independent experiments of triplicates. B) Cellular lysosomal content (green) was labeled with LysoTracker Green DND-26 (500 nM; 2 minutes) in cells treated with rapamycin (200 nM) and CdTe QDs (20 nM) for 1, 6 and 24 hours. Nuclei (blue) were labeled with Hoechst (10 μM; 30 minutes) and CdTe QDs are visible in red. Representative pictures are from at least 3 independent experiments of triplicates. Scale bars represent 20 μm. C) Intracellular LysoTracker Green DND-26 fluorescence intensity was quantified from fluorescent microscopy pictures. Data are presented as means ± SEM of three individual experiments of triplicates. Statistically significant differences from the control (untreated cells cultured in serum containing media) were tested by one sample t-test are indicated by *** $p < 0.001$

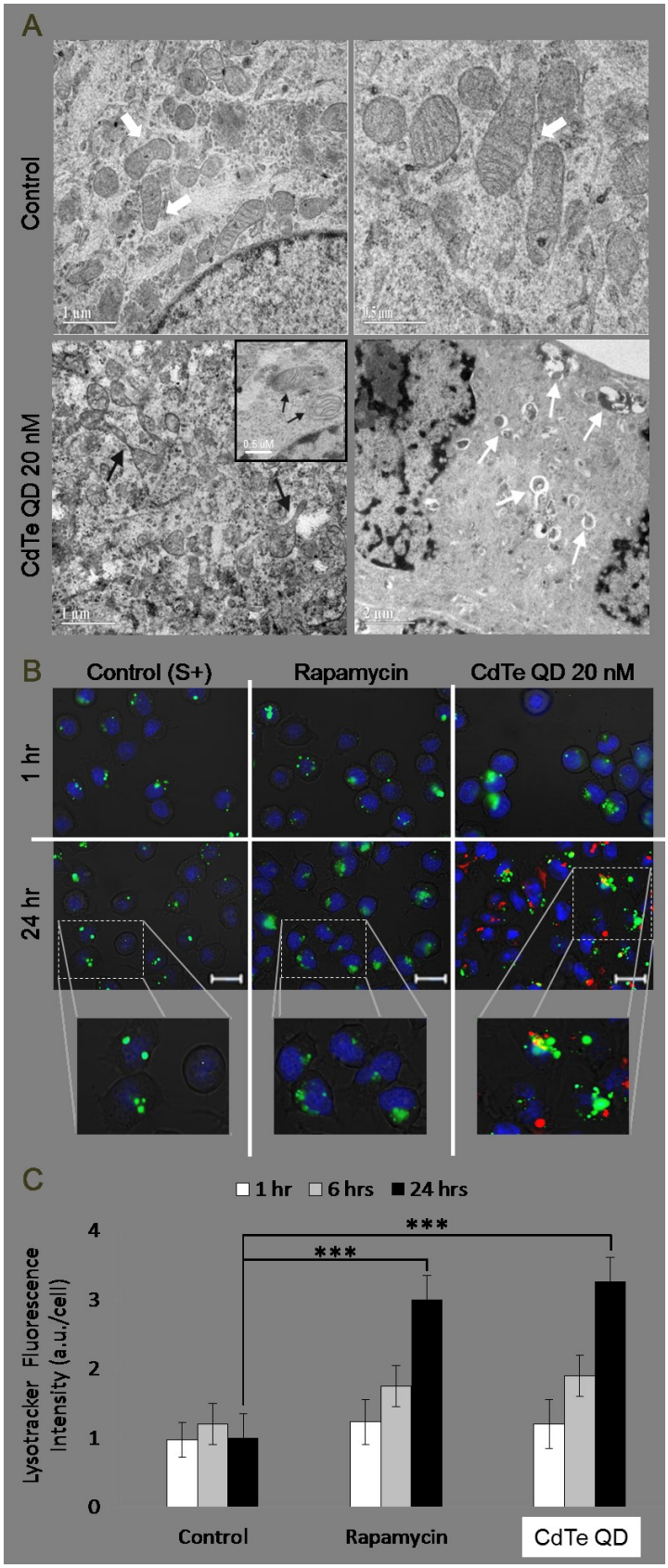
A
Control
CdTe QD 20 nM
1 μm
0.5 μm
0.5 μM
1 μm
2 μm
B
Control (S+)
Rapamycin
CdTe QD 20 nM
1 hr
24 hr
C
1 hr
6 hrs
24 hrs
Lysotracker Fluorescence Intensity (a.u./cell)
0
1
2
3
4
***
***
Control
Rapamycin
CdTe QD

Figure 2.5. Exposure to CdTe QDs leads to the progressive activation of transcription factor EB

A) LAMP1 expression (green) was assessed using a primary anti-LAMP1 antibody. Cells were treated with rapamycin (200 nM) and CdTe QDs (20 nM) for 6 hours. Nuclei (blue) were labeled with Hoechst (10 μM; 30 minutes) and CdTe QDs are visible in red. Representative pictures are from at least 3 independent experiments of triplicates. Scale bars represent 20 μm. B) LAMP1 fluorescence intensity was quantified from fluorescent microscopy pictures. Data are presented as means ± SEM of three individual experiments of triplicates. Statistically significant differences from the control were tested by one sample t-test are indicated by *** $p < 0.001$ C) TFEB subcellular localization (green) was assessed using a primary anti-TFEB antibody in cells treated with CdTe QDs (20 nM) for 1, 6 and 24 hours. Nuclei (blue) were labeled with Hoechst (10 μM; 30 minutes) and CdTe QDs are visible in red. Representative pictures are from at least 3 independent experiments of triplicates. Scale bars represent 20 μm. D) The nuclear/cytosolic TFEB subcellular location was quantified from fluorescent microscopy pictures. Data are presented as means ± SEM of three individual experiments of triplicates. Statistically significant differences from the control were tested by one sample t-test are indicated by *** $p < 0.001$

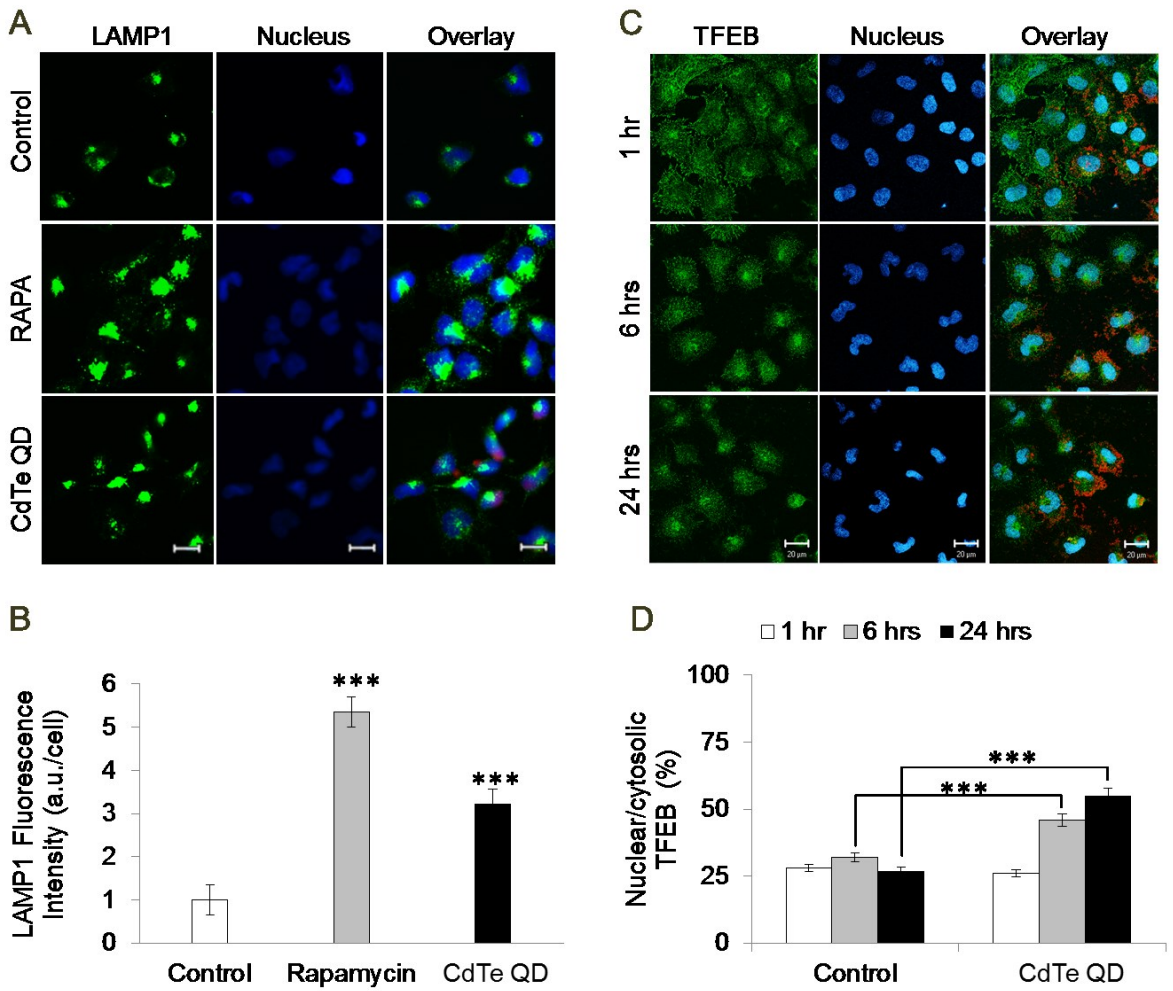
A
LAMP1
Nucleus
Overlay
Control
RAPA
CdTe QD
C
TFEB
Nucleus
Overlay
1 hr
6 hrs
24 hrs
B
LAMP1 Fluorescence Intensity (a.u./cell)
0
1
2
3
4
5
6
***
***
Control
Rapamycin
CdTe QD
D
1 hr
6 hrs
24 hrs
Nuclear/cytosolic TFEB (%)
0
25
50
75
100
***
***
Control
CdTe QD

Figure 2.6. Schematic outlining the proposed interactions between the antioxidant and lysosomal adaptive cellular response to oxidative stress

Activation of MAPKs leads to the expression of antioxidant genes and the strengthening of the antioxidant shield, which serves to maintain redox homeostasis. Activation of TFEB leads to enhanced formation and stability of lysosomes, essential for autophagy and endocytosis function. Together, these processes contribute to the adaptive cellular response to oxidative stress.

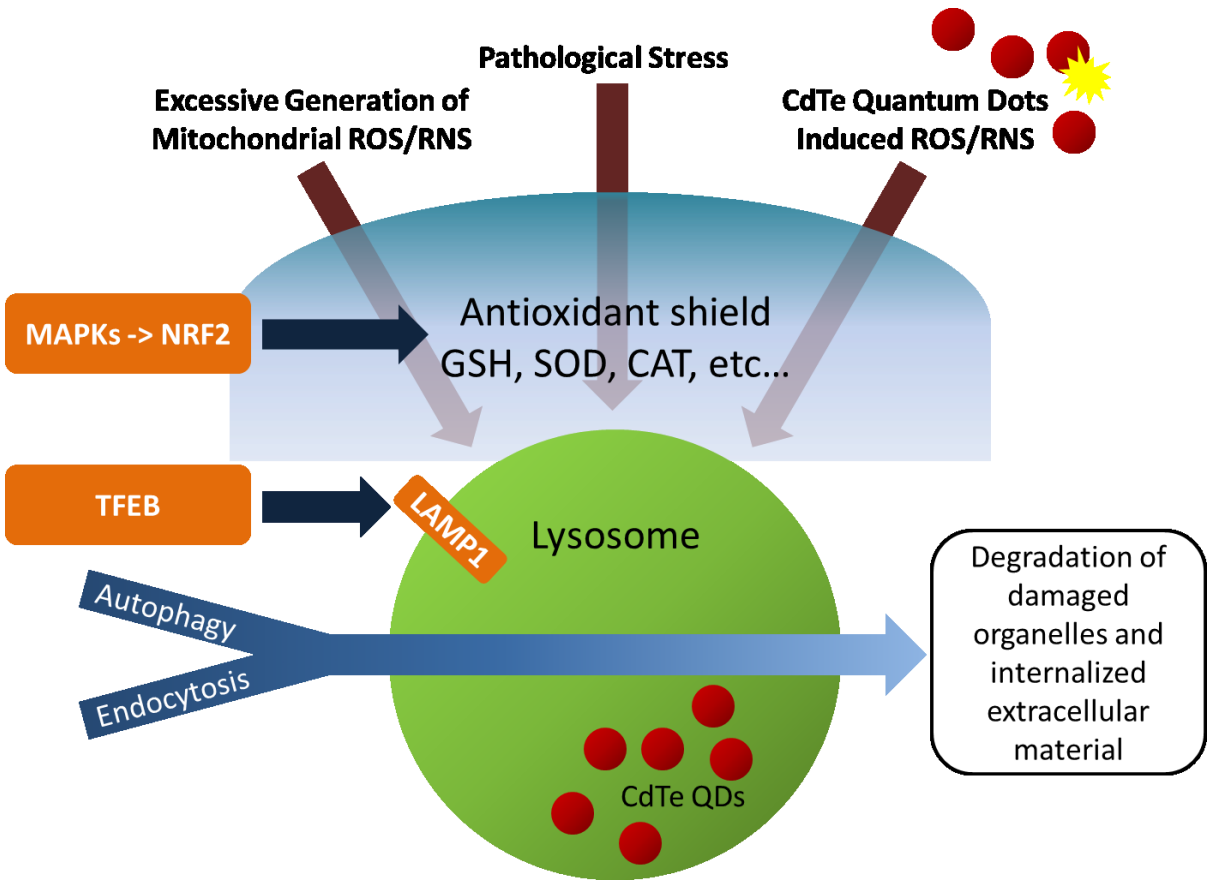

Figure S2.1. QD concentration correlates well with total cadmium content from stock solutions

A) The cadmium content of uncapped CdTe QDs and capped CdSe/ZnS QDs (4, 20, 40 nM) was determined using flame atomic absorption (FAA). QDs were dissolved in serum free media. Statistically significant differences were tested by independent t-test and are indicated by *** $p < 0.001$. Data are presented as means ± SEM of three individual experiments of triplicates.

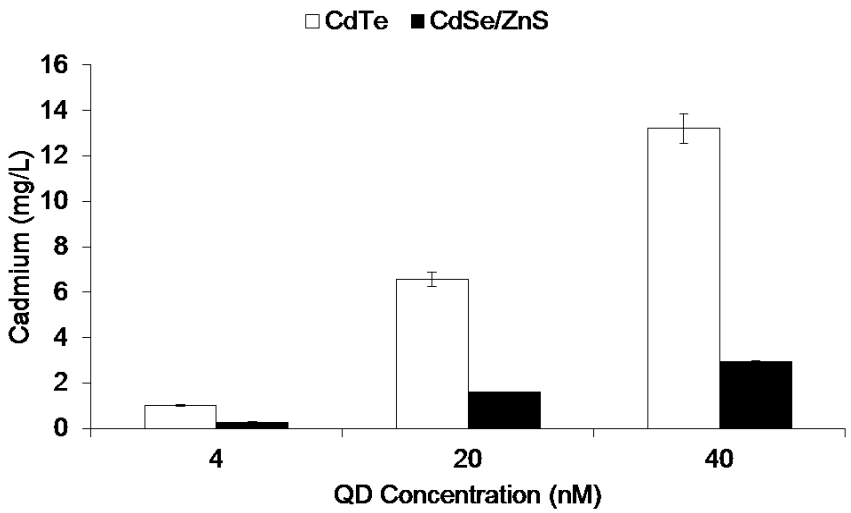

Figure S2.2.QDs form aggregates in the presence of biological media

The aggregation status of uncapped CdTe QDs (100 nM) was measured using dynamic light scattering (DLS) and data is expressed as A) number weighted and B) mass weighted distribution.

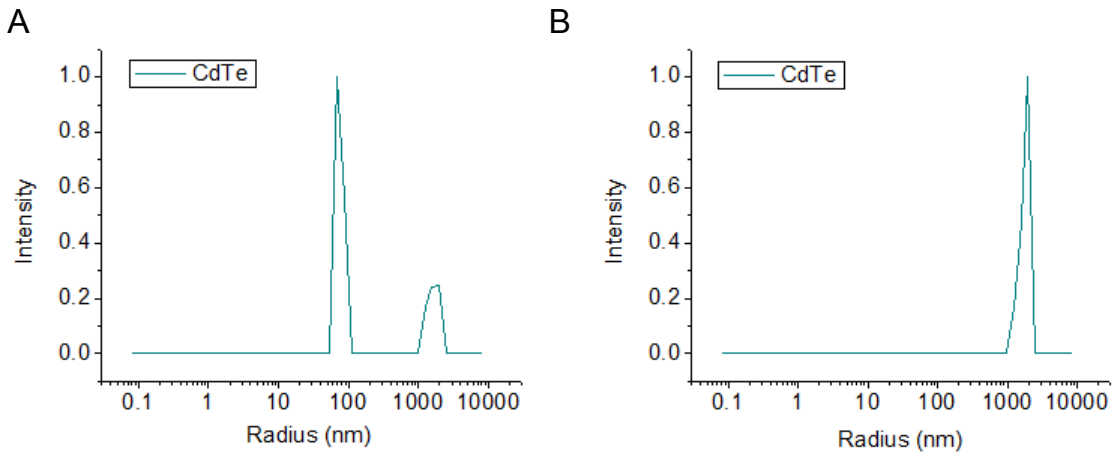

Figure S2.3. Fluorescence based assessment of intracellular glutathione correlates well with biochemical quantification

A) The relative fluorescent intensity of the mCBi-GS adduct was determined spectrofluoremetrically and compared to the biochemical tGSH determination (Figure 2.1B) in live cells treated with CdTe nanoparticles (4, 20 nM; 24 hours). Data are presented as means ± SEM of three individual experiments of triplicates.

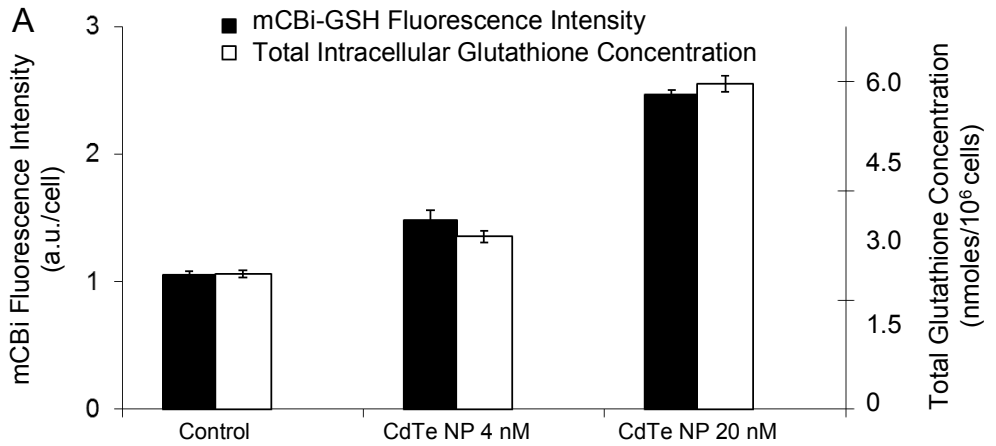

Connecting text

Early studies using nanoparticles with controlled surface charge, size or shape have begun to elucidate interactions at the nano-bio interface. For example, it was shown that increased QD uptake is correlated with increased cytotoxicity (Cho, Maysinger et al. 2007). However, it is still unclear how nanoparticle surface properties influence cell uptake and elimination mechanisms.

In Chapter 2, we showed that exposure to uncapped CdTe QDs resulted in the formation of reactive oxygen and nitrogen species (ROS/RNS). For cells with sufficient antioxidant defenses, cellular adaptation mechanisms could be activated, leading to cell survival. Cellular adaption involved recruitment of key redox sensitive transcription factors following QD internalization.

In Chapter 3, we investigated the role of surface charge on nanoparticle internalization using CdSe QDs with the same core composition and size (4.8 nm), but varied surface functionalization. Four small ligands: mercaptopropionic acid (MPA), dihydrolipoic acid (DHLA), L-cysteine (CYS) or cysteamine (CA) were non-covalently bound to the QD surface. These small ligands were of comparable size, but imparted varied surface properties. QDs capped with MPA and DHLA had a negative charge, those capped with CA had a positive charge while QDs capped with CYS were zwitterionic. We investigated ligand specific and non-specific QD uptake in two human cell lines, Hek 293 (kidney) and Hep G2 (liver). Internalization mechanisms were investigated using pharmacological inhibitors: methyl β-cyclodextrin (inhibitor of lipid raft mediate uptake) and threo-β-hydroxyaspartate (inhibitor of cysteine transporter). Results from these studies showed that nanoparticle toxicity could be reduced by altering the surface functional groups of QDs. More importantly, we found that QDs were differentially internalized based on their surface ligand and charge. Results from these studies show a strong dependence between the properties of QD-associated small ligands and modes of uptake in human cells.

Chapter 3. Short Ligands Affect Modes of QD Uptake and Elimination in Human Cells

Al-Hajaj N*, Moquin A*, Neibert K*, Soliman G, Winnik F, Maysinger D.

ACS Nano. 2011, 5(6), 4909-4918

3.1. Abstract

In order to better understand nanoparticle uptake and elimination mechanisms, we designed a controlled set of small, highly fluorescent quantum dots (QDs) with nearly identical hydrodynamic size (8-10 nm), but with varied short ligand surface functionalization. The properties of functionalized QDs and their modes of uptake and elimination were investigated systematically by asymmetrical flow field-flow fractionation (AF4), confocal fluorescence microscopy, flow cytometry (FACS) and flame atomic absorption (FAA). Using specific inhibitors of cellular uptake and elimination machinery in human embryonic kidney cells (Hek 293) and human hepatocellular carcinoma cells (Hep G2), we showed that QDs of the same size but with different surface properties were predominantly taken up through lipid raft-mediated endocytosis, however, to significantly different extents. The latter observation infers the contribution of additional, modes of QD internalization, which includes X-AG cysteine transporter for cysteine functionalized QDs (QD-CYS). We also investigated putative modes of QD elimination and established the contribution of P-glycoprotein (P-gp) transporter in QD efflux. Results from these studies show a strong dependence between the properties of QD-associated small ligands and modes of uptake/elimination in human cells.

3.1.1 Keywords

Quantum dot, human Hep G2, QD uptake, QD elimination, p-glycoprotein

3.2. Introduction

Semiconductor nanocrystals, or quantum dots (QDs), are powerful and versatile fluorescent probes for biomedical imaging and diagnostics, particularly for long-term, multiplexed, and quantitative detection (Goddette and Frieden 1986, Chan, Maxwell et al. 2002, Chithrani and Chan 2007, Guo, Huang et al. 2010). The wide adoption of QDs as imaging tools in biology and medical research stems from the fact that they readily penetrate into cells without losing their unique photophysical properties, in particular their size-tunable emission, high quantum yield, broad absorption spectrum, and resistance to photobleaching

(Panyam, Zhou et al. 2002, Wang, Gao et al. 2010, Stern, Adiseshaiah et al. 2012). Although successful application of *in vivo* imaging of QDs has been demonstrated in several animal models, their transition in human medicine is hampered by issues related to the safety of human exposure to QDs since they generally contain highly toxic elements, such as cadmium, tellurium and selenium (Lovric, Cho et al. 2005, Chang, Pinaud et al. 2008, Chazotte 2011). One fears that upon long term sequestration in the liver, kidney and other organs, QDs will gradually lose their protective cap causing toxic core components to be progressively released (Iversen, Frerker et al. 2012). The ambivalence surrounding the potential use of QDs in nanomedicine has prompted intensive efforts directed towards the development of cadmium-free and alternative "safe" QDs (Iversen, Frerker et al. 2012). Concerns over QD accumulation *in vivo* have additionally stimulated research aimed at elucidating the processes associated not only with their cellular uptake and intracellular fate, but also with their eventual exit from the cells (Meng, Liong et al. 2010, Moquin, Hutter et al. 2013).

Recent investigations into the nature of the relationship between cellular uptake and physicochemical properties of QDs indicate that in the absence of specific interactions, the entry of nanoparticles into cells and their cytosolic access are primarily governed by three factors: size, shape, and surface charge (Gaumet, Vargas et al. 2008, Gratton, Ropp et al. 2008, Jiang, Kim et al. 2008, Johnston, Semmler-Behnke et al. 2010, Verma and Stellacci 2010). Surface properties at the nano-scale strongly influence not only specific modes of internalization and subsequent subcellular localization but molecular and biological processes, including cell division and differentiation, ultimately dictating cellular fate (Jiang, Oberdorster et al. 2009, Variola, Brunski et al. 2011, Zhao, Zhao et al. 2011). It was also shown that QD internalization can only occur if the concentration of QDs at the plasma membrane is sufficient (Gaumet, Vargas et al. 2008). The initial contact of QDs with cells, namely their interactions with the lipid bilayer and the surface proteoglycans, are controlled by the QD charge and concentration (Nel, Madler et al. 2009). Since the proteoglycans are negatively charged, positively charged QDs are attracted towards the cell membrane by electrostatic interactions and accumulate readily at the plasma membrane, permitting internalization. Neutral or negatively charged QDs are only weakly bound to the lipid bilayer

and thus are less readily taken up (Xiao, Forry et al. 2010). Given their size (4 to 5 nm in radius), QDs cross the plasma membrane primarily through pinocytosis, a distinct set of endocytosis mechanisms, chiefly responsible for the uptake of cell nutrients and other small particles (< 100 nm). The contribution of each endocytosis pathway can be assessed using inhibitors that selectively suppress specific internalization processes (Zhang and Monteiro-Riviere 2009, Xiao, Forry et al. 2010, Zamborini, Bao et al. 2012). Many studies aimed at tracking the fate of internalized QDs by fluorescence imaging have revealed the preferential localization of QDs into lysosomes, a common terminus of several endocytic pathways. During uptake, QDs are internalized into endocytic vesicles which fuse with early endosomes, and subsequently with late endosomes and lysosomes (Stern, Zolnik et al. 2008, Behrendt, Sandros et al. 2009). These observations, together with evidence from inhibitor-based mechanistic studies, suggest that QDs are primarily internalized *via* lipid raft/caveolae and clathrin-dependent endocytosis (Zhang and Monteiro-Riviere 2009). Early endosomes which contain QDs have also been observed to traffic back to the plasma membrane in a process which likely contributes to the QDs exocytosis (Bouby, Geckeis et al. 2008). There is no consensus as yet on which of the specific processes leads to cytosolic release of QDs and on the possible involvement of exocytic mediators.

We report here the results of a mechanistic study of the cellular entry/exit pathways of QDs having the same CdSe(CdZnS) core coated with one of four different short ligands, such that their hydrodynamic diameters were nearly identical (8-10 nm). Cellular uptake experiments were performed in two human model cell lines: human embryonic kidney cells (Hek 293) and human hepatocellular carcinoma cells (Hep G2). These cell lines are particularly relevant to internalization and exocytosis studies as injected QDs tend to accumulate preferentially in the kidneys and liver of treated animals (Moquin, Winnik et al. 2013). QD internalization was observed by confocal fluorescence microscopy. The extent of QD uptake was estimated by plate-based fluorometry, flow cytometry (FACS), and analysis of intracellular cadmium concentrations using flame atomic absorption (FAA). To investigate the role of specific modes of QD entry and export, experiments were carried out in the presence or absence of a number of pharmacological inhibitors and activators. We focused on QD functionalized with cysteine ligands (QD-CYS) and compared their internalization *via*

the X-AG cysteine transport system and lipid rafts, with three other QDs with mercapto derivatives (Choi, Liu et al. 2007, Mullen, Fang et al. 2010, Moquin and Winnik 2012). To investigate the role of lipid raft-mediated endocytosis, methyl β-cyclodextrin (MBCD) was used due to its tendency to sequester cholesterol from the plasma membrane, thus disrupting the structure and function of lipid rafts (Nativo, Prior et al. 2008). In view of its high rate and broad substrate range, the P-glycoprotein (P-gp) transporter is likely to be involved in QD elimination (Gaumet, Vargas et al. 2008). To assess the potential role of P-gp in QD elimination, we used two pharmacological agents, elacridar and rifampin, that are, respectively, a P-gp inhibitor and a P-gp inducer (Aurell and Wistrom 1998, Hassellov, Readman et al. 2008). The types of QDs employed and the uptake/ elimination mechanisms probed are depicted schematically in Figure 3.1. This study has uncovered significant differences in the extent and mode of QD uptake/elimination, depending on the surface properties of the QD types tested. It also provides strong evidence for the involvement of the P-gp transporter in the release of QDs from cells.

3.3. Results and discussion

3.3.1. Preparation and characterization of the QDs (Figure 3.1 and Table 3.1).

All QDs were synthesized from a single batch of hydrophobic CdSe(CdZnS) nanoparticles with an average radius of 2.4 nm determined by transmission electron microscopy (TEM) (Figure 3.2A, left panel), by ligand exchange using either mercaptopropionic acid (MPA), dihydrolipoic acid (DHLA), L-cysteine (CYS) or cysteamine (CA) (Chan and Nie 1998, Clapp, Goldman et al. 2006).

Anionic ligands (MPA, DHLA) were efficient in keeping the QDs suspended within physiological pH and salt concentrations (Table S3.1.). QD-MPA and QD-DHLA were stable under these conditions for 7 days or more, even in mildly acidic media. However, in alkaline DMEM conditions, these QDs were unstable and rapidly aggregated due to high osmolarity and the presence of amino acids, salts *etc*.. The cysteine coating was not as efficient to stabilize the QDs: QD-CYS tend to aggregate after several (~ 4-5) days in conditions of

physiological pH and ionic strength. QD-CA on the other hand were very unstable within pH 4.22-8.6 and aggregated rapidly in the presence of phosphate ions. QD-CAs are only stable in deionized water, any salt in the solution causes them to aggregate over a few hours.

The zeta potential values for QD-MPA, QD-DHLA and QD-CYS (in Milli-Q water) are within -32.8 to -35.8 mV (Table S3.1.). The only positively charged QDs are QD-CA (zeta potential 48.25 mV). Zeta potential measurements confirmed that at physiological pH (7.4), QD-MPA, QD-DHLA, and QD-CYS are negatively charged, whereas QD-CA have a positive surface charge (Table 3.1.). When the zeta-potential of the particle falls below a threshold value, the surface charges are no longer strong enough to keep the particles from aggregating and precipitating out of solution. The hydrodynamic radius of the QDs, determined by dynamic light scattering (DLS), is on the order of 4 nm (Figure S3.1.), independently of the surface ligand (Table 3.1.).

The QDs were analyzed also by asymmetrical flow field-flow fractionation (AF4) chromatography coupled with UV-Visible, fluorescence, multi-angle light scattering (MALS) and dynamic light scattering detectors (DLS) (Figure S3.2.). Separation of nanoparticles by AF4 occurs according to their size by virtue of their diffusion coefficients in a very thin open channel (Florence 1997). Eluting nanoparticles are subjected to a longitudinal carrier flow and an applied field that acts perpendicularly to the length of the channel and causes particles to move towards the accumulation wall. Smaller particles are not affected to the same extent as larger particles. They travel faster than larger particles, resulting in size fractionation of the sample. The eluting fractions are monitored by a UV/Vis detector that responds to particle concentration and by a combination of MALS and DLS detectors that yield the particles size (Fraunhofer and Winter 2004). This technique provides the true size distribution of nanoparticles in aqueous media, unlike “batch-mode” DLS which tends to be biased towards the strongly scattering larger particles. The elution profile of a sample of QD-CA monitored by UV/Vis detection (λ = 300 nm) is presented in Figure 3.2C (short elution times) and Figure 3.2D (long elution times). The most intense band, with an elution time of 4 min, corresponds to the elution of QDs, whereas the weak band between 20 and 26 min is attributed to QD aggregates. Comparison of the areas of the two eluting bands reveals that the

fraction of aggregated QDs represents less than 1 % of the total QD concentration (Table 3.1.). The elution of QDs was monitored also by MALS and DLS detectors, which yield, respectively, the Rayleigh ratio and the hydrodynamic radius (Rh) of the eluting fractions. The dots in Figures 3.2C and 3.2D correspond, respectively, to the Rh values of isolated QD-CA nanoparticles and QD-CA aggregates. They were calculated from the diffusion constants extracted from the DLS auto-correlated functions determined for each fraction. Data from the fractograms were converted to size distributions represented as plots of the differential weight fractions as a function of Rh (Figure S3.2.). The size distributions obtained from AF4data are narrow in all cases and centered between 4 and 5 nm, depending on the sample. Based on these results, we will assume in the following sections that, in terms of cellular trafficking, the four QD samples have identical size. Such an assumption would have been less justified on the basis of batch-mode DLS data only, since size distributions recorded under these conditions are significantly broader (Figure S3.1.).

3.3.2. Uptake of QDs by human kidney and liver cells

QD uptake in human kidney (Hek 293) and liver (Hep G2) cells was assessed *spectrofluorometrically* (Ex/em 355/612 nm) as a function of time upon exposure to QDs (100 nM). Prior to analysis, cells were washed with acidified buffer solution (phosphate buffer saline (PBS, pH 5.5) for 5 minutes in order to disrupt weak electrostatic interactions between charged QDs and the plasma membrane, and to remove loosely bound and non-internalized QDs from the cell surface (Illum 2000). QD uptake in both cell types increased steadily for 6 hours. Then it remained constant, depending on the cell and QD types (Figure 3.3A and 3.3B). The extent of uptake of positively charged QDs (QD-CA) was significantly higher than that of the neutral (QD-CYS) and negatively (QD-MPA and QD-DHLA) charged QDs ($p<0.001$). A similar uptake pattern was found in both cell types at all time points examined. QDs were gradually eliminated over time. There was no significant cytotoxicity of QDs with different ligands within 24 hours exposure in Hek 293 and Hep G2 cell lines (Figure S3.3.).

Intracellular cadmium concentrations in cells exposed to QDs were determined by quantitative flame atomic absorption (FAA). Cells exposed to QDs (100 nM) had significantly higher intracellular cadmium concentration than those treated with comparable cadmium concentrations in $CdCl_2$ (23.66 μM). For example, Hek 293 cells exposed to QD or CdCl2 for 6 hours had intracellular cadmium concentration corresponding to 8.6 ± 0.5 μM and 0.4 ±0.4 μM, respectively ($p < 0.001$). These findings suggest that cadmium cations are either less effectively taken in or more rapidly eliminated from the kidney cells than QD (Figure S3.4.).

Determining factors influencing the rate and extent of nanoparticle internalization most likely depended on the physical and chemical surface properties, because the core of all four QD types was similar in size and composition. Interestingly, studies by Stellacci's group show that the small ligand, 11-mercapto-1-undecanosulphonate, arranged in sub-nanometer striations, enter the cells through different routes then those with the same ligand, but randomly distributed on the gold nanoparticle surface (Verma, Uzun et al. 2008).

To exclude possible artifacts resulting from non-specific association of the QDs with the cell membrane, we examined the QD localization within live cells using confocal fluorescence microscopy. To facilitate visualization, the plasma membrane and the nucleus were labeled with PHK67 (green) and Hoechst 33342 (blue), respectively. QDs were detected readily by their bright red emission. Representative micrographs recorded upon one hour treatment of human kidney cells (Hek 293) with QD-CA or QD-DHLA are presented in Figure 3.3C. Both types of QDs were localized predominantly within the cytosol (solid arrow). A small fraction of QD-CA appeared as clusters adhered to the plasma membrane (dashed arrow). These clusters may originate from the small fraction of QD aggregates present in the QD suspension (Table 3.1 and Figure 3.1) or because of the association of individual QDs on the plasma membrane surface (Mistry, Stolnik et al. 2009). Due to their size, such aggregates are expected to remain loosely associated with the plasma membrane or enter non-phagocytic cells rather slowly.

3.3.3. Mechanisms involved in QD internalization in Hek 293 and Hep G2 cells

The accumulation of QDs in lysosomal compartments is usually attributed to a mechanism (Figure 3.1.) involving QDs internalization by endocytosis, trafficking of the QDs from the plasma membrane by endocytic vesicles, fusion of the vesicles into early endosomes, then late endosomes, and finally fusion with lysosomes (Jiang, Rocker et al. 2010). To gain further insight into the mechanisms responsible for the transport of the QDs through the cell membrane, we examined the effect of temperature (Figure 3.3D) and of pharmacological inhibitors (Figures 3.4. and 3.5.). QD cellular uptake was determined experimentally by fluorometric measurements. The uptake of all types of QDs by either Hek 293 cells or Hep G2 cells was significantly reduced when the cells were kept at 4 ºC, rather than at 37 ^{o}C (Figure 3.3D). The strongest uptake inhibition (~85 %) was observed for QD-CYS. Incubation of cells at 4 ºC is believed to inhibit the ATP synthase complex, resulting in a reduction of the synthesis of the ATP required for the functioning of the cellular active transport machinery (Brown and Neher 2012). Exposure to low temperature also decreases the fluidity of the lipid bilayer, resulting in a tighter packing of the lipid rafts and other membrane-embedded cholesterol- rich structures (Neher, Neniskyte et al. 2012). Incubation of cells at low temperature causes a flattening of caveolae and a blockage of invagination clathrin-coated pits. These processes effectively inhibit pinocytosis, but their detailed mechanisms are still unclear (Hornung, Bauernfeind et al. 2008, Neher, Neniskyte et al. 2012).

Intrigued by the exceptionally strong inhibition of QD-CYS uptake in cells incubated at 4 ºC, we undertook a systematic study of two specific active transport mechanisms available for the transport of QD-CYS through the membrane: lipid rafts and the primary sodium dependent cysteine transporter (X-AG transport system) (see Figure 3.1). First, to examine the role of lipid-rafts in QD uptake, cells were treated for 30 min with methyl β-cyclodextrin (MBCD, 10 mM), washed, and thereafter incubated with QDs (100 nM) for 3 hours. The MBCD pretreatment of the cells, which depletes their membrane cholesterol and disrupts lipid rafts, led to a significant inhibition of QD internalization in Hek 293 cells and Hep G2 cells, compared with cells treated with QDs, but without MBCD (Figure 3.4A). Furthermore, the extent of QD uptake inhibition depended on the QD surface chemistry and

on the cell type. For example, the uptake inhibition of QD-CYS was much more pronounced in Hek 293 cells than in Hep G2 cells, whereas, in the case of QD-DHLA, the entry was reduced to the greatest extent (46 ± 4 %) in Hep G2 cells, compared to Hek 293 (20.2 ± 3.2 %). To test the hypothesis that QDs form specific supramolecular complexes with MBCD, we employed AF4technique. We selected AF4 with MALS/DLS/UV-Vis detection due to its sensitivity to small changes in nanoparticle size. AF4 elution profiles of suspensions of QDs preincubated with MCBD are shown in Figure S3.5, C and D. A shift of the elution peak, corresponding to an increase in Rh of about 1 nm, was observed in pretreated QD-CYS, but not in the case of QD-DHLA. This suggests that complexation occurred between MBCD and QD-CYS, but not with QD-DHLA. It is not clear whether or not QD-CYS/MBCD complexation occurred in the living cells, after removal of the excess MBCD prior to QD treatment. To elucidate the mechanisms involved in lipid raft mediated QD uptake, additional experiments should be performed, such as time lapse measurements of QD-lipid raft interactions and experiments using lipid raft interfering agents other than MBCD. Multiple knockdown and mutation experiments of proteins involved in signaling steps within and downstream from the lipid rafts warrant further investigations to clarify the role of individual components implicated in QD-lipid raft interactions and internalization process. The structural and functional role of lipid rafts and caveolin in endocytosis of small molecules was recently discussed and some common mechanisms were proposed (Lambeth 2004, West, Brodsky et al. 2011).

Cysteine, the ligand on the surface of QD-CYS, has a specific transport machinery, the primary sodium dependent cysteine transporter (X-AG transport system), in both model cell lines selected in this study. Threo-β-hydroxyaspartate (THA), an inhibitor of the X-AG transporter, is a substrate for cysteine, glutamate and aspartate (Vallhov, Qin et al. 2006). We selected THA as a competitive inhibitor of QD-CYS uptake. Hek 293 and Hep G2 cells were treated with THA (5 mM, 1 hour), prior to incubation of QD-CYS (100 nM, 3 hours) (Figure 3.4B). Under these conditions the uptake of QD-CYS was significantly inhibited in Hek 293 cells (35 ± 4 %; ***$p<0.001$) and in Hep G2 cells (48 ± 6 %; ***$p<0.001$). To confirm that the cysteine transporter is indeed implicated in QD-CYS internalization, competition experiments with free ligand were performed. Cells were co-treated with equal amount of

D,L-cysteine (0.1 mM) or excess (1 mM and 2 mM) and QD-CYS (100 nM, 15 minutes) (Figure 3.4C). Free D,L-cysteine effectively competed with the uptake of QD-CYS in both cell lines, significantly inhibiting internalization in Hek 293 cells (42 ± 2 %; ***$p<0.001$) and Hep G2 cells (45 ± 3 %; ***$p<0.001$) cells. Taken together, these observations indicate that the X-AG active cysteine transport contributes to the internalization of QD-CYS.

To complement the results from the *spectrofluorometric* determinations, we performed flow cytometry (FACS) (Figure 3.4D). Following exposure to QD-CYS (100 nM, 3 hours, 37 ^{o}C, no pretreatment, red lines), FACS histograms revealed a large population of highly fluorescent cells. A decrease of the incubation temperature from 37 ºC to 4 ºC or treatment with THA significantly reduced the population of fluorescent cells containing QD-CYS revealing three almost overlapping peaks with significantly lower mean fluorescence intensities ($p<0.001$).

3.3.4. Elimination of multifunctional QDs and the involvement of P-glycoprotein

The efflux of QD-CYS and QD-CA from Hek 293 and Hep G2 cells was measured after a 3-hour incubation of the cells with QDs (100 nM), followed by aspiration of the cell medium and replacement with fresh medium. The percentages of QD efflux after 1, 3 and 6 hrs for each cell/QD pair are presented in Figure 3.5A-B. Significant differences in the fraction of exported QDs were detected depending on the cell type and on the QD surface chemistry. The efflux of QD-CA was greater from Hep G2 cells than from Hek 293 cells within the first 3 hours. After 6 hours, the percent of QDs left in the cells (~ 30 to 40 %) was similar in both cell lines. The efflux of QD-CYS increased with time for both cell lines, but the efflux from Hep G2 cells was inefficient: after 6 hours nearly 80 % of QD-CYS remained trapped within Hep G2 cells, compared to 20 % in the case of Hek 293. There are known differences in P-gp activity and expression in the kidneys and liver, pointing to a possible involvement of P-gp in QD elimination (Magalhaes, Lopes et al. 2007).

We used two pharmacological modulators of P-gp activity, rifampin and elacridar, to investigate the role of P-gp in QD elimination. Rifampin is a P-gp inducer known to increase

P-gp activity through mechanisms that are still poorly understood (Matheny, Ali et al. 2004). Elacridar is a competitive inhibitor of P-gp that competes with P-gp substrates such as azidopine and inhibits its action (Smulders, Kaiser et al. 2012). Pretreatment of cells with rifampin (50 nM) for 15 hours resulted in significantly increased QDs efflux in both cell lines (Figure 3.5C) while pretreatment of cells with elacridar (25 μM, 1 hour) caused a significant decrease in QD elimination from both cell lines (Figure 3.5D).

In summary, these studies show how the properties of four functionalized QDs with conserved size, but varied surface ligands are differently taken up and eliminated from the human kidney and liver cells. The QDs investigated in the present study were internalized by endocytosis involving lipid rafts in human liver Hep G2 cells and kidney Hek 293 cells. Ligand-specific uptake through the X-AG cysteine transporter was shown to be involved in QD-CYS internalization. In addition, the results suggest a role of P-gp transporter in QD elimination. Further studies are warranted to define signal transduction pathways involved in QD uptake and elimination.

3.4. Conclusion

Similar to the present studies, P-gp was previously proposed to have a role in the efflux of hydrophobic cytokines, steroid metabolites and lipids (Dobrovolskaia, Neun et al. 2010). P-gps have been found within lipid raft membrane domains. Cholesterol was established as a modulator of P-gp functions, suggesting that the elimination QDs is at least in part, dependent on the cholesterol content at the plasma membrane (Michaud, Halle et al. 2013). It would be interesting to extend these studies by employing cells with knockdowns of enzymes involved in cholesterol synthesis and metabolism as well as physical measurements of membrane stiffness to address the real contribution of cholesterol in QDs elimination by P-gp. We are currently exploring the role of different proteins involved in QD uptake and elimination by their systematic elimination or knock-down in different cell types.

3.5. Experimental section

3.5.1 Quantum dot preparation

All chemicals were purchased from Sigma-Aldrich unless mentioned otherwise. CdSe(CdZnS) core-shell QDs were synthesized and purified based on a method developed by Pons *et al*., with some modifications as indicated below (Demento, Eisenbarth et al. 2009). Preparation of precursors: Cadmium oxide (n moles) was mixed with tetradecylphosphonic acid (TDPA, 2.05n moles, from PCI Synthesis) in 1-octadecene (ODE) for a final cadmium concentration of 0.5 M. The mixture was heated to 300 ºC and kept at this temperature for 30 minutes under nitrogen yielding a white gel with a melting point around 200 ºC. Cadmium oleate $Cd(OA)_2$ and zinc oleate $Zn(OA)_2$ were prepared as 0.5 M stock solutions by heating cadmium oxide CdO and zinc oxide ZnO powders in oleic acid at 180 ºC and 240 ºC respectively, for 1 hour. The resulting solutions were then degassed at 80 ºC under vacuum. Stock solutions of trioctylphosphine sulfide (TOPS 0.5 M) and trioctylphosphine selenide (TOPSe 1.0 M) were prepared by dissolution of sulfur or selenium powders in trioctylphosphine (TOP) at ambient temperature under inert atmosphere, followed by vortex agitation and sonication until all the solid sulfur/selenium is dissolved.

The cadmium selenide CdSe cores were prepared by mixing of $Cd(TDPA)_2$ (3.2 g, 0.5 M) in ODE (~2 mmol Cd) with 2 mL of TOP, 2 mL of oleylamine and 5 mL of ODE in a three-neck flask. The preparation was degassed for 30 minutes under vacuum at 70-80 ºC and then heated to 280 ºC under nitrogen. TOPSe (150 µL, 1 M) was mixed in TOP (1 mL) and swiftly injected. The solution was then kept at 230 ºC for 10-20 min. Controlled QD growth was performed by drop wise injection of TOPSe 1 M at a 1.5 mL/h rate and the addition was stopped when the desired QD emission wavelength was obtained (~600 nm). The reaction was then cooled to room temperature. The mixture was precipitated in ethanol, and re-suspended in hexanes (9 mL) and TOP (1 mL). The shell of CdZnS was then added by mixing 2 mL of CdSe core solution with trioctylamine (5 mL), along with TOP (0.5 mL), $Cd(OA)_2$ (0.5 M, 0.6 mL) and $Zn(OA)_2$ (0.5 M, 1.2 mL). The mixture was first degassed at 70-80 ºC for 30 min under vacuum before being heated to 230 ºC. TOPS (0.5 M, 1 mL) solution was then injected drop-wise over a few minutes, and the reaction mixture was kept at 230 ºC for 30 min or until the desired wavelength was obtained. The luminescence intensity

increased significantly upon successful addition of the shell. The nanocrystals were precipitated twice in ethanol and re-suspended in 10 mL of chloroform.

3.5.2. QD surface modification

Mercaptopropionic acid or dihydrolipoic acid (excess of MPA/DHLA to QDs) was added to a suspension of CdSe(CdZnS) in chloroform. The resulting mixture was heated to 60 ºC for 1 hour. In the cases of L-cysteine and cysteamine the ligands were first solubilized in methanol, then mixed with the suspension of QDs and heated to 60 ºC for 1 hour. The QDs were separated by adding ethanol to the reaction mixture, followed by centrifugation for 5 min at 8000 rpm. A sodium hydroxide solution (0.01 M) was used to resuspend QDs with carboxylic groups (MPA, DHLA and cysteine) to improve their solubility. QD-CA was readily re-dispersible in deionized water. The precipitation step with ethanol was repeated followed by centrifugation for 5 min at 8000 rpm. The precipitates were kept and the ethanol was evaporated under vacuum before re-suspending the QDs in either deionized water or aqueous NaOH (0.01 M).

3.5.3. Zeta-potential measurements

The zeta potential of the different QDs dispersions was determined at 37 ºC by using a Malvern Zetasizer Nano ZS (Worcestershire, UK).

3.5.4. QD characterization by AF4/UV-VIS/MALS+DLS System

The principle of AF4 has been described elsewhere (Aubin-Tam and Hamad-Schifferli 2008). An asymmetrical flow field-flow fractionation (AF4) system (AF 2000 MT, Postnova Analytics) with a channel thickness of 350 μm fitted with either a special regenerated cellulose membrane (10 kDa cut-off, RC amphiphilic, Z-MEM-AQU-631, Postnova Analytics) for analysis of positively charged QD-CA or a special polyethylene sulfonate (10 kDa cut-off, PES, Z-MEM-AQU-615, Postnova Analytics) for negatively charged QDs (QD-MPA, QD-DHLA, QD-Cys). The AF4 was connected to an UV-VIS

variable wavelength spectrophotometric detector (SPD-20A, Postnova Analytics), a fluorescence detector (RF-10A_{XL}, Postnova Analytics), a multi-angle light scattering (MALS, Dawn Heleos 8+, Wyatt Technology, Santa Barbara, USA), and a quasi-elastic light scattering (QELS) detector (WyattQELS, Wyatt Technology) which is an add-on unit connected to the 90º angle of the MALS Dawn Heleos 8+ detector. The MALS detector is equipped with a K5 cell and a GaAs laser operating at 658 nm and takes measurements at 0.5 s intervals. Data collection and analysis were done using ASTRA version 5.3.4.20 (Wyatt Technology).

3.5.5. AF4 separation conditions

The carrier medium was prefiltered (0.1 μm) deionized water. After flow equilibration, the sample was injected with a flow rate of 0.2 mL/min (injection loop volume: 21.5 μL), followed by a 6 min-focusing with a cross-flow rate of 1.5 mL/min and a detector flow rate of 0.5 mL/min. Following a 1 minute transition, a two-step cross-flow rate gradient was initiated for the elution mode. The starting cross-flow rate (1.5 mL/min) was decreased linearly to 0 mL/min within 20 minutes. The cross-flow rate was then kept constant at 0.0 mL/min for 15 minutes to allow elution of any large aggregates. The detector flow rate was kept at 0.5 mL/min throughout. All the flow rates were controlled by the AF2000 Control software (Postnova Analytics, Salt Lake City, USA). The cross-flow was generated by Khloen syringe pumps (Postnova Analytics) while the axial and focusing flows were delivered by isocratic pumps (Postnova Analytics). The detection of the eluted fractionated QDs/aggregates was performed sequentially by UV absorbance at 300 nm, fluorescence with λ_{ex} 365 nm and λ_{em} 615 nm, MALS and DLS. Each fractogram presented is representative of a triplicate sample.

3.5.6. QDs characterization by UV-Vis and spectrofluorometry

Suspensions in water of hydrophilic QDs were diluted to reach an absorbance of the first excitonic peak (~ 590-600 nm) around 0.1. UV-Vis absorbance spectra were recorded on a Hewlett Packard Diode Array Spectrophotometer model 8452 A, between wavelengths of

200-800 nm. The empirical formulae proposed by Yu *et al*. were used to determine the diameter and extinction coefficient of cadmium selenide particles from the wavelength of their first excitonic peak (~590 nm) (Yu, Qu et al. 2003). The concentration was then determined using the Beer-Lambert law.
Fluorescence spectroscopy measurements were performed on an Eclipse instrument from Varian Cary. The fluorescence spectra were taken on samples diluted to an absorbance at the excitation wavelength inferior to 0.1 (monochromator excitation and emission slits were set at 5 nm, photomultiplier voltage was set at 600V).

3.5.7. Cell cultures and treatments

Human embryonic kidney cells (Hek 293) (CRL-1573, ATCC) and Human hepatocellular liver carcinoma cells (Hep G2) (HB-8065, ATCC) were cultured in Dulbecco's modified eagle medium (DMEM) (Gibco) containing 10 % and 5 % of fetal bovine serum (Gibco), respectively. Cells were maintained at 37 ºC, 5 % CO_2 in a humidified atmosphere. Culture media contained 1 % penicillin–streptomycin (Gibco). Cells were grown in serum containing media for 24 hours before cell treatments. Culture media was then aspirated, cells were washed with PBS (Gibco), QDs and/or drugs were added and incubated at 37 ºC for the times indicated. All inhibitors were from Sigma. And the following concentrations and times of incubations were applied: MBCD (10 mM, 30 mins), THA (5 mM, 1 hour), D,L-cysteine (0.1-2 mM, 15 mins), elacridar (50 nM, 1 hour), rifampin (25 µM, 15 hours). QDs (100 nM) were used in all experiments.

3.5.8. Fluorescence microscopy imaging

Cells were seeded at a density of 50,000 cells/well into 8-well chamber slides (Lab-Tek) and incubated with and without QDs (100 nM) for 1 hour. Following QD treatment, cells were washed and the nucleus and plasma membranes were stained with 10 µM Hoechst 33342 (Invitrogen) for 1 hour and 2 µM PHK67 (Sigma) for 10 minutes respectively. Fluorescence micrographs were acquired with a Leica DFC350FX monochrome digital camera connected to a Leica DMI4000B inverted fluorescence microscope using a DAPI-

1160A filter at 63x oil immersion (Leica). UV (Hoechst), GFP (PKH) and CYS3 (QD) filters were used and images were acquired and pseudo colored using Leica Application Suite (LAS).

3.5.9. Determination of QD uptake by spectrofluorometry

Cells were seeded at a density of 80,000 cells/well into 96 clear bottom, black well plate (Costar) and incubated with and without QDs (100 nM) for the times indicated. Following QD treatment, cells were washed and DMSO was added to each well. Mean fluorescent intensity was measured with a FLUOROstar Optima fluorometer (BGM, Labtech) with filters set to Ex/Em = 355/612 nm and employing 4x4 matrix well scanning.

3.5.10. Determination of QD efflux by spectrofluorometry

Cells were seeded at a density of 80,000 cells/well into 96 clear bottom, black well plate (Costar) and incubated with and without QDs (100 nM) for 3 hours. Following QD treatment, cells were washed and fresh serum free media was added to initiate efflux for the times indicated. Cells were then washed and DMSO was added to each well. Mean fluorescent intensity was measured with a FLUOROstar Optima fluorometer (BGM, Labtech) with filters set to Ex/Em = 355/612 nm and employing 4x4 matrix well scanning.

3.5.11. Determination of QD uptake by flame atomic adsorption (FAA)

Standard solutions were prepared by serial diluting 1000 ppm Cd certified standard (SCP Science). Deionized distilled water was used as the diluent and blank. The concentration of cadmium from standard QD solutions (0-100 nM) was measured with a flame atomic absorption spectrophotometer (Perkin Elmer AAS-700). Hek 293 cells were treated with equimolar concentrations of cadmium, in the form of QDs (100 nM) and $CdCl_2$ (23.66 μM). Following treatment, cells were washed and detached gently by adding PBS containing 0.5 % bovine serum albumin (BSA). Cell samples were counted, spun down and resuspended in deionized distilled water for cadmium determination.

3.5.12. Determination of QD uptake by flow cytometry (FACS)

Cells were seeded in 12-well plates (Millipore). Following QD treatment, cells were washed and detached gently by adding PBS containing 0.5 % BSA. Samples were collected and analyzed by FACSAria Sorter (BD Biosciences) using PE-Texas Red (Ex 594 nm) filter and expressed as mean fluorescence intensity (MFI).

3.5.13. Statistical analysis

Data were analyzed using SYSTAT 10 (SPSS). Statistical significance was determined by analysis of variance (ANOVA) followed by post hoc, Dunnett's test, independent *t*-test or by one sample *t*-test where specified. Significant differences are indicated by * $p<0.05$, ** $p<0.01$, and *** $p<0.001$.

Table 3.1. Physicochemical characteristics of quantum dots

	λ_{em} (nm)	R_{UV} of CdSe core (nm)	R_{TEM} of core-shell (nm)	Rh by AF4 (nm)	Zeta potential (mV)	% of aggregates
QD-MPA	620	2.4	2.0 ± 0.3	4.24 nm ± 0.23	-32.8	0.0 %
QD-DHLA	620	2.4	_	5.03 nm ± 0.31	-33.7	1.32 %
QD-CYS	620	2.4	_	4.41 nm ± 0.22	-35.8	0.08 %
QD-CA	617	2.4	_	3.99 nm ± 0.29	+41.9	0.22 %

Figure 3.1. Proposed modes of QD uptake and elimination

A) Schematic representation of the investigated modes of QD uptake and elimination by: (1) lipid raft endocytosis, (2) X-AG cysteine transporter and (3) P-glycoprotein (P-gp). Pharmacological inhibitors and activators are indicated. B) Diagram of representative QD structures and list of abbreviations used.

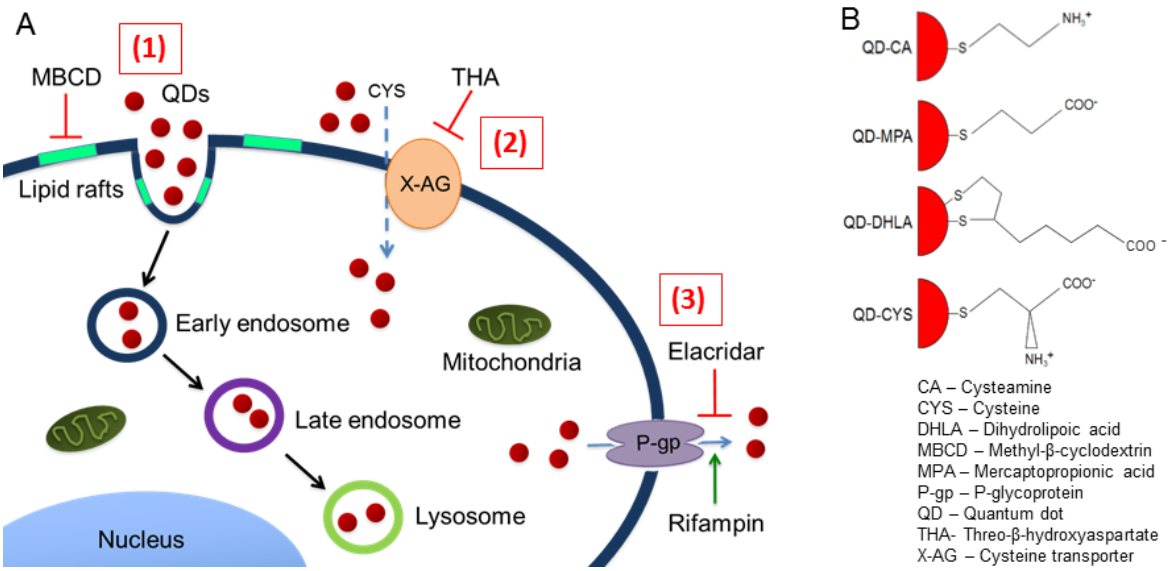

Figure 3.2. Characterization of QDs

A) Representative TEM micrographs of un-functionalized CdSe(CdZnS) QDs (left) and functionalized QD-MPA (right). Scale bars represent 5 and 20 nm, respectively. B) Normalized size distribution of QD-MPA compiled from several TEM images. C) Asymmetrical flow field-flow fractionation (AF4) fractograms of QD-CYS. D) Elution of aggregated QD-CYS.

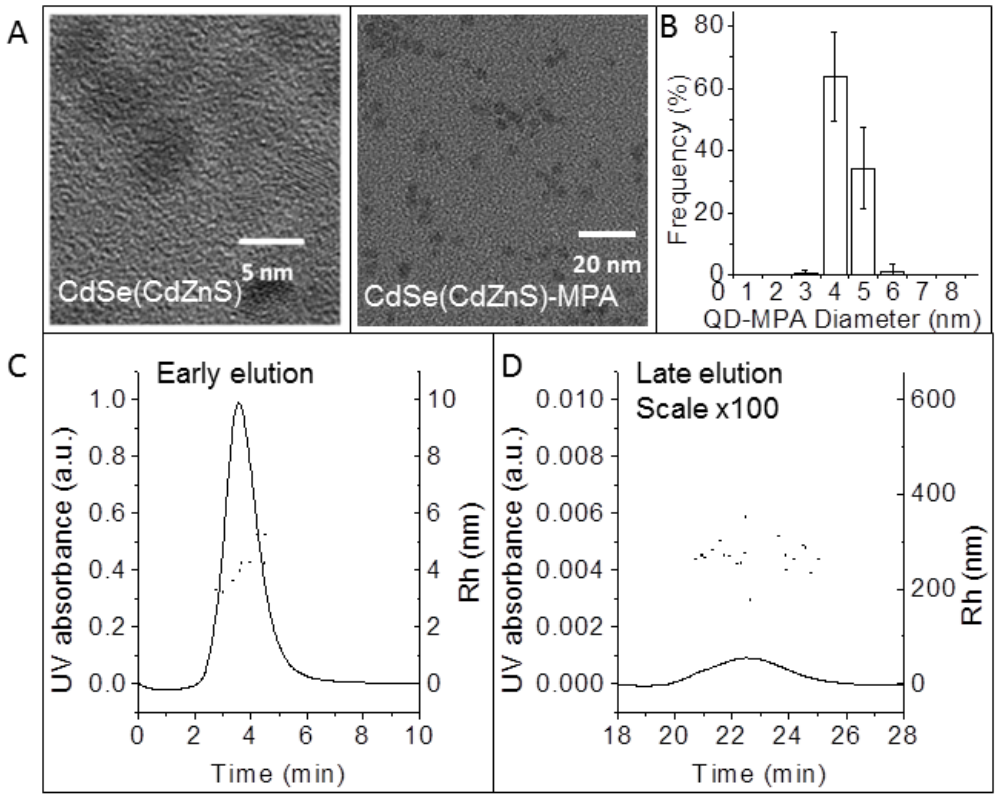

Figure 3.3 QD uptake by human kidney and liver cells

A) Hek 293 kidney cells and B) Hep G2 liver cells were exposed to QDs (100 nM, 1-24 hrs). Uptake values are the means ± SEM from three independent experiments expressed relative to the maximal QD-CA uptake given 1 a.u. (100 nM; 6 hrs). C) Confocal micrographs of QD-CA and QD-DHLA taken up by Hek 293 cells within 1 hour. QDs (red), N= nucleus (blue), PM = plasma membrane (green). Dashed arrows indicate partially internalized QDs and solid arrows indicate fully internalized QDs. Scale bars represent 10 μm. D) Effect of temperature on QD uptake in Hek 293 cells (black bars) and Hep G2 cells (white bars) exposed to QDs (100 nM; 1 hrs). The means ± SEM of uptake inhibition (%, at 4 °C) are relative to the uptake of QDs at 37 °C (100 %), *** $p<0.001$.

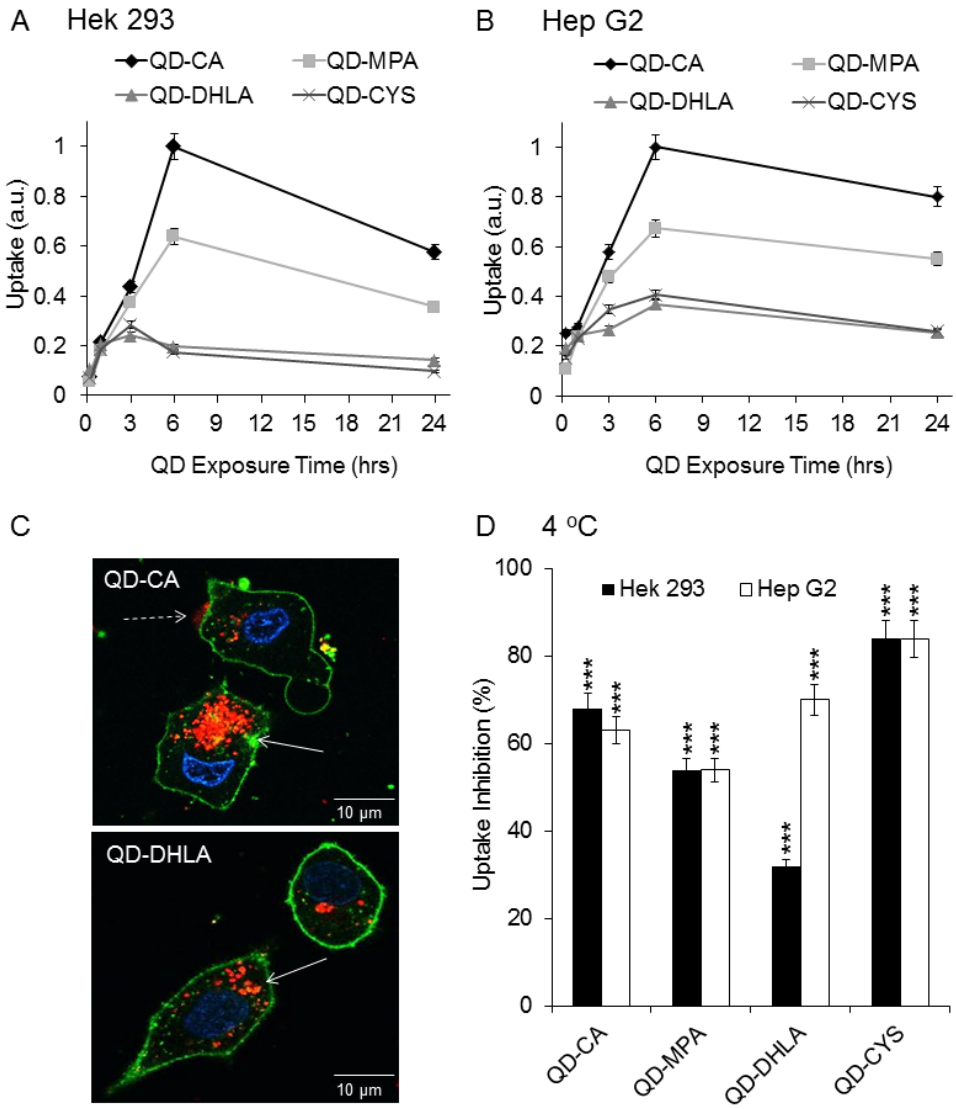
A
Hek 293
QD-CA
QD-MPA
QD-DHLA
QD-CYS
Uptake (a.u.)
QD Exposure Time (hrs)
B
Hep G2
C
QD-CA
QD-DHLA
10 μm
D
4 °C
Hek 293
Hep G2
Uptake Inhibition (%)
***

Figure 3.4. Inhibition of QD uptake in human kidney Hek 293 and liver Hep G2 cells – involvement of lipid rafts and the X-AG cysteine transporter

A) Effect of lipid raft disruption by MBCD (10 mM, 30 min) on QD (100 nM, 3 hrs) uptake in Hek 293 cells (black bars) and Hep G2 cells (white bars). B) Effect of cysteine transport inhibition by THA (5 mM, 1 hrs) on QD-CYS (100 nM, 3 hrs), and C) Effect of D,L-cysteine (0.1-2 mM, 15 min) on QD-CYS uptake. All values for uptake inhibition (%) in panels A-C are the means ± SEM (n = 9), *** $p<0.001$. D) Inhibition of QD uptake by MBCD, THA or at 4 °C measured by flow cytometry (FACS). The scatter histograms are representative of three independent experiments.

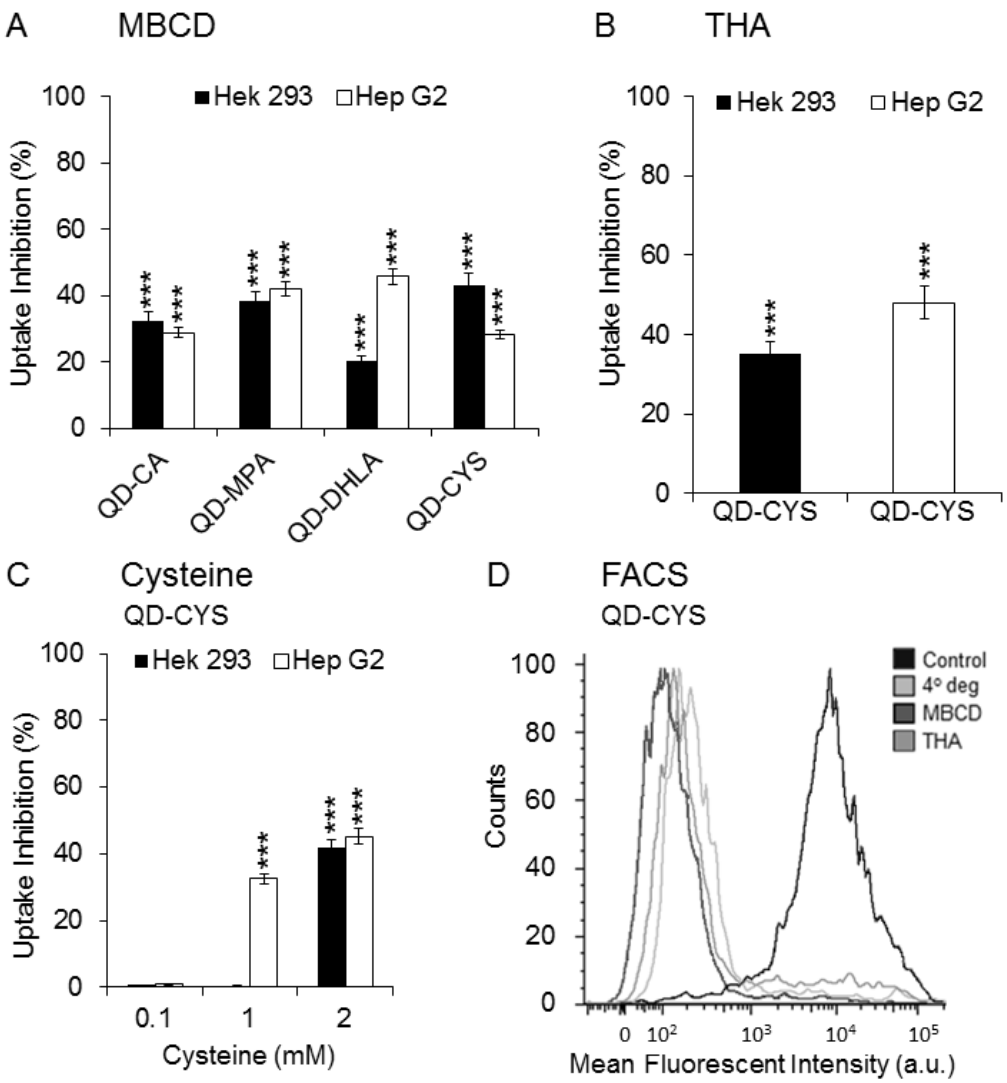
A
MBCD
Hek 293
Hep G2
Uptake Inhibition (%)
100
80
60
40
20
0
***
QD-CA
QD-MPA
QD-DHLA
QD-CYS
B
THA
Hek 293
Hep G2
Uptake Inhibition (%)
***
QD-CYS
QD-CYS
C
Cysteine
QD-CYS
Hek 293
Hep G2
Uptake Inhibition (%)
***
0.1
1
2
Cysteine (mM)
D
FACS
QD-CYS
Control
4° deg
MBCD
THA
Counts
0
10²
10³
10⁴
10⁵
Mean Fluorescent Intensity (a.u.)

Figure 3.5. The role of P-gp transporter in QD elimination from human cells

A) Hek 293 cells and B) Hep G2 cells were exposed to QDs (100 nM) for 3 hrs and QD elimination was measured over time (1-6 hrs). Data represent the means ± SEM (n = 9), *** $p<0.001$. C) Activation of P-gp by rifampin (25 μM, 15 hrs) and elimination of QDs (100 nM). All values (the means +/- SEM) represent the change in QD efflux (%) relative to the values from cells exposed to QDs only (no rifampin), *** $p<0.001$. D) Inhibition of P-gp by elacridar (50 nM, 1 hrs) and elimination of QDs (100 nM). Reduction (%) of QD efflux is relative to the efflux in the absence of elacridar. Data points represent the means +/- SEM from three independent experiments of triplicates, *** $p<0.001$.

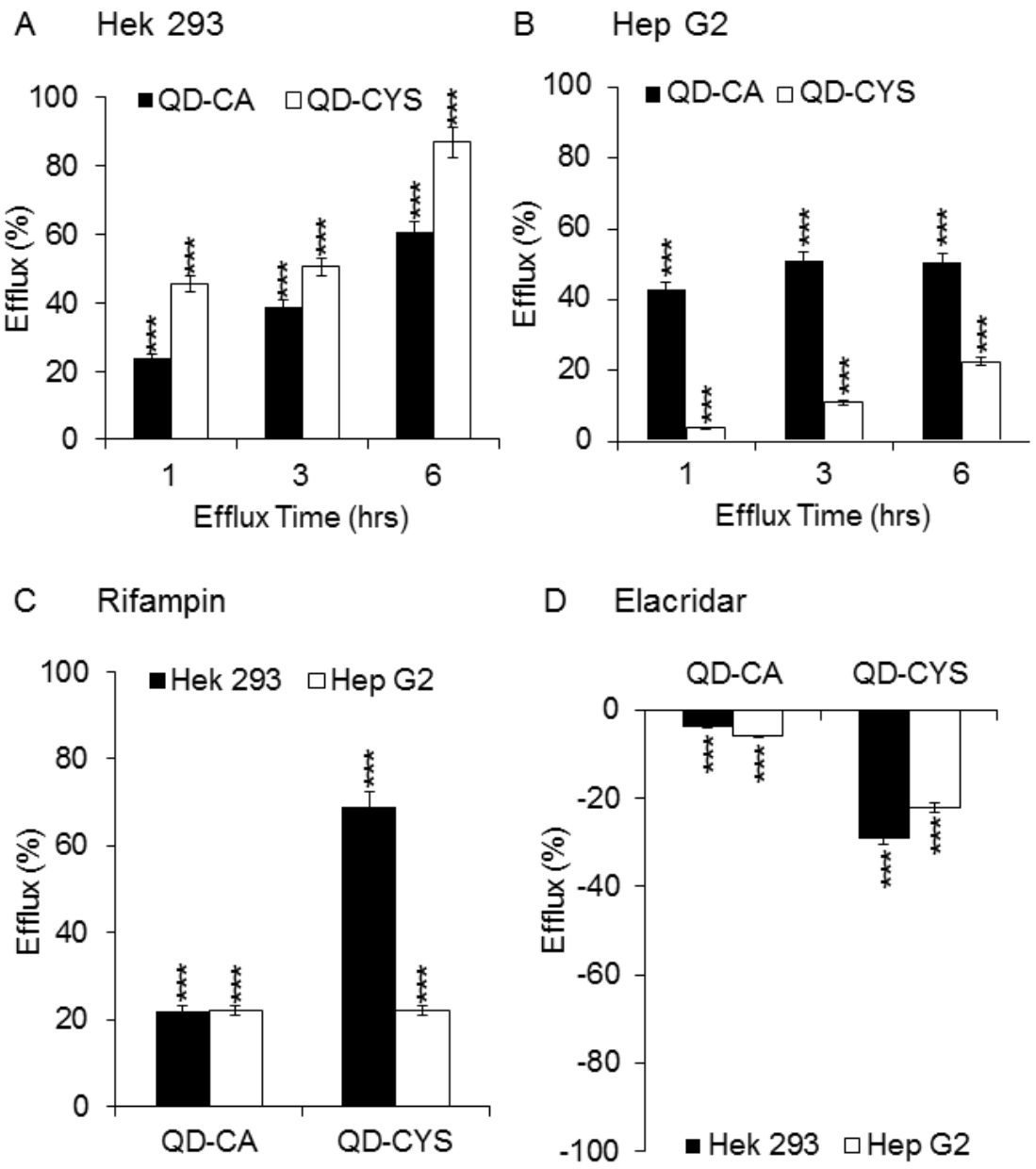
A
Hek 293
QD-CA
QD-CYS
Efflux (%)
Efflux Time (hrs)
B
Hep G2
C
Rifampin
Hek 293
Hep G2
D
Elacridar

Figure S3.1. Size distributions of differently coated QDs prepared from the same QD batch

Compared to the size distribution obtained from DLS measurements of filtered QD-CA (thick line), the AF4 results show that fractionation prior to light scattering measurements yield greater precision on the medium size and the size distributions of the QDs, and allows us to observe reproducibly slight differences in the radius of the QDs, depending on the length of their surface ligands. The differential weight fractions were plotted using the Astra software (Wyatt Technologies, USA) from the Rh data plotted as a function of elution time, with a UV-Vis detector to monitor the concentration of QDs.

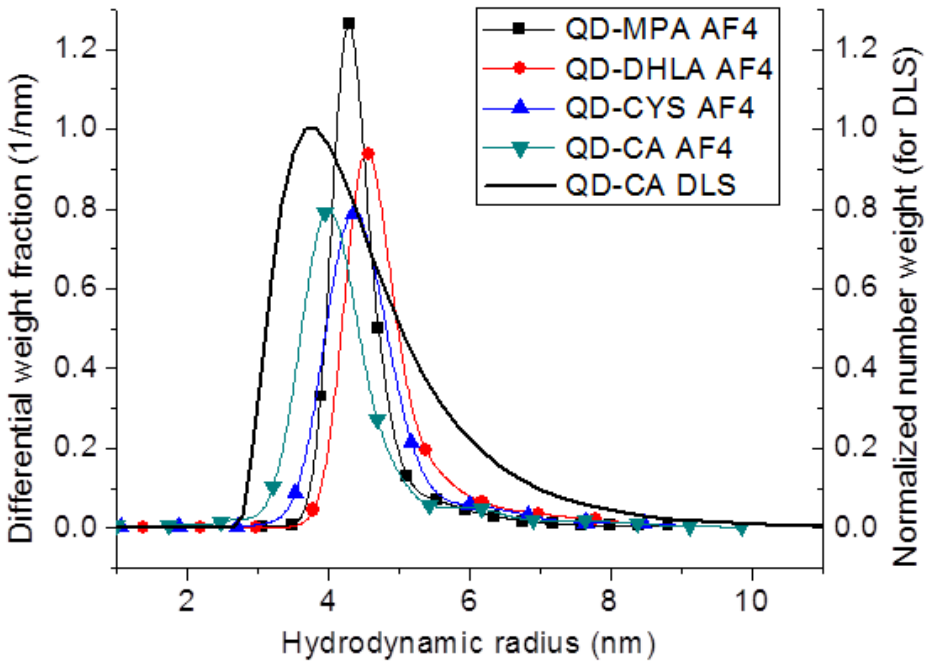

Table S3.1. Zeta-potential and hydrodynamic diameter of differently coated quantum dots (QDs) in different conditions of pH and ionic strength

All zeta-potential measurements were done at 37 °C on a Zetasizer Nano ZS (Malvern Instruments, UK).

	QD-MPA	QD-DHLA	QD-Cys	QD-CA
Milli-Q water *(Conductivity: 0.49 mS/cm)*	Soluble (> 7days)	Soluble (> 7days)	Soluble (4-7 days)	Soluble (4-7days) Dh = 25 ± 3.7 nm
	-32.8 mV	-33.7 mV	-35.8 mV	48.25 ± 1.55 mV
pH 4.22 [PO_4] 100mM *(9.54 mS/cm)*	Soluble (> 7days) Dh = 46 ± 0.4 nm	Aggregates <1day D>10µm	Soluble 1 day after R>15µm	Not-soluble (<1day)
	-31.4 ± 0.46 mV	-30.53 ± 1.9 mV	-12.1 ± 0.62 mV	6.6 ± 0.5 mV
pH 5.5 [PO_4] 10mM *(1.57 mS/cm)*	Soluble (> 7days) Dh = 20 ± 1.2 nm	Soluble 4-7days Dh = 33 ± 3.5 nm	Soluble 1 day Dh= 128 ± 25 nm	Not-soluble (<1day)
	-34.87 ± 1.53 mV	-42.3 ± 0.9 mV	-33.98 ± 0.56 mV	15.45 ± 0.39 mV
pH 6.5 [PO_4] 10mM *(1.59 mS/cm)*	Soluble (> 7days) Dh = 17 ± 0.5 nm	Soluble (4-7days) Dh = 63 ± 1.8 nm	Soluble 1 day Dh = 95 ± 11 nm	Not-soluble (<1day)
	-35.42 ± 0.77 mV	-40.93 ± 1.42 mV	-37.48 ± 1.27 mV	8.61 ± 0.76 mV
pH 7.5 [PO_4] 10mM *(2.16 mS/cm)*	Soluble (> 7days) Dh = 15 ± 0.2 nm	Soluble (> 7days) Dh = 26 ± 1.0 nm	Soluble 3 days Dh = 130 ± 51 nm	Not-soluble (<1day)
	-59.65 ± 2.23 mV	-42.85 ± 2.26 mV	-40.68 ± 1.88 mV	1.41 ± 0.70 mV
pH 7.4 [PO_4] 10mM, [NaCl] 137mM *(9.66 mS/cm)*	Soluble (> 7days) Dh = 18 ± 0.1 nm	Soluble (> 7days) Dh = 26 ± 3.0 nm	Soluble 1 day Dh = 245 ± 12 nm	Not-soluble (<1day)
	-26.1 ± 1.93 mV	-30.43 ± 0.9 mV	-28.4 ± 1.15 mV	5.53 ± 0.94 mV
DMEM pH 8.6 *(18.3 mS/cm)*	Not soluble, aggregates rapidly D>2.5µm	Not soluble, aggregates rapidly D>5µm	Not soluble, aggregates rapidly D>5µm	Soluble 1 day Dh = 84.7 ± 53
	-18.65 ± 0.44 mV	-19.4 ± 4.1 mV	-4.02 ± 1.12 mV	-8.81 ± 0.60 mV

Figure S3.2. Characterization of quantum dots using asymmetrical flow field-flow fractionation

Asymmetrical flow field-flow fractionation (AF4) fractogram of CdSe(CdZnS) QDs coated with mercaptopropionic acid (top), dihydrolipoic acid (center) and L-cysteine (bottom). Elution of the QD-MPA, QD-DHLA and QD-CYS, respectively, in a size-dependent manner (left column). Elution of aggregates of QD-MPA, QD-DHLA and QD-CYS, respectively (right column).

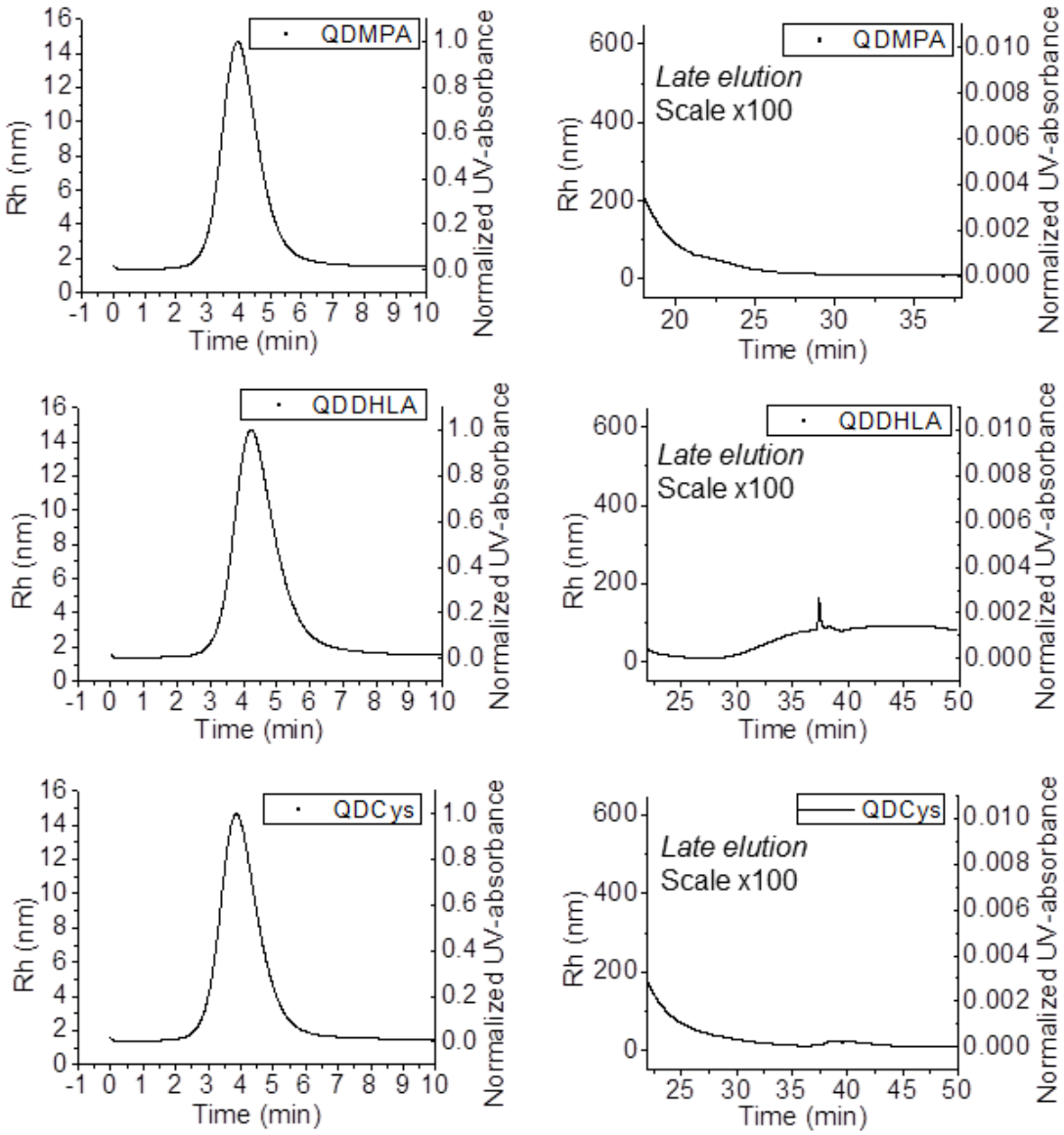

Figure S3.3. Quantum dots are well tolerated in Hek 293 and Hep G2 cells up to 24 hours

A) Hek 293 kidney cells and B) Hep G2 liver cells were exposed to QDs (100 nM, 1-24 hrs) in serum free DMEM media. Following QD treatment, cellular metabolic activity was assessed using the Alamar blue viability assay. All vales are expressed as % metabolic activity with respect to cells incubated for the same time but in the absence of QDs (taken as 100%). Data points represent the means ± SEM from three independent experiments of triplicates. Cell number was not significantly reduced within 24 hours exposure to the QDs.

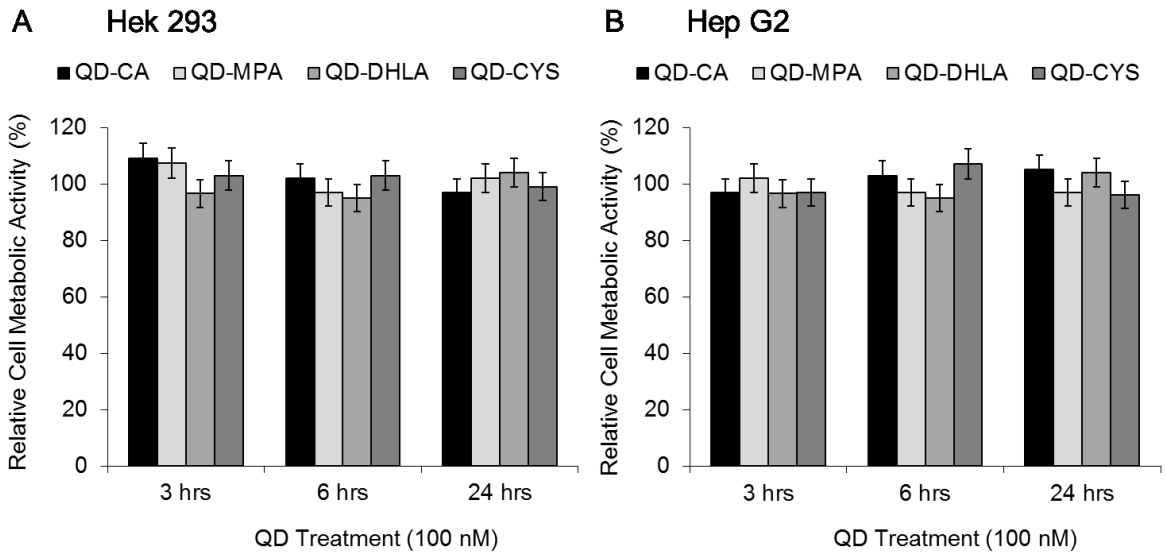

Figure S3.4. Intracellular cadmium concentrations increase following exposure to quantum dots

A) Total intracellular cadmium content (μM) was assessed using flame atomic absorption (FAA) and the values were plotted with respect to QD concentrations (nM). Cadmium concentrations from stock QD solutions were determined using FAA. Standard curves were generated using 0, 5, 10, 25, 50 and 100 nM QDs. B) Hek 293 cells were treated with QD-CYS and $CdCl_2$ in equimolar concentrations with respect to cadmium (100 nM and 23.66 μM respectively). Data points represent the means ± SEM from three independent experiments of triplicates. Statistically significant differences from control were tested with independent t-tests and are indicated by *** $p<0.001$.

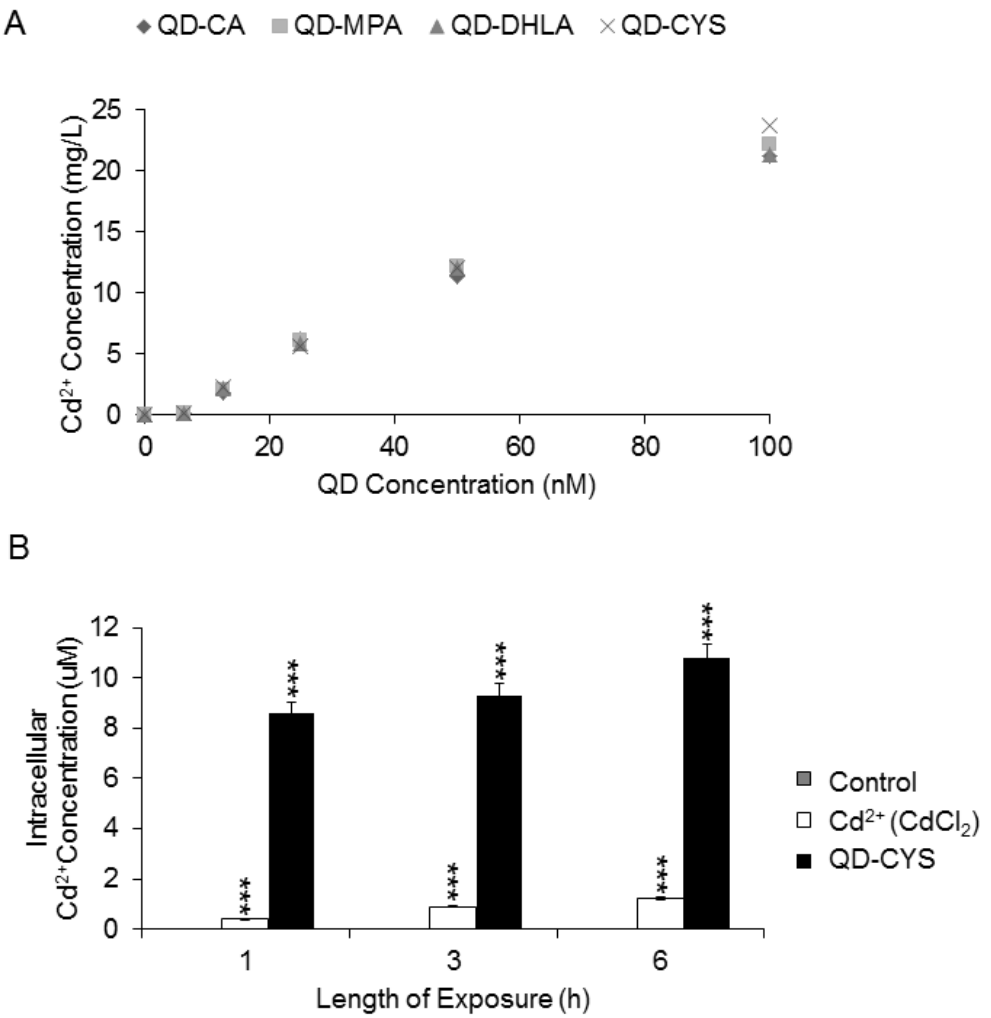

Figure S3.5. QD-MBCD interactions

A and C) AF4/UV/QELS fractograms showing the UV/Vis signal as a function of elution time for QD-DHLA and QD-CYS, respectively upon incubation for 3 or 5 hours at 37 °C with methyl-β-cyclodextrin (MBCD, 10 mM in deionised water). The dots underneath the curves represent the hydrodynamic radii determined by the online QELS (Wyatt Technologies). The same fractionation method was used as previously described for all 4 QDs. B and D) Differential weight fraction obtained from the Rh data combined with the concentration provided by the UV/Vis detector for QD-DHLA and QD-CYS, respectively.

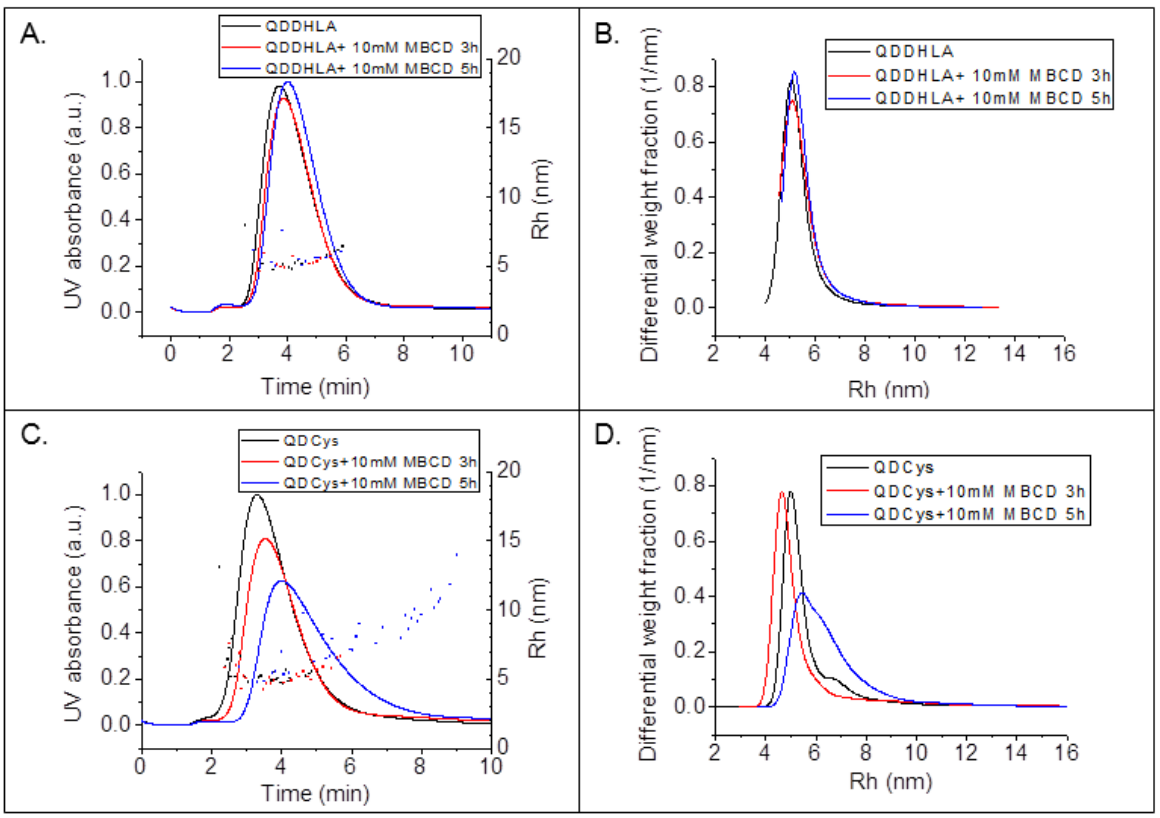

Connecting text

In previous chapters, we presented evidence for the involvement of several different cellular mechanisms which mediate QD-cell interactions. More specifically, we showed in Chapter 3 that QD surface properties modulate cellular internalization processes. However, we did not consider the effect of particle aggregation/agglomeration in the previous studies. The agglomeration state of nanoparticles plays a critical role in at least two ways: it can re-direct the mode of nanocrystal internalization and it can contribute either positively or negatively to the cell survival.

In the follow-up study, we characterized CdSe QD agglomeration states, tracked the agglomerates in a time and concentration dependent manner *in vitro* and measured the viability of cells with predominantly agglomerated QDs against the finely dispersed QDs. These studies focused on investigating particle agglomeration induced by high concentrations of salts and proteins within the physiological medium. We used asymmetric flow-field flow fractionation (AF-4) as the major approach for the determination of QD size and stability. This technique provided particle by particle size determination and dynamics of agglomerate formation. Traditional characterization techniques for size determinations such as transmission electron microscopy (TEM) and dynamic light scattering (DLS) were used as complementary techniques.

The major findings from these studies were: 1) serum proteins were differentially adsorbed to the particle surface depending on the conjugated surface ligand, 2) QD stability modified interactions at the cell membrane, driving particle uptake and 3) AF-4 is a suitable technique for characterization of nanoparticles in complex biological media because it provides quantitative data needed to establish the relationship between the agglomeration status and internalization by cells. Results from Chapter 4 highlight key differences between the “synthetic” and “biological” identity of nanoparticles while in the presence of cell culture medium. Understanding particle stability in the biological microenvironment is essential to properly interpret cellular mechanistic studies and diagnostic assays.

Chapter 4. Relating the chemical and biological identity of quantum dots in N9 microglia cells through asymmetrical flow field-flow fractionation analyses

Alexandre Moquin*, Kevin D. Neibert*, Dusica Maysinger, Françoise M. Winnik

(to be re-submitted)

4.1. Abstract

The *in vitro* or *in vivo* fate of nanoparticles is determined primarily by their size and surface chemistry in the biological environment, two properties that remain difficult to determine experimentally. In this work, we determined the size of PEGylated quantum dots (QDs) and QDs bearing short ligands dispersed in biological media of increasing complexity, using asymmetrical flow field-flow fractionation (AF4) with UV-Visible absorbance, dynamic light scattering and static light scattering detection. AF4 analyses, carried out over a 1-hrs incubation of QDs in biological media, gave a precise description of the time-dependent status of QD aggregation, as a function of the medium and of their initial structure in water. In parallel, we determined the preferred mode(s) of entry of the same QDs in N9 microglia cells using confocal fluorescence imaging of live cells pre-treated with pharmacological inhibitors that block specific modes of cellular entry. We observed an excellent correlation between the aggregation status of QDs in cellular media derived from AF4 analyses and their preferred mode of cellular uptake. Furthermore, we report for the first time, that QDs are transported within the N9 microglial protrusions towards the cell soma. Since N9 microglia are the main cells in the central nervous system that respond strongly to nanoparticles, this study provides important new insights into the mode of entry of particles in the brain.

4.1.1. Key Words

Aggregation status, internalization, nano-bio interface

4.2. Introduction

Cells use various modes of particle internalization and elimination to preserve their homeostasis (Kumari, Mg et al. 2010). Routing of particles is carefully regulated through dynamic morphological changes of the plasma membrane and activation of signal transduction pathways (Duncan and Richardson 2012). Luminescent semi-conductor nanocrystals or quantum dots (QDs) are frequently used in the biomedical field for *in vitro* studies, diagnostics, and small animal imaging, in view of their high quantum yield, size-

tunable optical properties, and outstanding photostability (Dubertret, Skourides et al. 2002, Gao, Yang et al. 2005, Michalet, Pinaud et al. 2005). Their cellular internalization involves multiple endocytotic pathways, such as clathrin and lipid raft-dependent endocytosis, as well as specific receptor-mediated endocytosis. PEGylated QDs are routinely used for *in vitro* and *in vivo* imaging due to their excellent stability in water and the ability of PEG chains to reduce non-specific binding and to alleviate cytotoxicity. Moreover PEGs with functional end groups are convenient handles for conjugation of targeting groups or drugs, thus facilitating biomedical applications. Zhang et al. reported recently that PEGylated QDs with different end groups trigger different endocytic pathways in human pulmonary epithelial cells and macrophages culture in serum-free media (Zhang, Pan et al. 2013). QDs bearing short ligands are also useful bioimaging tools. As prepared, short-ligand QDs are smaller than PEGylated QDs. Their small size is expected to facilitate their elimination during *in vivo* studies. This may not be the case, since the size of QDs in cellular media and *in vivo*, their "biological identity", may in fact be quite different from their size determined by standard analytical tools, such as dynamic light scattering (DLS). Proteins present in biological fluids tend to adsorb onto the QD surface and to modify their surface properties and size (Cedervall, Lynch et al. 2007, Lundqvist, Stigler et al. 2008, Casals, Pfaller et al. 2010, Lundqvist, Stigler et al. 2011, Tenzer, Docter et al. 2011, Walkey and Chan 2012, Walkey, Olsen et al. 2012). Protein-coated QDs often associate into larger assemblies of broad size distribution and undefined surface chemistry (Walczyk, Bombelli et al. 2010).

In order to interpret properly cellular mechanistic studies and diagnostic assays, it is necessary to know the size of QDs in the cell culture medium employed (Nel, Madler et al. 2009, Walkey and Chan 2012). Currently, there is no simple, reliable method to determine the size of QDs in complex cellular media. Transmission electron microscopy (TEM) can be used to monitor the location and state of aggregation of QDs in cells, but only for fixed cells, which cannot be used for further biological studies (Nabiev, Mitchell et al. 2007, Zhang and Monteiro-Riviere 2009, Xiao, Forry et al. 2010). Confocal fluorescence microscopy is the tool of choice to follow the fate of QDs in live cells, but its spatial resolution is not sufficient to determine accurately the size of QDs in cells (Iversen, Skotland et al. 2011, Duncan and Richardson 2012). Fluorescence correlation spectroscopy was applied recently to monitor the

concentration, distribution, and dynamics of QDs in living cells. It may prove to be very useful once the technique becomes readily accessible, but currently there is no standard analytical method to assess the size of QDs in relevant biological milieus (Powers, Palazuelos et al. 2007, Murdock, Braydich-Stolle et al. 2008, Warheit 2008, Zhu, Yeh et al. 2011, Hondow, Brydson et al. 2012, Muro, Fragola et al. 2012, von der Kammer, Ferguson et al. 2012). So far asymmetrical flow field-flow fractionation (AF4) has not been applied to the characterization of QDs or metallic particles in complex cell culture media. Yet, AF4 is a mild separation technique that permits the quantitative determination of the size and concentration of particles ranging in size from a few nanometers to several microns. It has been used to analyze QDs (Al-Hajaj, Moquin et al. 2011), gold (Zattoni, Rambaldi et al. 2009, Cho and Hackley 2010, Calzolai, Gilliland et al. 2011, Schmidt, Loeschner et al. 2011, Yang, Shang et al. 2013), and silver nanoparticles/clusters in buffers (Hagendorfer, Kaegi et al. 2012, Pettibone, Gigault et al. 2013). We present here convincing evidence that there is an excellent correlation between the QD size data acquired by AF4 and the aggregation status of QDs *in vitro*, as inferred from by their preferred internalization pathways in cells.

The cellular experiments were conducted with N9 microglia, which bear many similarities with primary microglia (Stansley, Post et al. 2012). Microglia are the brain "surveyors" whose main function is to maintain brain homeostasis by elimination of aggregated and misfolded proteins, particles, microorganisms, or cellular debris from injured neurons (Kettenmann, Hanisch et al. 2011). Recent studies show that microglia also play a role in brain remodeling throughout the normal lifespan (Sierra, Abiega et al. 2013). Microglia constantly move and change shape, from amoeboid to ramified (Nimmerjahn, Kirchhoff et al. 2005). Although microglial activation is often regarded as neurotoxic, microglia can also be protective and facilitate functional recovery in the central nervous system. We used immortalized microglial cells (N9) because these cells, like primary microglia, respond to particulate matter (Kettenmann, Hanisch et al. 2011). QD uptake by N9 microglia was examined after treatment of the cells with pharmacological inhibitors known to block specific nanoparticle entry modes. Specifically, we used chlorpromazine (CPZ), which prevents clathrin dependent pathways, cytochalasin D (CytoD), which interferes with actin polymerization thereby inhibiting macropinocytosis and likely other modes (Gratton, Ropp et

al. 2008), Y-27632, which blocks the Rho kinase pathway involved in pinocytosis (Ishizaki, Uehata et al. 2000), methyl-β-cyclodextrin (MBCD), which extracts cholesterol from the plasma membrane thereby depleting lipid rafts and strongly inhibiting both caveolae and receptor mediated internalization (Gratton, Ropp et al. 2008), and SB-203580, an inhibitor of phagocytosis. Effectively, the inhibitors screen QDs and QD aggregates according to their size as they encounter the outer cell membrane. Using relatively simple serum-containing media to illustrate how the high salt concentration and protein content in the QD environment change the QD aggregation state, we demonstrate that there is an excellent relationship between the size of QDs in these media, measured by AF4 analysis, and their preferred mode of cellular uptake. The robustness of the AF4 technique is such that it can be used to monitor the aggregation of QDs and other nanoparticles in more complex media.

4.3. Results and discussion

4.3.1 Characterization of the QDs

The structure, spectral characteristics, size, and charge of the QDs employed here are given in Figure 4.1. The QDs were prepared by conventional ligand exchange, starting with CdSe(CdZnS) nanocrystals (core diameter ~ 7 nm) obtained according to standard protocols (Yang, Wang et al. 2012). The ligands were mercaptopropionic acid (MPA), dihydrolipoic acid (DHLA), and α-carboxyl-ω-mercapto-poly(ethylene glycol) (PEG-COOH), all of which are commonly used for *in vitro* studies (Clapp, Goldman et al. 2006, Mei, Susumu et al. 2009). All QDs were negatively charged in Dulbecco's modified Eagle's medium (DMEM) supplemented with FBS (5 %) and in serum-free DMEM. The ζ-potential of QD-DHLA and QD-MPA in phosphate buffered saline (10 mM, pH 7.4) were slightly negative (ionic strength: 137 mM), and also slightly negative in DMEM (ionic strength 130 mM) and in FBS-DMEM. In agreement with previous reports, the ζ-potential of PEGylated QDs was slightly negative in phosphate buffered saline (10 mM, pH 7.4) and kept the same value in DMEM and FBS-DMEM.

4.3.2 QD aggregation status

The aggregation status of QDs dispersed in water, DMEM, and FBS-DMEM was evaluated by AF4 analysis using an instrument equipped with a UV-visible absorbance detector acting as concentration detector, a multiangle light scattering (MALS) detector and a dynamic light scattering (DLS) detector that yield, respectively, the gyration and hydrodynamic diameters (Dg and Dh) of the eluting nanoparticles. AF4 separation principles and details of the measurements are reported elsewhere (Schimpf, Caldwell et al. 2000, Zattoni, Rambaldi et al. 2009). The elution profiles (fractograms) recorded for QD-DHLA dispersed in water and after a 5-min incubation in DMEM or DMEM-FBS are presented in Figure 4.1D. The median Dh values, which correspond to the Dh at the maximum elution determined by the UV-vis detector, are given in Figure 4.1B. The UV-absorbance fractograms (λ = 280 nm, black line) feature bands after ~ 7 and ~ 10 min, for QD-DHLA in water and in DMEM + 5% FBS (Figure 4.1D, left and right panels). The bands correspond, respectively, to the elution of nanoparticles of Dh ~ 12 nm and 24 nm, as determined by DLS (blue open circles, Figure 4.1D). A small fraction of aggregated QD-DHLAs in water (~ 6 weight %) eluted at very long times (~ 24 min) (not shown in Figure 4.1D, see fractogram in Figure S4.1.). The fractogram of QD-DHLA incubated with FBS-DMEM (Figure 4.1D, right panel) presents two bands: 1) a band at very short time (3.75 min, Dh 7 nm), corresponding to the elution of the proteins present in FBS and 2) a broad band with a maximum at ~ 10 min and a shoulder at long elution times corresponding to the elution of particles of Dh ranging from ~ 16-20 nm to nearly 80 nm. The broad size distribution is indicative of the formation of assemblies of 2 to 5 QDs, presumably kept together by adsorbed serum proteins. QD-MPAs also showed a tendency towards association in FBS-DMEM, whereas the QD-PEG-COOH retained their original size (~ 31 nm) (Figure 4.1B).

4.3.3 Interactions at the nano-bio interface

Protein/nanoparticle interactions and nanoparticle aggregation in serum or cell culture media are dynamic processes (Jiang, Oberdörster et al. 2009, Maiorano, Sabella et al. 2010). Therefore, we monitored by AF4, the evolution of the size of the QDs as a function of their incubation time (5 min to 1 hrs) in FBS-DMEM and in DMEM. Representative fractograms

are presented in Figure 4.2. As described above, QD-DHLA show a strong tendency towards association is small clusters immediately upon exposure to DMEM-FBS. From the shape of the broad band in the time-dependent fractograms shown in Figure 4.2A, we conclude that the aggregation status of QD-DHLA does not change with time to any significant extent, indicating that the protein corona surrounding QD-DHLA particles stabilizes them against further aggregation, in accordance with previous reports (Murdock, Braydich-Stolle et al. 2008). QD-MPA dispersions also underwent immediate aggregation upon treatment with DMEM-FBS (Figure 4.2C). During the first 5 min of incubation, all QD-MPAs were incorporated into larger aggregates, ranging in size from 5 to 130 nm; further incubation led to the formation of increasingly large aggregates. After a 1 hrs-incubation most aggregates eluted at times exceeding 20 min. Their size ranged from 140 nm < Rh < 1000 nm. Panel E in Figure 4.2 and Figure S4.2 present fractograms recorded for QD-PEG-COOH incubated in DMEM-FBS. The elution band has a tail of ~ 0.5 min on the long elution time side. It corresponds to an increase in Dh of ~ 10 nm (Figure S4.2.). It would appear that the PEG corona surrounding the nanocrystals does not entirely prevent protein adsorption, as suggested previously (Walkey and Chan 2012, Walkey, Olsen et al. 2012, Salvati, Pitek et al. 2013). Yet, the limited amount of adsorbed proteins has no deleterious consequences on the dispersion stability of PEGylated QDs, as confirmed by the absence of signals in the long elution time sections of the fractograms.

Panels B, D, and F of Figure 4.2 display the time-dependent UV-absorbance fractograms recorded for QDs dispersed in DMEM. In the case of QD-DHLA the elution pattern changed gradually as a function of time: after a 30-min incubation, a shoulder appeared on the long elution time side of the QD-DHLA elution band. Its intensity increased gradually with time. After a 1hr-incubation, the Dh values of QD-DHLA aggregates ranged from 11 to 60 nm. Samples of QD-MPA, also, proved to have little resistance against aggregation in DMEM (Figure 4.2D). After a 5-min incubation, a large fraction of QD-MPAs formed aggregates (10 nm < Dh < 80 nm). QD-MPA association continues with increasing incubation time, but the size of the aggregates does not change significantly over time, in contrast with the case of QD-DHLA. MPA ligands are attached to the QD surface through a monodentate thiol bond, while the DHLA linkage is bidentate and bulkier. It has been

suggested that the ligand packing density is higher in the case of QD-MPA, compared to QD-DHLA (Mattoussi, Mauro et al. 2000, Zhang and Clapp 2011). The enhanced stability of QD-MPA in DMEM, compared to QD-DHLA, may be due to the tighter ligand packing. In the presence of serum proteins, the situation is different: the lower packing density of DHLA, vs. MPA, leaves more space available for the adsorption of proteins, which can enhance the long-term stability of QDs against aggregation. Fractograms recorded for QD-PEG-COOH incubated in DMEM (Figure 4.2F) revealed that the size of QD-PEG-COOH did not change significantly within 1 hrs. Moreover, the elution pattern did not change over the course of 24-hrs incubation (data not shown).

4.3.4. Internalization of QDs in N9 microglia: time dependence

Using a combination of confocal fluorescence microscopy and phase contrast imaging, we examined qualitatively the extent of QD internalization by N9 microglia within the course of 1 hrs and confirmed that the three QD types were internalized by N9 microglia in DMEM and DMEM-FBS. Microglia adopt various shapes depending on their environment. Characteristically, they feature many ramifications, which are readily visible in confocal micrographs of N9 microglia labeled with a green membrane-specific dye (PKH). In Figure 4.3A, we present depth-dependent micrographs of N9 microglia in DMEM after a 1hr-treatment with QD-MPA (red emitting). Z-stack slices were taken at 0.64 μm intervals, starting from the surface of the coverslip (left-hand side of Figure 4.3A). Membrane ruffling is observed in most sections. During the membrane ruffling, there is extensive actin filament reorganization involving activation of p38 signal transduction pathway (Ferreira, Santos et al. 2012). The QD-MPA aggregates accumulate primarily near the tips of the ramifications (white arrows), although QD-MPA aggregates are also observed in the cell body (yellow arrows). By examining confocal micrographs taken at various time points following exposure to QD-MPA, we observed that QDs were transported within the microglial protrusions from their tip towards the cell soma. Micrographs, recorded within a single focal plan after various time lapses are presented in Figure 4.3B. The same protrusion section examined at times 0, 10 and 50 min, is outlined by a white rectangle on the left-hand micrographs that present a wide observation area. Within 50 min, the specific QD aggregate indicated by the white

arrows moved towards the soma (rate: 90.5 ± 10 nm/min), by reference to a fixed point, indicated by yellow arrows. Anterograde and retrograde movements of intracellular organelles in neurites and axons have been frequently reported, particularly mitochondria and vesicles (Tsukita and Ishikawa 1980, Cui, Wu et al. 2007).

4.3.4 Internalization of QDs in N9 microglia: QD ligand dependence

To study the preferred endocytotic pathways adopted by QDs bearing different ligands, the N9 microglia were pretreated with pharmacological inhibitors used in concentrations non-toxic to the cells (Figure S4.4). We confirmed also that the inhibitors did not interact with the QDs and did not affect their dispersions stability (Figure S4.5). The percent uptake inhibition caused by each inhibitor was determined fluorometrically for N9 microglia exposed to each type of QDs for 1hr in either DMEM-FBS (Figure 4.4A) or DMEM (Figure 4.4B). Inhibiting phagocytosis with SB-203580 reduced the uptake of QD-MPA by N9 microglia by nearly 50 % in the presence of serum proteins, but it had no significant effect on the uptake of QD-DHLA and QD-PEG-COOH under the same conditions. The effect of SB-203580 on QD-MPA uptake by N9 microglia in serum-free DMEM was noticeable, but the % uptake inhibition was much lower (~ 15 %). Disrupting lipid rafts with MBCD markedly attenuated the uptake of all QDs by N9 microglia cultured with or without serum. Inhibiting clathrin mediated endocytosis with CPZ slightly decreased QD-MPA uptake by cells in DMEM-FBS, but did not affect uptake of QD-DHLA and QD-PEG-COOH. The macropinocytosis inhibitor CytoD slightly affected uptake of QD-DHLA and QD-MPA in serum-free DMEM, but had no effect in the presence of serum protein. These data confirm that the internalization of all QDs examined here, including the PEGylated sample, relies significantly on lipid raft-dependent endocytosis, as reported earlier (Al-Hajaj, Moquin et al. 2011, Zhang, Pan et al. 2013). They also give a strong indication that the internalization of QD-MPAs in N9 microglia primarily involves phagocytosis for cells cultured in the presence of serum.

Confocal fluorescence micrographs of QD-treated N9 microglia cells cultured in FBS-DMEM and DMEM are presented in Figures 4.5A and 4.5B, respectively. Micrographs in the

top row of panels A and B present QD-treated cells without inhibitor; the bottom row of each panel presents images of cells treated with the phagocytosis inhibitor SB-203580. Micrographs of cells in FBS-DMEM treated with QD-DHLA and QD-PEG-COOH present small luminescent clusters distributed in the periphery of the cytoplasm, whereas QD-MPA are found inside the cells as large luminescent clumps (Figure 4.5A). Cells cultured in serum-free DMEM also internalize all three QD types (Figure 4.5B) but in this case QD-DHLA form large assemblies, whereas QD-MPA particles form much smaller assemblies distributed mainly in the proximity of the inner plasma membrane. These observations are in full agreement with results of AF4 measurements, which indicate that QD-MPA in DMEM form smaller aggregates, compared to FBS-DMEM, whereas the opposite is true in the case of QD-DHLA (Figure 4.2.).

Turning our attention to micrographs of cells pre-treated with SB-203580 prior to exposure to QDs. For N9 microglia cultured in the presence of serum (Figure 4.5A), small QD-DHLA assemblies are detected within the cell, embedded in the plasma membrane, and on the outer surface of the membrane, indicating that a fraction of the QD-DHLAs cannot enter the cell. In contrast, it appears that nearly all the QD-MPA population is either adsorbed on the outer cell surface or imbedded in the plasma membrane, as reflected by the yellow color of the membrane, which indicate co-localization of the red QDs and the membrane labeled with the green-emitting dye. Only a very small proportion of QD-MPA is found intracellularly. We note also that the phagocytosis inhibitor does not restrict the uptake of QD-PEG-COOH by N9 microglia cells in FBS-DMEM. The situation is quite different when N9 microglia pre-treated with SB-203580 and cultured in DMEM in the absence of serum are exposed to QDs (Figure 4.5B, bottom row). In this case, most of the QD-DHLAs enter the cell and reside within the cell cytoplasm. Only a few QD-DHLA assemblies can be seen on the outer membrane surface. In contrast, QD-MPAs are not taken up by the cells. They are retained on the outer plasma membrane surface or embedded in the membrane. The Cd^{2+} concentration within N9-microglia treated with QDs under various conditions was measured by graphite furnace atomic absorption spectrometry. Their values are presented graphically on the right-hand side of Figure 4.5 in the cases of QD-MPA-treated cells pre-incubated with SB-203580, or without inhibitor. The intracellular Cd^{2+} concentration was significantly

reduced for cells pretreated with the phagocytosis inhibitor and cultured in serum, confirming the visual assessments of micrographs and the fluorimetric data presented in Figure 4.4. They are also in good agreement with AF4 data that indicate that QD-MPA form aggregates very rapidly in DMEM, whereas the aggregation rate of QD-DHLA nanoparticles is slower (Figure 4.2.).

4.4. Experimental section

4.4.1. Materials and instrumentation

4.4.1.1 Quantum dots

Water was deionized using a Millipore Milli-Q system. All chemicals were purchased from Sigma-Aldrich, unless specified otherwise. Dihydrolipoic acid (DHLA) was prepared by reduction of thioctic acid following a known procedure (Ishizaki, Uehata et al. 2000). α-Carboxyl-ω-mercapto poly(ethylene glycol) (HS-PEG-COOH, Mw 5,000 Da) was obtained from Iris Biotech. Chemicals were used without further purification unless otherwise stated. TOP/TOPO-coated CdSe(CdZnS) core–shell QDs were synthesized and purified by a protocol described in detail elsewhere (Al-Hajaj, Moquin et al. 2011). They were stored as a suspension in chloroform prior use. Mercaptopropionic acid (MPA) and dihydrolipoic acid (DHLA)–modified QDs were prepared as described previously.27 QD-PEG-COOH nanoparticles were prepared from TOP/TOPO-coated CdSe(CdZnS) core–shell nanoparticles synthesized and purified as described in detail elsewhere (Al-Hajaj, Moquin et al. 2011). A suspension of QD-TOP/TOPO in chloroform (~ 500 mL, ~ 5 μM) was treated with an excess ethanol (5 mL). The resulting turbid solution was subjected to centrifugation (5 min, 1,900 g, room temperature). The pellet was treated with HS-PEG-COOH (~ 0.5 g) and ethanol (~ 0.5 mL). The mixture was purged with N2 for 10 min in a sealed vial. It was heated to 60 °C and kept at this temperature for 3 hrs while stirring. A mixed solution of hexane, ethanol and chloroform (11:10:1 v/v/v, 22 mL) was added to the cooled reaction mixture. The resulting turbid mixture was subjected to centrifugation (5 min, 1,900 g, room temperature). The pellet was resuspended in deionized water (5 mL). It was filtered through a Millex-LCR filter. The

filtrate was diluted with deionized water (15 mL) and concentrated with an Amicon Ultra-15 centrifugal filter unit. Two more filtrations were performed to remove unbound ligand. The concentrated phase was diluted with deionized water (~ 1-2 mL) and kept refrigerated (~ 4 °C) until use. The UV-Vis absorbance spectrum of the QDs was recorded on an Agilent diode array spectrometer model 8452 A. relative fluorescence intensity (RFI) measurements were performed on an Eclipse fluorescence spectrometer from Varian Cary (excitation and emission slits: 5 nm; λexc 365 nm). TEM studies were performed on a FEI Tecnai 12, 120 kV transmission electron microscope equipped with an AMT XR80C CCD Camera System. Samples were deposited from dispersions in water or CHCl3 onto Formvar-coated copper grids or a polymer-coated carbon grids. ζ-potentials were measured on a Malvern Zetasizer Nano ZS (Worcestershire, UK).

Suspensions of QDs (absorbance ~ 0.1 at 590-600 nm) in DMEM and FBS-DMEM for AF4 analysis were prepared by dilution of a stock solution in deionized water. Their concentration was calculated using an empirical correlation between optical absorption, particle size, and concentration(Yu, Qu et al. 2003). The solutions were diluted to a concentration of 200 nM (nanoparticles).

4.4.1.2 Asymmetrical flow field-flow fractionation

An asymmetrical flow field-flow fractionation (AF4) system (AF 2000 MT, Postnova Analytics, Salt Lake City, USA) with a channel thickness of 350 µm and controlled by the AF2000 Control software (Postnova Analytics, Salt Lake City, USA) was used. The cross-flow was generated by Khloen syringe pumps (Postnova Analytics) while the axial and focusing flows were delivered by isocratic pumps (PN1130, Postnova Analytics). The system was connected to a UV-Vis. variable wavelength spectrophotometric detector (SPD-20A, Postnova Analytics), a fluorescence detector (RF-10AXL, Postnova Analytics), a multi-angle light scattering (MALS, Dawn Heleos 8+, Wyatt Technology, Santa Barbara, USA), and a quasi-elastic light scattering (QELS) detector (WyattQELS, Wyatt Technology) which is an add-on unit connected to the 90° angle of the MALS Dawn Heleos 8+ detector. The MALS

was equipped with a K5 cell and a GaAs laser operating at 658 nm. It takes measurements at 1 s intervals. Data collection and analysis were done using the ASTRA software version 5.3.4.20 provided by Wyatt Technology. A regenerated cellulose membrane (Z-MEM-AQU-627, Mw cut-off 10 kDa, Postnova Analytics) was used throughout.

The carrier medium (1 mM phosphate buffer, pH 7.4) was filtered through a 0.1 μm Whatman filter prior to use. After flow equilibration, the sample was injected with a flow rate of 0.2 mL/min (injection loop volume: 21.5 μL), followed by a 5-min focusing period with a cross-flow rate of 1.2 mL/min and a detector flow rate of 0.3 mL/min. Following a 1 min transition, the cross-flow rate was decreased linearly from 1.2 mL/min to 0 mL/min within 20 minutes. The elution was continued for 10-min elution without cross-flow to allow elution of large aggregates (size > 60 nm). The detector flow rate was kept at 0.3 mL/min throughout. The detection of the eluted fractionated QDs/aggregates was performed sequentially by UV absorbance at 280 nm, fluorescence (λex 365 nm, λem 635 nm), MALS, and DLS. For MALS, data from the detector positioned at a scattering angle of 90° are reported. The z-average effective spherical hydrodynamic radius of the eluting particles/aggregates was determined by DLS based on cumulant analysis of the scattered intensity correlation functions measured across each eluting band. Each fractogram presented is representative of a triplicate sample. A calibration of the instrument with QD-DHLA samples of increasing concentration was performed first in order to verify that there was no sample loss due to irreversible interactions with the ultrafiltration membrane used as the channel wall and that the signal at the detector was proportional to the concentration of the sample (Figure S4.6.).

4.4.2. Cell culture, stimulation, and analysis

Murine microglia cells (N9) were generously provided by Philippe Séguéla (Montreal Neurological Institute, Montreal, Que., Canada). They were maintained in Dulbecco's Modified Eagle Media (DMEM, Gibco) containing 5 % of fetal bovine serum and 1 % penicillin–streptomycin at 37 ºC, 5 % CO2 in a humidified atmosphere. Culture media was aspirated and the cells were washed with PBS and maintained in DMEM at 37 ºC. They were treated with pharmacological inhibitors purchased from Sigma-Aldrich as follows: Y-27632

(10 μM, 30 min), SB-203580 (10 μM, 30 min), methyl-β-cyclodextrin (5 mM, 30 min), chlorpromazine (5 μM, 30 min) and cytochalasin D (5 μM, 30 min). Subsequently, cells were incubated with QD suspensions in deionized water (100 nM) for 60 minutes in cell culture media (DMEM), in the presence and absence of 5 % FBS as indicated. Subsequently, cells were washed with a PBS/citric acid solution (pH 5.4) to remove QDs weakly bound to cells by non-specific interactions. For fluorescence confocal microscopy imaging, cells were seeded at a density of 20,000 cells/well onto rat tail collagen (Invitrogen) coated cover slips (Fisher) and incubated with/without inhibitors as described above. At the end of the treatment, plasma membranes were labeled with 2 μM PHK67 (Sigma) for 15 minutes, and subsequently washed with PBS containing 1 % BSA (Sigma) for 5 minutes. Fluorescence micrographs were acquired with a Zeiss LSM 710 confocal microscope using Zeiss Zen imaging software. For fluorometric determination of QD uptake, cells were seeded at a density of 80,000 cells/well into 96 clear bottom, black well plate (Costar) and incubated with/without QDs (100 nM) following incubation in presence/absence of inhibitors. Following QD treatment, cells were washed and DMSO was added to each well. The mean fluorescent intensity was measured with a FLUOROstar Optima fluorimeter (BGM, Labtech) with filters set to ex/em = 355/612 nm, employing 4x4 matrix well scanning.

4.4.3. Quantitative Cd^{2+} analysis by flame atomic absorption (FAA)

Standard Cd^{2+} solutions were prepared by diluting a certified standard (SCP Science) Cd^{2+} solution (1000 ppm) with deionized water. The concentration of Cd^{2+} from standard QD solutions (0-100 nM) was measured with a graphite furnace atomic absorption spectrophotometer (Perkin Elmer AAS-700). Cells were seeded at a density of 1,000,000 cells/well into 6 well plates (Sarstedt) and incubated with equimolar concentrations of QDs (100 nM nanoparticle concentration). Following treatment, cells were washed and detached gently by adding PBS containing 0.5 % bovine serum albumin (BSA). Cell samples were counted, spun down and re-suspended in deionized distilled water for determination of cadmium concentration.

4.4.4. Determination of QD uptake by flow cytometry (FACS)

Cells were seeded in 12-well plates (Millipore) and incubated with QDs as described above. At the end of the QD treatment, cells were washed and detached gently by adding PBS containing 0.5 % BSA. Samples were collected and analyzed by a FACS Aria Sorter (BD Biosciences) equipped with a Cyan A laser (Ex 488 nm) and a 612 nm bandpass filter.

4.4.5. Statistical analysis

Data were analyzed using SYSTAT 10 (SPSS). Statistical significance was determined by analysis of variance (ANOVA) followed by post hoc, Dunnett's test, independent t-test or by one sample t-test where specified. Significant differences are indicated by * $p<0.05$, ** $p<0.01$, and *** $p<0.001$

4.5. Conclusion

The responses of cells to QDs are determined by the physicochemical properties of the QDs' surface ligands. These properties change when QDs are exposed to biological media because of interactions between the ligands and various components of the media. The present studies examined these interactions, and consequent changes in cellular responses.

We combined several complementary approaches: 1) AF4 for the separation and characterization of the QD aggregation status, 2) confocal imaging to visualize *in vitro* the aggregation state of the same QDs in simple and complex media and to determine the localization in microglia of these now physically-altered nanocrystals, and 3) pharmacological manipulations to block selected routes of QD internalization by microglia cells. The N9 microglia cells were selected because they are the main cells in the central nervous system that respond strongly to biological and "artificial" aggregates (i.e. man-made nanostructures which self-assemble into aggregates either spontaneously or intentionally in a controlled manner) and serve as biological sensors in the brain. The present study proposes AF4 as a rapid, quantitative and reliable technique for the analyses of aggregate formation and stability in biologically relevant media, such as cell culture media supplemented with

serum. In the case of QDs with short ligands, we observed that aggregates are not formed to the same extent in media enriched with serum proteins, compared to serum-free media. This implies that the protein corona protects QD-DHLA against aggregation, whereas this is not the case for QD-MPA.

Although we used relatively simple media to illustrate how the high salt concentration and protein content in the QD environment change the QD aggregation state, the robustness of AF4 is such that it can be used to monitor the aggregation of QDs and other nanoparticles in more complex media. The important concept is that the biological identity of a nanoparticle rather than its chemical identity will determine the cell response. This concept is valid for any *in vitro* or *in vivo* study using nanoparticles. It is applicable to very complex cellular environments where the acquired biological QD identity is even more profoundly altered. However, determination of essential parameters of each ligand and of the QD itself in its initial, chemically defined state, is critical for making predictions of the possible extent and kind of interactions of nanocrystals with biological molecules, thereby allowing the prediction of at least some of the consequent biological responses. Proteomic analyses of QDs exposed to different proteins, not only from serum, but also from different cellular compartments, are now needed and we are pursuing this line of research. Some initial observations establishing the types of proteins interacting with QDs *in vitro* have been already made (Walczyk, Bombelli et al. 2010, Walkey and Chan 2012). The next step will be to extend these kinds of analyses so as to provide not only qualitative, but also quantitative, data in order to establish the QD biological identity. Such information is critically important for the prediction of aggregate formation in intracellular and extracellular compartments, and their impact on cellular functions. This is particularly relevant to the brain because it is so readily accessed by nanocrystals, accidentally or intentionally.

Figure 4.1. QD characterization

A) Schematic structures of the quantum dots bearing mercaptopropionic acid (MPA), dihydrolipoic acid (DHLA), or poly(ethylene glycol-COOH) (PEG-COOH, 5000 Da). B) Median hydrodynamic diameter, determined by AF4, and zeta-potential, measured using a Zetasizer Nano ZS of the QDs in 10 mM phosphate buffered saline (pH 7.4, 137 mM NaCl), DMEM (pH 7.2) and DMEM + 5% FBS (pH 7.2). C) Absorption and emission spectra of QD-DHLA in water (λex 365 nm. D) AF4 fractograms monitored by UV absorbance (280 nm, full line, left axis) and DLS (Dh, blue open circles, right axis) for QD-DHLA in water, and after a 5-min incubation in DMEM and in DMEM + 5 % FBS.

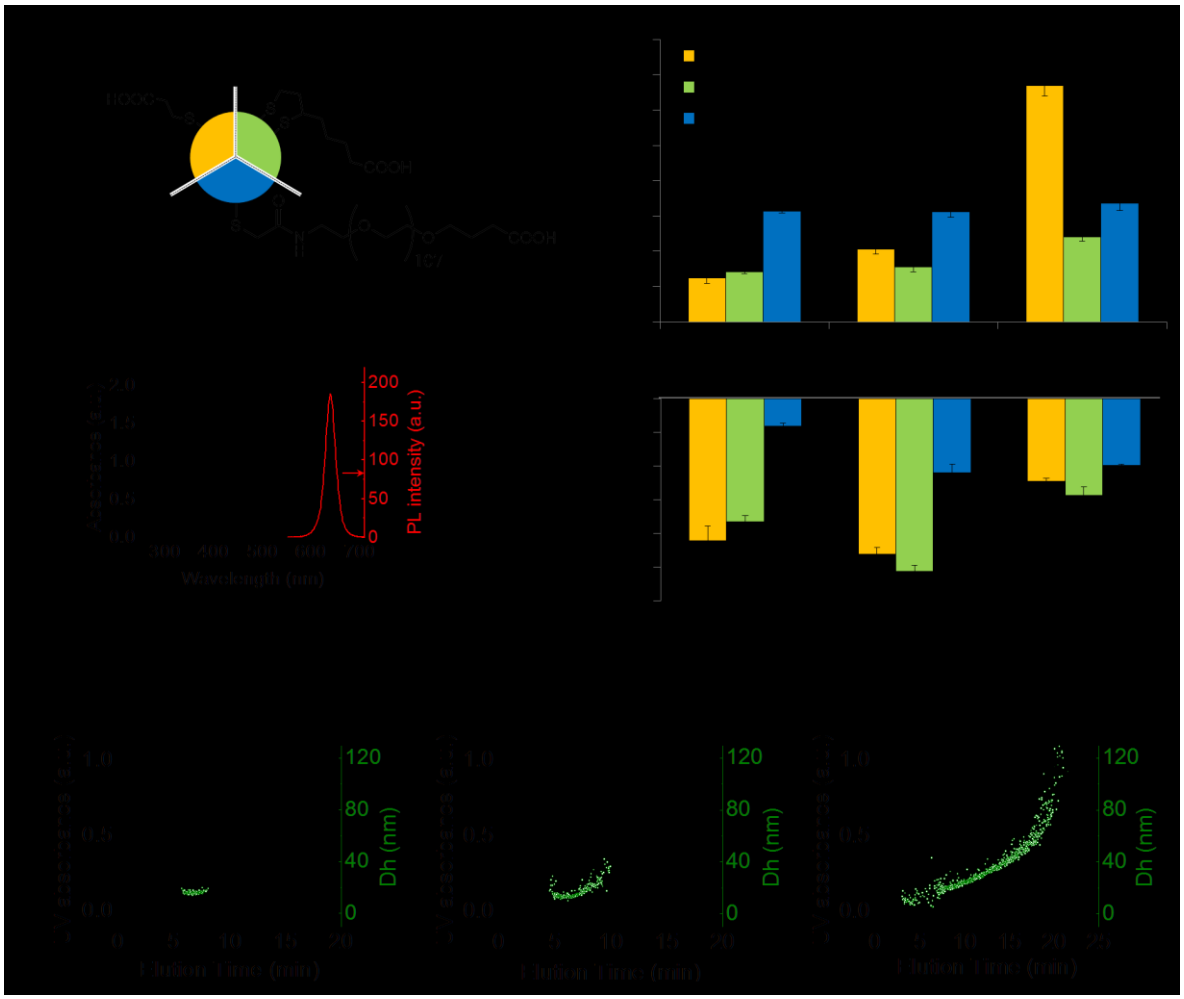

Figure 4.2. QD aggregation status is surface and serum dependent

AF4 fractograms of QD suspensions in DMEM (left) and serum-containing DMEM (right) monitored by UV-absorbance at 280 nm for A) QD-DHLA, B) QD-MPA, and C) QD-PEG-COOH after incubation times of 5 min, 30 min, and 1 hrs; in each panel, the backmost fractogram corresponds to the elution of QDs in deionized water.

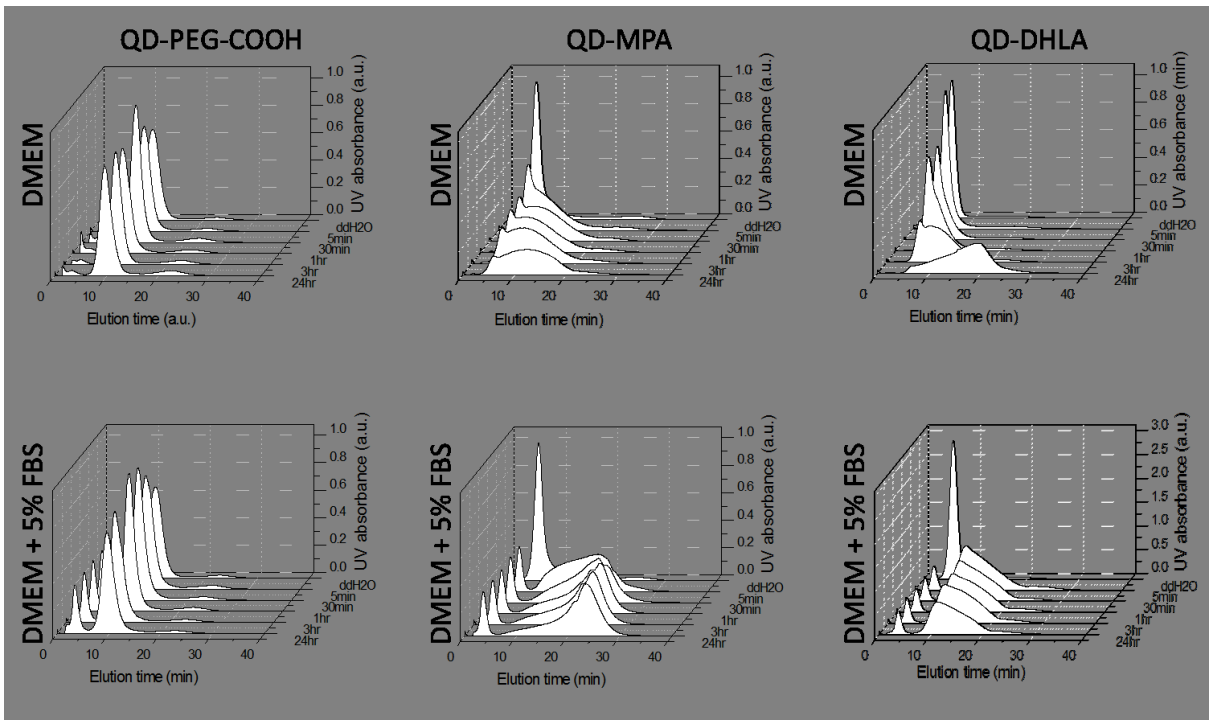

Figure 4.3. QDs are rapidly internalized by microglia cells

A) Live cell fluorescence confocal micrographs of N9 microglia incubated with QD-MPA (100 nM) for 1hr in DMEM. The plasma membrane is labeled in green (PKH) and QDs are visible in red. Z-stack slices were taken at 0.64 μm intervals (from left to right) starting from the surface of the coverslip. Note regions of QD aggregate accumulation primarily near the tips of microglia ramified processes (white arrows) as well as in the cell body (yellow arrows). B) Time course of QD uptake. All confocal images are from the same z-stack. Superpositions of phase contrast and fluorescence images are presented in the middle column, the scale bar representing 30 μm applies for all three phase contrast images. Regions of interest are highlighted in yellow and zoomed in in the last column. Internalized QD-MPA travel towards the microglia cell body 0, 10, and 50 minutes post QD-MPA treatment (100 nM). The QDs monitored are indicated by white arrows. The distance between the representative QDs and a fixed reference point (green arrow) is reported. Representative pictures are selected from triplicates of at least 3 independent experiments. Scale bars represent 20 μm.

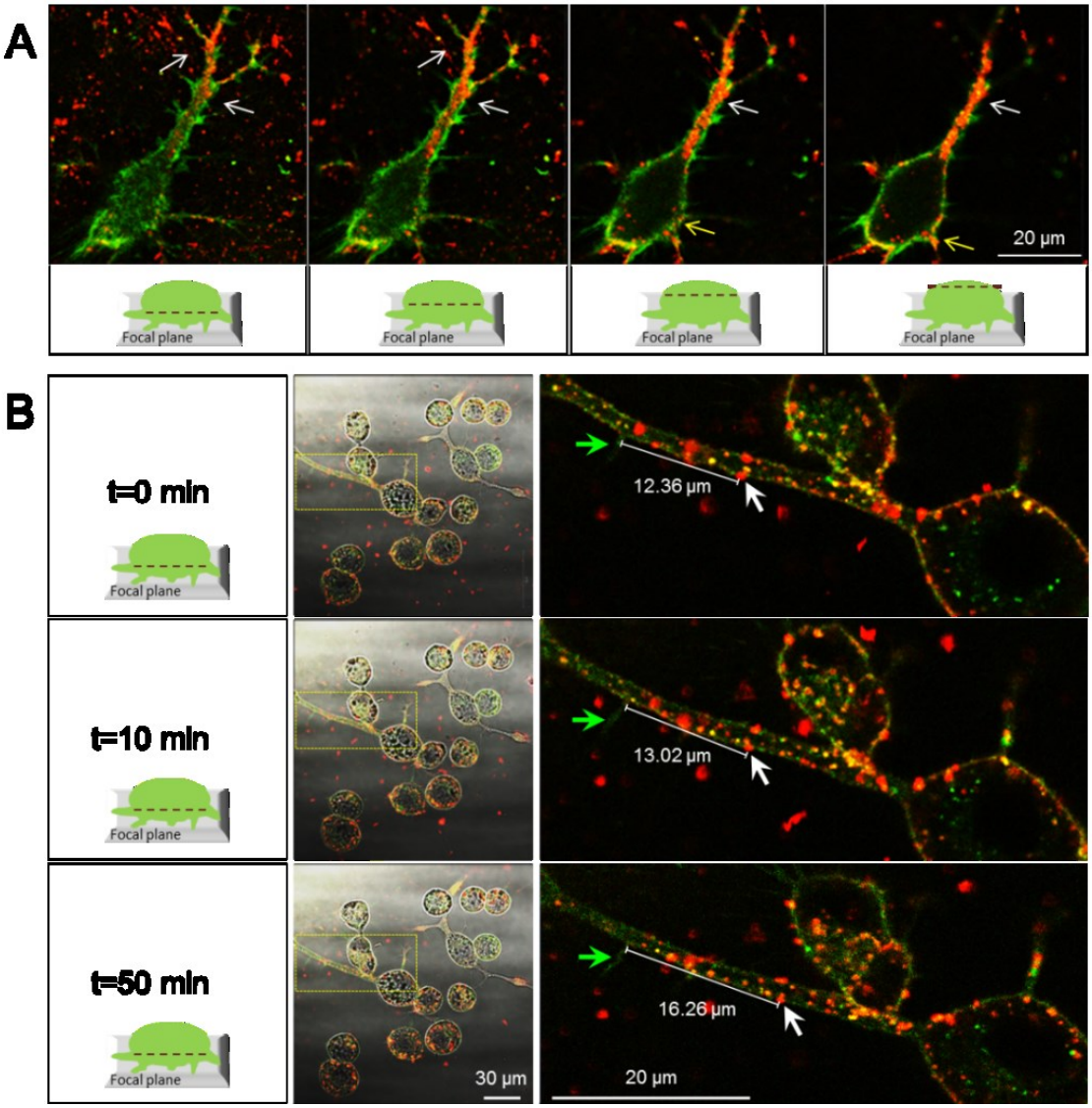
A
20 µm
Focal plane
Focal plane
Focal plane
Focal plane
B
t=0 min
Focal plane
12.36 µm
t=10 min
Focal plane
13.02 µm
t=50 min
Focal plane
16.26 µm
30 µm
20 µm

Figure 4.4. QD aggregation status drives primary mode of uptake

Fluorometric assessment of QD uptake inhibition in N9 microglia in DMEM + 5 % FBS A) and DMEM B) incubated with QD-DHLA, QD-MPA and QD-PEG-COOH (100 nM; 1 hrs) following pre-incubation with MBCD (5 mM), CPZ (5 µM), CytoD (5 µM), SB-203580 (10 µM), and Y-27632 (10 µM) for 1 hrs. The QD uptake inhibition % was calculated with respect to the QD uptake in the absence of inhibitor (set to 100 % uptake). The data represent the means ± SEM (n = 9). *p≤0.05, **p≤0.01, ***p≤0.001.

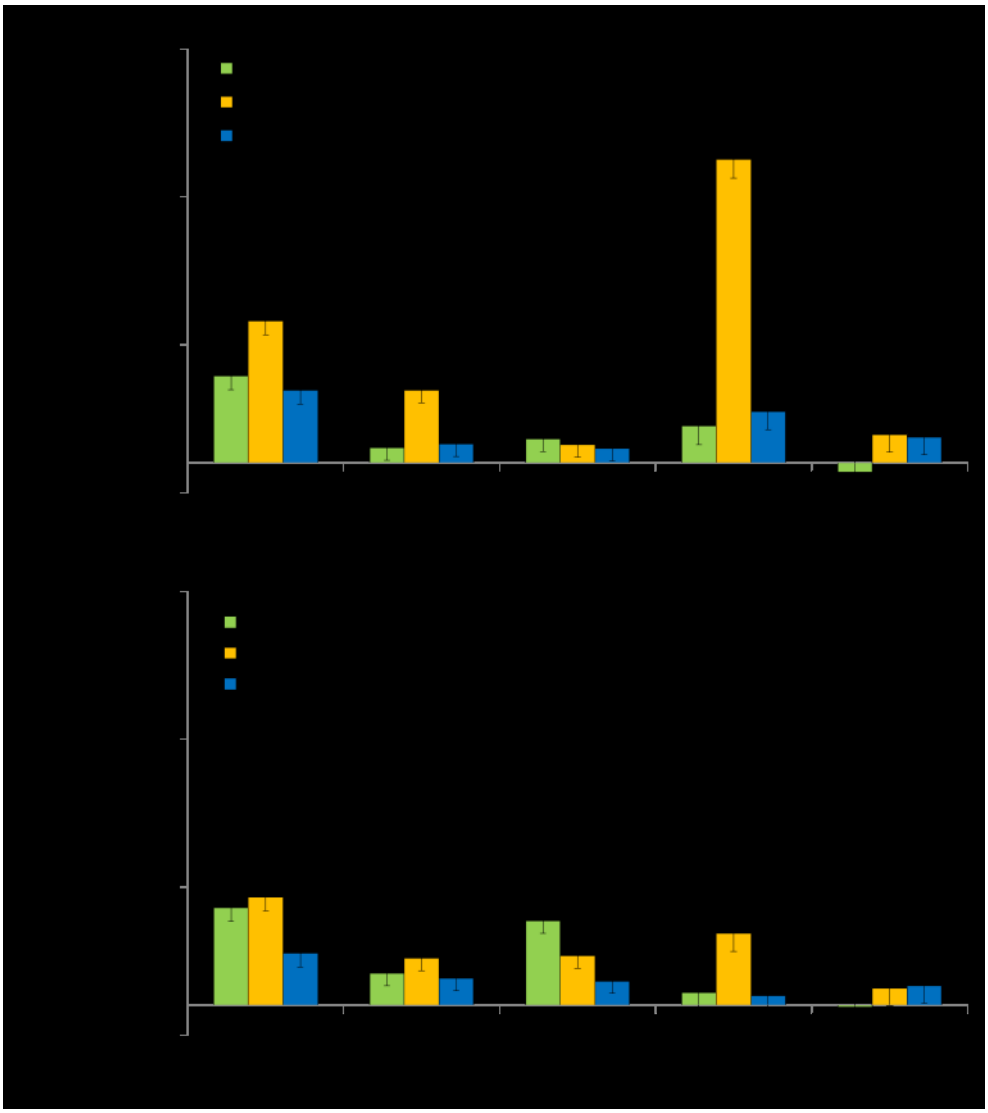

Figure 4.5. Confirmation of QD uptake using intracellular cadmium determination
Live cell fluorescence confocal micrographs of N9 microglia incubated with QD-DHLA, QD-MPA and QD-PEG-COOH (100 nM; 1 hrs) in FBS-DMEM A) or DMEM B). The cells were pre-treated, or not, with SB-203580 (10 µM), inhibitor of phagocytosis. The plasma membrane is labeled in green (PKH) and QDs are visible in red. Representative pictures are selected from triplicates of at least 3 independent experiments. Scale bars represent 20 µm. (right column) Intracellular cadmium content determined by graphite furnace atomic absorption spectrometry.

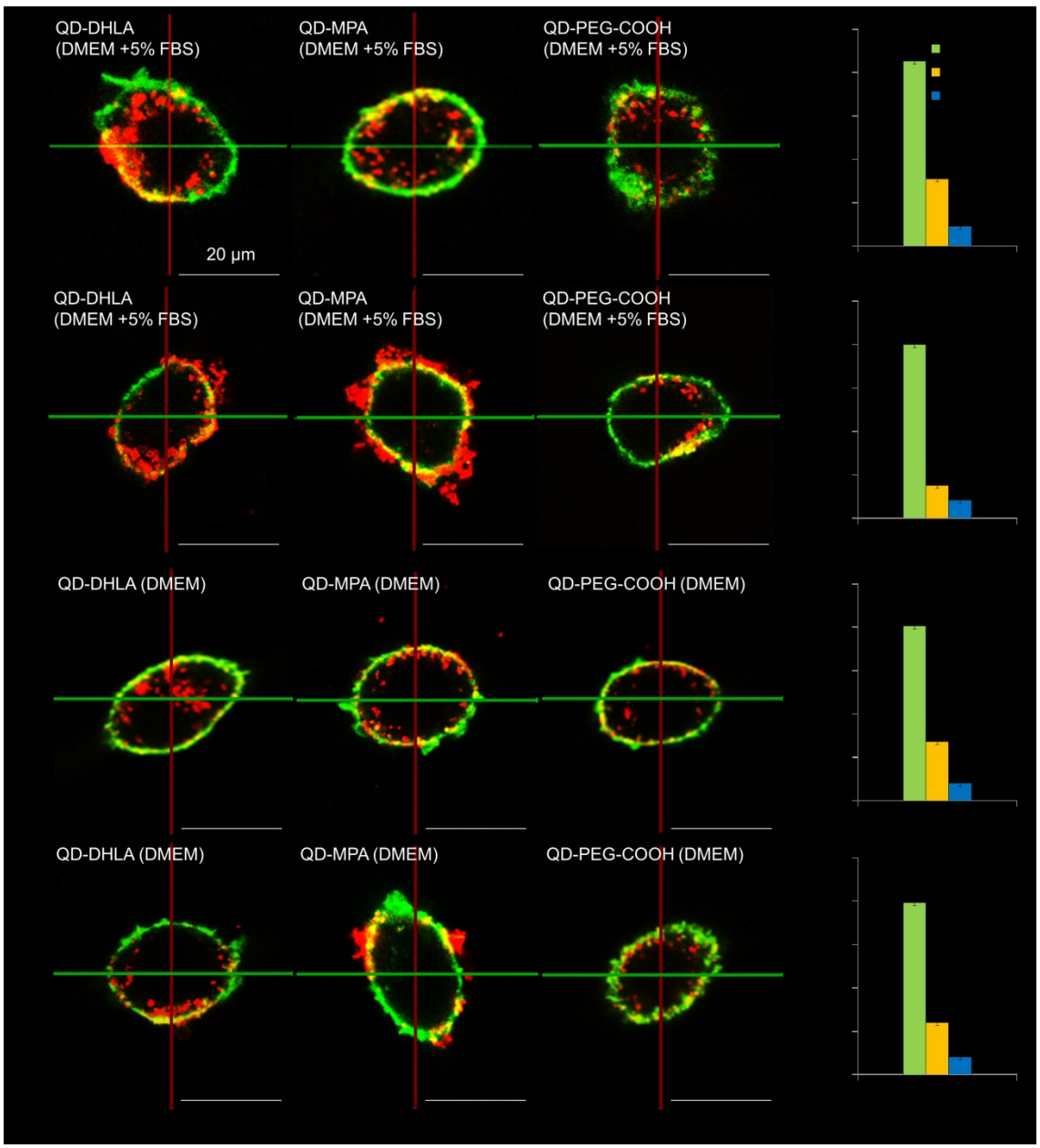

Figure S4.1. QD characterization

AF4/UV/MALS/QELS fractograms of QD-DHLA, QD-MPA and QD-PEG-COOH suspended in deionized water. The fractograms report the UV absorption at 280 nm (black solid line), MALS (red dashed line) and z-averaged hydrodynamic radius, R_h (blue open circles), as function of elution time. Phosphate buffer (1 mM, pH 7.4) was used as an eluent and 21.5 µL of a 200 nM solution of QDs was injected.

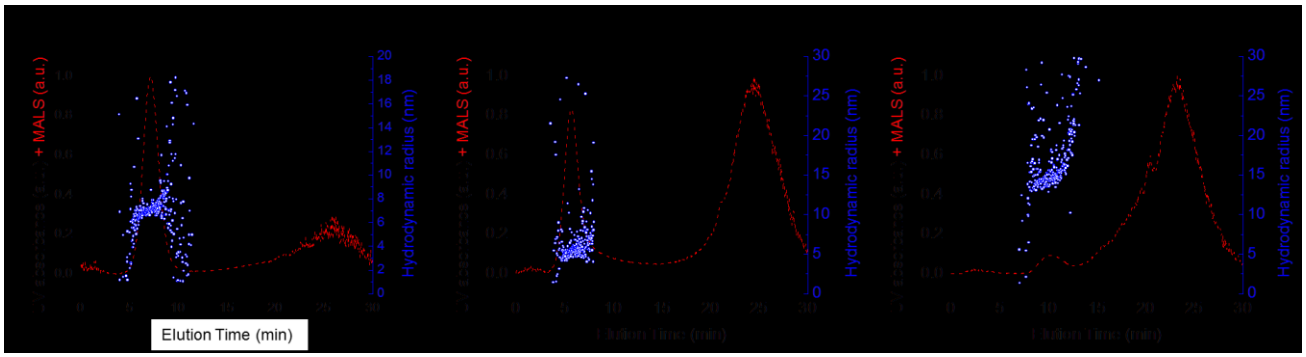

Figure S4.2. QD-PEG are highly stable in serum containing media

Fractograms of QD-PEG-COOH monitored by UV-Vis absorbance at 280 nm (black and grey lines) and hydrodynamic radii of the eluting species (full dots: QD-PEG in water; open squares: QD-PEG in FBS-DMEM). The QDs were incubated in deionized (DI) water or FBS-DMEM for 30 min before injection in the AF4 instrument. The UV-Vis fractogram of FBS-DMEM alone is also reported for comparison. It is superimposed with the peak at 5 min of QD-PEG in FBS-DMEM. Eluent: phosphate buffer (pH 7.4, 1 mM).

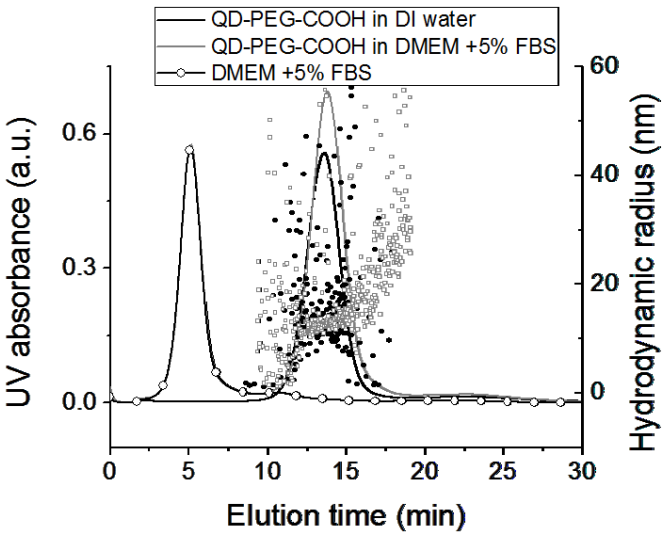

Figure S4.3. Z-stacks from live cell confocal microscopy confirm intracellular localization following QD uptake

Live cell confocal microscopy of N9 microglia cells incubated with QD-MPA (100 nM; 1 hrs) in serum containing media (DMEM + 5 % FBS) in the absence and with SB-203580 (10 μM, 30 min). Representative pictures are selected from triplicates of at least 3 independent experiments. 3D reconstructions (top left panel) were made by compiling 20 z-stacks (0.64 μM intervals), with orthogonal sectioning shown (top right panel). Individual z-stacks are shown (bottom panel). Scale bars represent 20 μm.

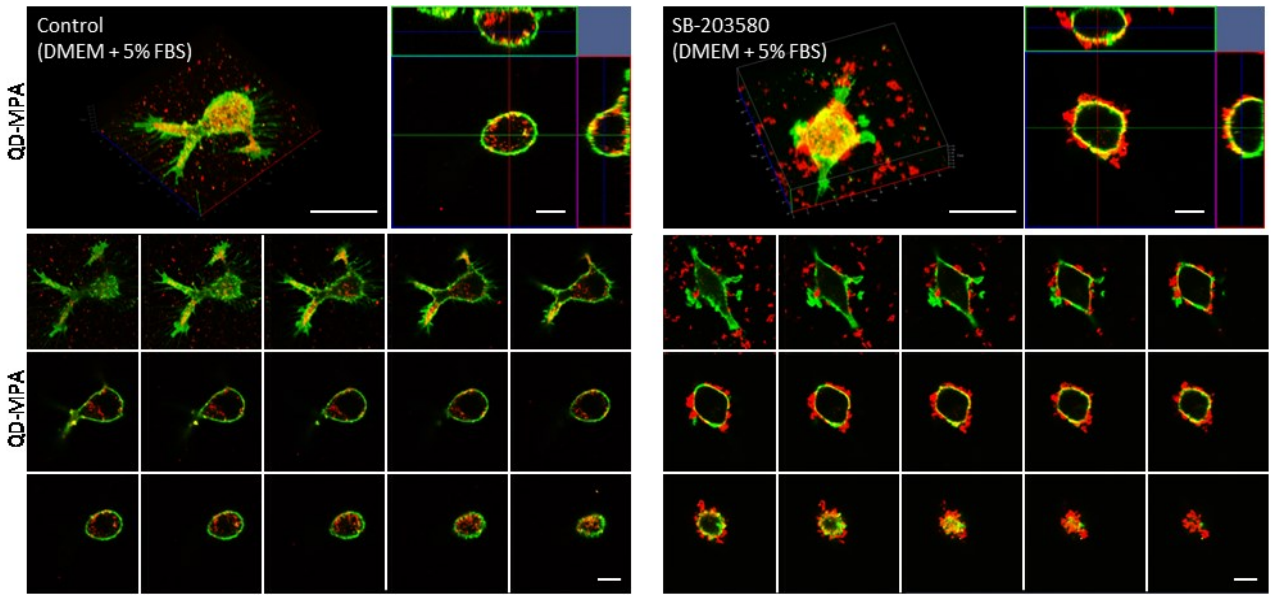

Figure S4.4. Pharmacological inhibitors of internalization are non-toxic at the concentrations used

N9 cells were pre-treated with inhibitors of internalization (MBCD, CPZ, CytoD, SB-203580 and Y-27632) for 1 hrs, followed by incubation with QDs for 1 hrs (100 nM). Cell viability was measured using the MTT cell viability assay and expressed as relative cell viability with respect to control (set to 100 %).

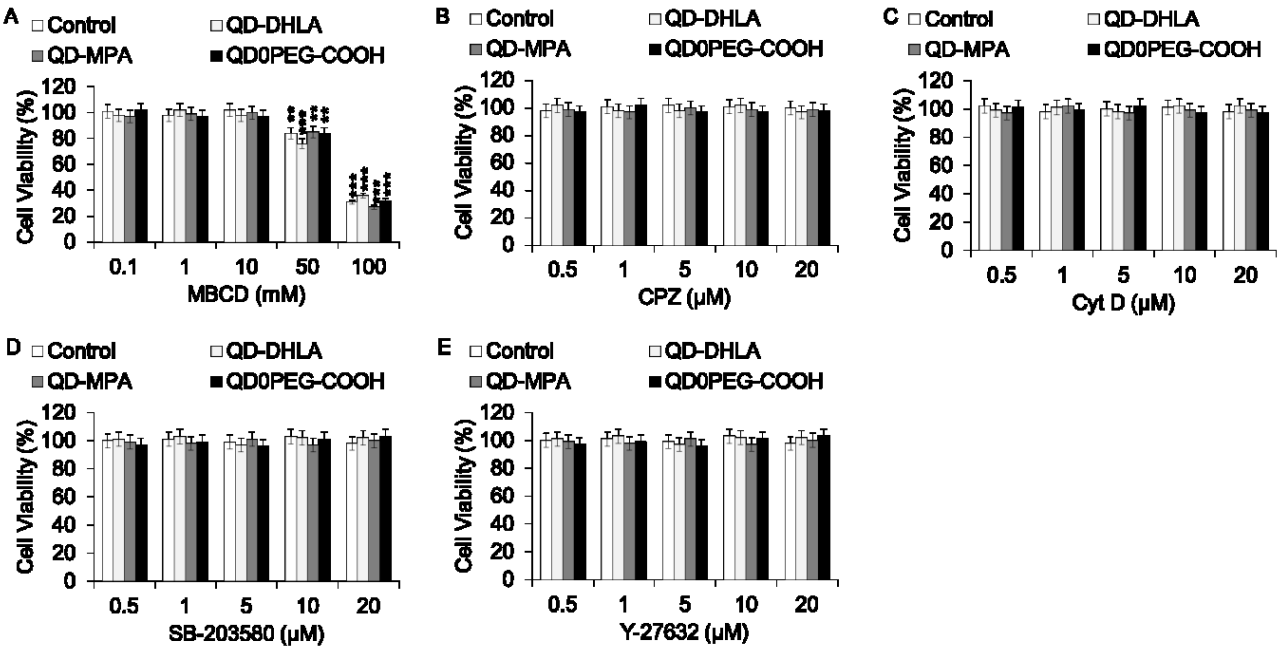

Figure S4.5. QDs are highly stable in deionized water

AF4/UV-VIS fractograms of three differently coated QDs (from back to front: QD-PEG-COOH, QD-MPA, QD-DHLA) in deionized water (DI) with or without SB-203580 (10 mM) or Y-27632 (10 mM). Eluent: phosphate buffer (pH 7.4, 1 mM).

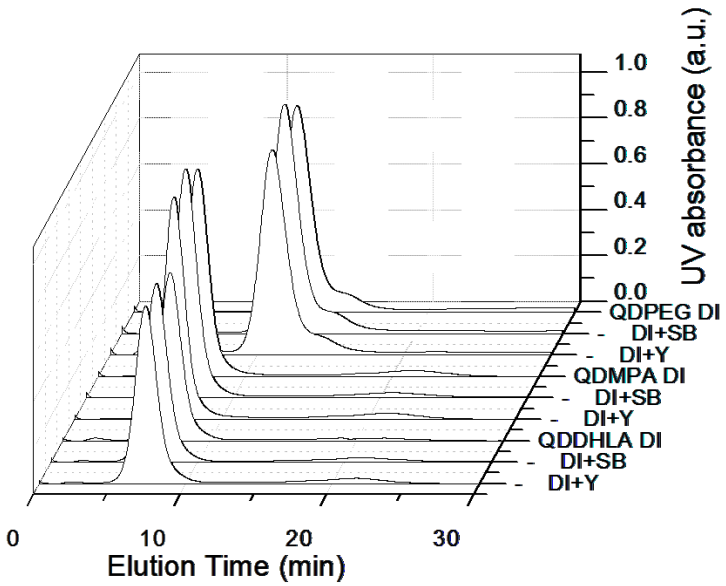

Figure S4.6. AF4 instrument calibration

Calibration of the AF4 instrument using increasing concentrations of QD-DHLA suspended in deionized water. The concentration of the QDs was determined by measuring the absorbance at the first excitonic peak. Linear relationship between the area under the curve measured of the QD-DHLA in water and the concentration of the solution injected over the range of 7.8 nM to over 261 nM. Eluent is phosphate buffer (pH 7.4, 1 mM).

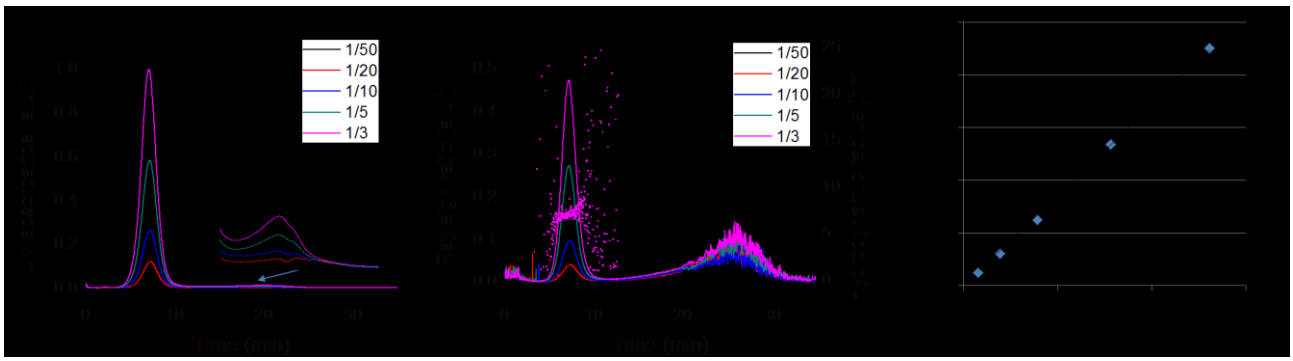

Figure S4.7. Aggregation dependent toxicity

Cells were incuabed at 30°C with QDs in DMEM media containing 10% FBS for 24 hours. For the preincubation treatment, QDs were incubed at 30°C in DMEM media containing 10% FBS for 24 hours prior to the start of the experiment. Relative metatbolic activity was assessed via cell counting. Data represents the mean +/- SEM from triplicates. Statistically significant differences are indicated by p* <0.05, p** <0.01, p*** <0.00

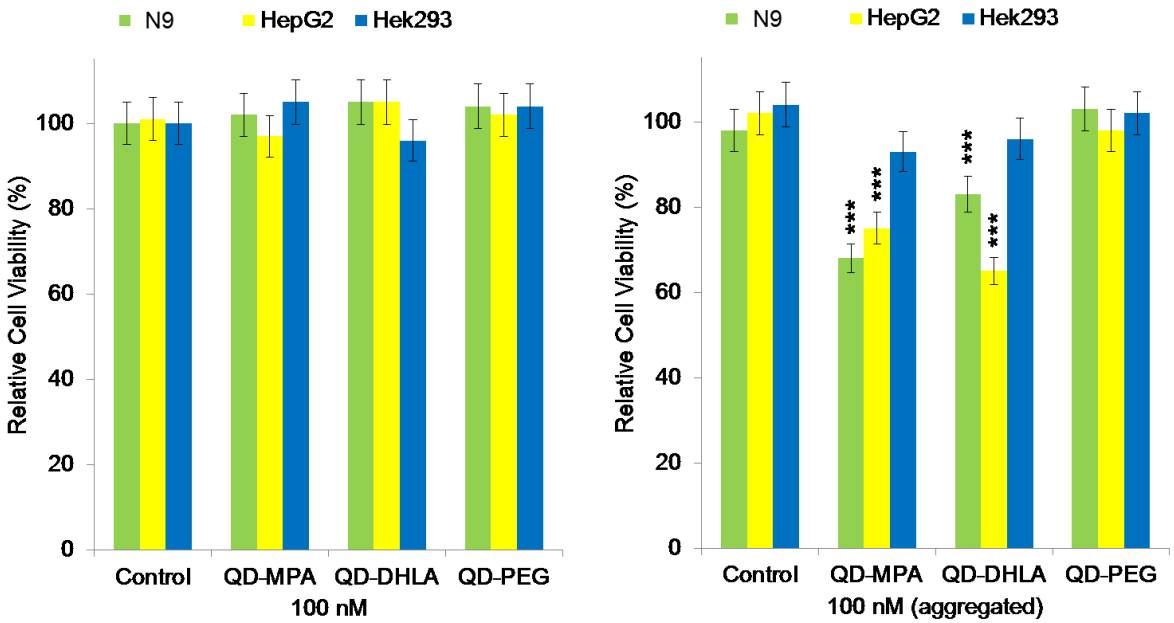

Chapter 5. General Discussion

Recent developments in nano-scale technologies have unlocked new and exciting avenues of biomedical research. Since the 1980s, regulatory agencies have approved several nanoparticles specifically designed for applications in the human body, in addition to a multitude of others that have the potential to gradually bio-accumulate in humans over time following indirect routes of exposure. As a result, concerns are now being raised with regards to the growing production, use and subsequent disposal of engineered nanoparticles as well as their potential to accumulate in ground and surface waters and soils. In the biological environment, nanoparticles may present a significant environmental risk as they are degraded, bio-transformed and accumulated in a variety of ways (Colvin 2003).

Once nanomaterials enter the human microenvironment through inhalation, ingestion and/or dermal absorption, they encounter a complex milieu of ions, proteins, cells, tissues and organ systems. Despite their unique physical and chemical properties and promising widespread applications in biology, we presently have a very poor understanding of how cells within the body will respond to these nanoparticles, and equally important, how the nanoparticles will react to components of the biological microenvironment. A dynamic back and forth occurs between the synthetic and biological components, a phenomenon which is often overlooked and can lead to a significant confusion in the literature. Therefore, there is a growing need for studies investigating how these nanomaterials will interact with the biological milieu and what is the overall impact on cell function. The studies described herein aim to uncover the underlying nature of these interactions.

The objectives of this thesis are three-fold; 1) to elucidate the mechanisms underlying the adaptive cellular response to quantum dots, 2) to investigate modified quantum dot surfaces with small ligands and to study the nanoparticle-cell interactions at the nano-bio interface and 3) to explore the effect of the biological microenvironment on particle stability and cellular fate. We showed in Chapter 2 that exposure to uncapped cadmium telluride QDs resulted in the generation of oxidative stress, detectable by functional changes at individual subcellular organelles, including the mitochondria and lysosome. We noted that cytotoxicity could be controlled by modifying QD surfaces with short capping ligands. These studies highlighted the role of QD surface properties in determining the cellular response and led us

to further investigate this relationship. In Chapter 3, we systematically investigated the influence of surface charge on nanoparticle internalization. We prepared QDs with different surface functionalization and showed that surface properties play a major role in determining the primary mode of uptake into human cells. We furthered these studies in Chapter 4 by demonstrating the effect of biological molecules such as salts and proteins on QD stability and uptake.

These studies have advanced our understanding of how nanoparticles interact with cells, and the biological consequences of these interactions. With this knowledge, we can better predict how nanoparticles will behave in biological systems, guiding sensible design strategies for future nanomedicines. In this final chapter, we discuss the implications of the work that was carried out and the relevance to ongoing investigations in nanomedicine. In addition, we reflect on the limitations of our findings and how our investigations could be pursued further.

5.1. Nanoparticle characterization

In the previous chapters, we highlighted the role that nanoparticle surface properties play in directing interactions at the nano-bio interface, ultimately driving cellular fate. Findings from Chapter 3 in particular, have emphasized that the size distribution of nanoparticles is sensitive to changes in the microenvironment, in particular due to serum proteins adsorbed at the particle surface. Therefore, it is important to characterize nanomaterials in the context of the biological environment, as the size change may affect how the particle will be distributed in the body, its toxicity and its immunological profile. Since the challenges of nanoparticle characterization are becoming more apparent, a multitude of complementary characterization techniques have been developed to accurately assess nanoparticle size, shape and surface properties (Murdock, Braydich-Stolle et al. 2008, McNeil 2011, Cho, Holback et al. 2013). In the following section, we discuss the advantages and limitations of several techniques currently used to characterize nanoparticles.

5.1.1 Dynamic light scattering

Dynamic light scattering (DLS) is one of the most commonly used techniques to determine nanoparticle size. The DLS technique owes its popularity to its simplicity, speed and ease of use. A monochromatic light beam is used to illuminate the sample. Light scattered by the sample is measured by a sensor which is placed at 90° relative to the laser beam. The intensity of light scattering depends on the size of the nanoparticle; the larger the particle, the greater the light scattering.

DLS is a useful technique to measure the size of nanoparticles ranging from 10-1000 nm (Chen, Zhao et al. 2007). However, DLS can provide only low resolution between species in a polydisperse sample due to the nonlinear dependence of scattered light intensity to nanoparticle size. Since only a small number of larger particles can completely saturate the signal of the smaller particles, DLS is not useful for measuring polydisperse samples. In addition, the sizes obtained by DLS are made assuming the particle has a spherical shape.

5.1.2. Fluorescence correlation spectroscopy

Fluorescence correlation spectroscopy (FCS) is a characterization technique that is based on a similar principle to that of DLS. It determines the hydrodynamic size based on the photophysical properties of the nanoparticle. As such, it is only applicable for fluorescent particles. The technique uses a laser to excite the fluorescent sample and measure the diffusion coefficient which is related to particle size by the Stokes-Einstein equation (Haustein and Schwille 2007). FCS is much more sensitive than DLS, but it is applicable only to a narrow concentration range.

5.1.3. Nanoparticle tracking analysis

Nanoparticle tracking analysis (NTA) is a newly developed technique which provides the direct sizing and counting of nanoparticles. The system combines conventional optical imaging and fluorescence imaging to visualize the sample under a microscope (Wright 2012). The technique works by tracking individual particles, relating the degree of movement under Brownian motion to particle size, allowing high resolution particle size distributions of polydisperse samples to be obtained within minutes (Filipe, Hawe et al. 2010). NTA provides a particle by particle count, not a weighted average. This technique can be used to characterize particles ranging in size from 30-1000 nm, however the samples must be sufficiently diluted. This technique is unique in allowing the direct determination of sample concentration, which can be difficult for other techniques, especially in complex biological media. Nanosight Inc., a private developer of this technology, is actively working to increase the sensitivity of the technique so that smaller nanoparticles (<30 nm), such as quantum dots, can be analyzed.

As opposed to DLS and FCS related techniques, microscopy can provide information on the size, shape or structure of the particles investigated. The visualization of the samples can be made using beams of electrons or photons, or by moving a fine probe across the sample surface. Some of these techniques can also be used to obtain the elemental composition, or even the surface charge.

5.1.4. Transmission electron microscopy

Traditional optical microscopy is limited in the analysis of nanoparticles above 200 nm due to the diffraction limit of transmitted light. For the purposes of nanoparticle characterization, microscopy using a beam of electrons as the illumination source is more suitable, due to the shorter wavelength of photons compared to visible light.

In transmission electron microscopy (TEM), an electron beam is passed over a thin layer of the test sample, which is placed on a grid of a conductive material. After passing through the sample, the electrons that have not been absorbed are focused onto a detector. The resulting image is a function of the electron density of the sample species present on the grid and its thickness. For analysis of an organic material, the sample must be first fixed by a mixture of heavy metals such as uranyl acetate or osmium tetroxide. TEM can also be used to determine the intracellular localization of electron dense materials, particularly relevant for metallic nanoparticles (Nativo, Prior et al. 2008). The high-resolution TEM (HRTEM) can generate images with sub-nanometer resolution (0.2-0.3 nm) and can provide information on the atomic arrangement of the surface of the nanoparticles (Pasricha 2011).

The limitations of electron microscopy are mainly the cost of the instrument and the sample preparation steps. Nanoparticle samples must be treated and dried before analysis, which can change the size of the species producing artifacts. Further evaporation of the solvent may induce the agglomeration between species where the concentration is artificially increased.

5.1.5. Asymmetrical flow field-flow fractionation

As opposed to optical characterization techniques, field-flow fractionation can be used to separate a complex mixture of nanomaterials depending on the sizes of the species present in the sample. Asymmetrical flow field-flow fractionation (AF4) is a separation technique where a sample suspension is applied to a carrier liquid which is pumped through a long and narrow channel. A cross flow can be applied to the sample, perpendicular to the

direction of flow, in order to cause a separation of the particle present in the solution. Particles are separated depending on their differing mobility under the force exerted by the flow of the carrier liquid. Under ideal conditions (in the absence of interactions between the sample and the components of the instrument), the elution rate in the channel depends directly on the particle size of the injected species.

Typical AF4 operation involves three distinct steps. First, the sample is injected into the system using a known sample volume. The volume depends on the type of AF4 instrument, but is typically in the microliter range. Next, in the focusing step, particles in solution are pushed towards the membrane that lines the bottom of the channel by the cross flow. The particles scatter against the membrane and rest at a distance according to their diffusion coefficient. The smaller particles, having a higher diffusion coefficient, will rest closer to the center of the channel, while larger particles will rest closer to the membrane. Thus, a gradient of particle sizes is formed in the channel. Finally, in the elution step, the opposite longitudinal flow is turned off and the particles can begin to elute out of the column due to the channel flow. The channel dimensions are such that the elution exhibits laminar flow, so the distribution of the velocities is parabolic with the maximum at the center of the channel. At the edges of the channel, the velocity is almost zero. Small particles will elute with greater velocity compared to larger particles that are retained close to the walls by the applied field. The eluted species may be subsequently recovered following separation to purify the sample and/or perform complementary characterization steps using other techniques.

In order to monitor the output of the eluting particles, several detectors can be coupled to the instrument. The most common is the UV absorbance detector which measures the concentration of species emerging. In addition, highly sensitive elemental detectors such as inductively coupled plasma mass spectrometry (ICP- MS) can be used to characterize the composition of the particles as they elute. Particle detectors including dynamic light scattering can be installed for obtaining information on the particle size or the molecular weight regardless of the retention time. The main drawback to the AF4 is the time required to optimize the fractionation conditions for a new sample. Many parameters will play on the

retention time of particles in the system. Two of the most important will be the nature of the composition used and the accumulation of the membrane solvent. These parameters should be chosen to minimize particle-particle and particle-membrane interactions.

The AF4 technique is particularly useful in the analysis of complex samples and offers several advantages over other characterization techniques. AF4 allows a wide range of particle sizes to be simultaneously analyzed following separation by the instrument, from a few nanometers to several microns in diameter. In addition, it is suitable for analyzing neutral and charged particles alike. When coupled to fluorescence analysis or dynamic light scattering, AF4 can measure the size and quantity of each species that eluted out of the instrument. Thus it is possible to make a complete analysis of the species present in the sample. This is particularly useful in the analysis by dynamic light scattering because particles of different sizes elute separately, allowing for the sequential analysis of several distinct monomodal populations. The size distribution can then be related precisely to the concentration and the size of each population within the sample. Several examples of AF4 applications for nanoparticles and pharmaceutics have been recently highlighted in the literature (Yohannes, Jussila et al. 2011, Moquin and Winnik 2012).

Nanoparticle size and by extension, the degree of particle aggregation, will have a significant effect on its physical interactions when in contact with the biological environment. Thus, proper characterization is an essential component of any valid nanoparticle evaluation. AF4 is one of very few techniques that can be used to accurately assess particle sizes in complex biological media. Therefore, it is essential to use several complementary techniques, which together provide reliable information concerning particle size and aggregation status in the aqueous environment or biological media of interest (Rogers, Franklin et al. 2007, Gaumet, Vargas et al. 2008, Hassellov, Readman et al. 2008).

5.2. Nanoparticle-cell interactions

In addition to the covalent functionalization of nanoparticles with proteins for targeting, delivery or stability purposes, there is a tendency for other proteins present in

biological medium to spontaneously adsorb to the nanoparticle surface, especially given the large surface area to volume ratio (Nel, Madler et al. 2009, Zhu, Posati et al. 2012). This type of adsorption is driven by the abundance of proteins in the serum which readily come into contact with the particle surface. Serum proteins are particularly significant, given that the primary route of administration for most medically relevant nanoparticles is intravenous (IV). Interactions with components of the serum play an important biological role, especially in the case of the immune system, where foreign particles can be specifically marked for ingestion and destruction by phagocytes following the binding of an opsonin such as immunoglobulin (IgG). Alternatively, the non-specific adsorption of molecules, atoms, ions, or larger particles to the nanoparticle surface will increase recognition and uptake by the mononuclear phagocyte system (MPS) (Ehrenberg, Friedman et al. 2009). The MPS plays an important role in the host immune response and is primarily made up of monocytes and macrophage cells which accumulate in the liver and spleen.

2.3. Biological vs. synthetic identity

When a population of proteins become adsorbed and coat the particle surface, it is referred to as the protein corona. The protein corona can be composed of several sub-layers according to the strength of the molecular interactions between proteins and the particle surface (Walkey and Chan 2012). The composition of the protein corona can be varied and plays an important role in the function and distribution of the nanoparticle (Cedervall, Lynch et al. 2007, Cedervall, Lynch et al. 2007, Casals, Pfaller et al. 2010, Maiorano, Sabella et al. 2010, Walczyk, Bombelli et al. 2010, Lundqvist, Stigler et al. 2011, Kah, Chen et al. 2012). One of the most commonly used serum proteins in cell culture is serum bovine albumin (BSA). Electrostatic forces appear to play a major role in attracting the BSA to surface of the nanoparticles (Wang, Zhang et al. 2012). Although albumins are a major component of the serum, other proteins are commonly found adsorbed to the particle surface. Therefore it is necessary to consider the exact composition of the protein corona.

The structure and composition of the protein corona depends on 3 key factors: 1) the synthetic identity of the nanomaterial (size, shape and composition), 2) the nature of the

physiological environment (blood, interstitial fluid, cell cytoplasm, etc.), and 3) the duration of exposure (Walkey and Chan 2012). Adsorbed proteins can be identified and quantified using mass spectrometry, gel electrophoresis, centrifugation, differential sedimentation, western blot and proteomic analysis (Cedervall, Lynch et al. 2007, Cedervall, Lynch et al. 2007). A recent study investigating the composition of the protein corona identified over 125 different plasma proteins which interacted with nanoparticles of varied size and shape, forming the "adsorbome" (Walkey and Chan 2012). The physiological function of the proteins in the adsorbome varies, but they are generally involved in lipid transport, blood coagulation, complement activation, pathogen recognition or ion transport (Lundqvist, Stigler et al. 2008). The protein corona appears to follow a general structure, with 2 to 6 proteins (ex. apolipoprotein AI, albumin, IgG and fibrinogen) adsorbed at high abundance, and many more adsorbed at low abundance, depending on the composition of the nanomaterial (Walkey and Chan 2012). The amount and identity of adsorbed proteins at the particle surface depends on the intrinsic properties of the ligand, inducing packing density, molecular weight and length. The opsonization process is a major obstacle to the controlled delivery of drugs or nanoparticles, because it hides the surface ligands used for their active targeting (Salvati, Pitek et al. 2013).

Addition of PEG or other macromolecules (e.g. polysaccharides) on the nanoparticle surfaces prevents protein adsorption, interactions among particles and interactions with immune cells; thereby avoiding premature elimination from the circulation (Cheng, Teply et al. 2007). Furthermore, the length of PEG chains on QD surfaces was found to greatly influence their uptake by the MPS (Daou, Li et al. 2009). Regardless of QD size, the ones coated with longer chained PEG (>12 kDa) have longer blood circulation half-life, and were found to accumulate less in the liver.

A cell does not recognize the nanoparticle as has been characterized in aqueous solution. The synthetic identity is not what comes in contact with the cell, but rather the biological identity which includes the protein shell covering the surface of the nanoparticle. It is the biological identity that will dictate the physiological response of the cells, including the activation of signaling pathways and nanoparticle uptake. It is also important to consider that

the biological identity is sensitive to changes in the nanoparticle microenvironment, which can be altered depending on the location of the nanoparticle. Indeed, as nanoparticles pass from the bloodstream to other physiological compartments such as the cytoplasm of a cell, its biological identity can be modified accordingly (Clift, Bhattacharjee et al. 2010, Lundqvist, Stigler et al. 2011).

5.4. Quantifying nanoparticle uptake

The fundamental unit of nanoparticle dose should be considered as the number of particles internalized per cell. Assessing the dose in nanoparticle–cell interactions is inherently difficult due to the complexity of nanoparticle uptake and lack of sensitive quantification techniques (Summers, Brown et al. 2013). The extent and rate of nanoparticle internalization can be measured using several different techniques, but comparability of data between different research groups and industry partners is hindered by lack of standardized methods (Elsaesser, Taylor et al. 2010, Gottstein, Wu et al. 2013). Furthermore, the distinction between internalized particles (within the cytosol) and those strongly associated with the plasma membrane though specific and non-specific interactions, has remained a challenge for many years, although this distinction is critical for proper interpretation of the results. Traditional methods to verify intracellular location, such as confocal microscopy, are typically not quantitative and do not lend themselves to high-throughput analysis. Several recent studies have outlined new useful strategies for quantifying the extent of nanoparticle uptake which include low-throughput, high resolution electron microscopy (Summers, Brown et al. 2013) and high-throughput flow cytometry techniques (Gottstein, Wu et al. 2013).

Throughout this body of work, we used several complementary techniques to indirectly measure nanoparticle uptake in cells. Fluorescence based semi-quantifications were made used micro-plate and flow cytometry techniques, yielding comparable results (Figure 3.4.). As previously discussed, there are certain limitations that are inherent to any fluorescent based assay, especially those which involve QDs as their photophysical properties are highly sensitive to changes in the local extracellular and intracellular environment. As such, we also carried out elemental analysis for Cadmium, which is normally present in very

low concentrations within the cell and cell culture media, as an indirect measure of QD uptake (Figure S3.4 B). Our results show that fluorescence based approaches and intracellular cadmium determinations yielded similar results with regards to total QD uptake (Figure S3.4. and Figure 4.5.).

To better estimate the number of QDs present in a cell (or QD dose), we can correlate intracellular cadmium with the cadmium present in known concentrations of QD stock solutions. In Aim 3, we measured the intracellular cadmium concentration at the peak of QD uptake (6 hrs; 10.79 mg/L - Figure S3.4.). Assuming that all the cadmium within the cell lysate derived from intact QDs, we can indirectly calculate the amount of internalized QDs. This is not entirely true, given the possibility that the stock QD solutions contain a certain amount of free cadmium leftover from the synthesis, which we show can accumulate in the cell (white bars - S3.4.). With this in mind, we believe that the vast majority of cadmium does indeed come from the QD core. Back calculating the QD concentration from the standard curve (10.79 = 0.2358x), we get a QD-CYS concentration of 45.75 nM per sample. Using Avogadro's number, we can then calculate the number of QDs (45.75 nM x 6.022e+23 mol^{-1}) which gives us 2.755e+16 QDs per sample. Since we seeded 1,000,000 cells per sample, this corresponds to approximately 2.755e+10 QDs per cell. A study measuring QD internalization using flow cytometry have estimated uptake to range between 2-100 million QDs/cell in a dendritic cell line (Mittal and Bruchez 2009). Another study using high resolution TEM imaging, estimated between 1-10 million QDs/cell, but showed a high degree of variability within the cell population suggesting that nanoparticle-cell interactions are not consistent on a cell by cell basis (Summers, Brown et al. 2013). It is possible that small variations in cell morphology, plasma membrane composition, receptor expression or intracellular parameters such as endogenous redox potential or lysosomal content (as described in Chapter 2) may be responsible for the observed variability in nanoparticle uptake and cellular response. The mechanisms which drive these interactions are still unclear and require further study.

5.4.1. Subcellular localization

Following internalization by endocytosis, nanoparticles tend to be found in endosomal compartments. The contents of these dynamic transport vesicles are often degraded by fusion with lysosomes. Lysosomes contain many proton pumps which progressively decrease the pH of the compartment which activate resident hydrolases. Under these harsh acidic and proteolytic conditions, most endosomal materials are degraded, including many nanoparticles. It is possible to avoid destruction by escaping the endosomal compartments into other organelles such as the cytosol, mitochondria or nucleus. One such strategy is termed the proton sponge effect (Nel, Madler et al. 2009). Cationic nanoparticles bind with high affinity to lipid groups at the plasma membrane. Following endocytosis and transport through endosomes, these cationic nanoparticles enter into an acidifying compartment following fusion with lysosomes. The amino groups are capable of sequestering protons supplied by the v-ATPase (proton pump), required for the activation of hydrolytic enzymes present in the lysosome. This process keeps the proton pump activated and leads to the retention of one Cl- ion and one water molecule per proton. Subsequently, the lysosome swells with the excess water and eventually ruptures, leading to the escape of particles in the cytoplasm and the spillage of the lysosomal content (Stern, Adiseshaiah et al. 2012, Crist, Grossman et al. 2013). This strategy is used to specifically target cargo to the cytosol and other cellular organelles, such as siRNA (Dominska and Dykxhoorn 2010).

5.4.2. Fluorescence lifetime imaging

While the favourable optical properties of QDs have been exploited and improved for molecular imaging applications in recent years, the vast majority of studies have used emission intensity-based techniques. This is primarily due to the fact that these methods require relatively inexpensive instruments and offer greater ease of operation. New modalities of fluorescence imaging, namely fluorescence lifetime imaging (FLIM), have recently become more accessible and offer significant advantages over traditional bioimaging techniques such as improved resolution, sensitivity and concentration independent effects of the fluorophore (Marcu 2012).

The fluorescence lifetime refers to the average time a molecule stays in its excited state before emitting a photon. Quantum dots have an average lifetime of 10-100 ns depending on their composition, while organic fluorophores have a shorter lifetime of 1-10 ns (Grecco, Lidke et al. 2004). The long fluorescent decay times of QDs make them easily distinguishable from intrinsic background cell autofluorescence and other fluorophores, improving selectivity in sensing for bioimaging applications (Durisic, Godin et al. 2011).

In recent studies, has been shown that QD lifetime is highly sensitive to changes in the microenvironment, which permits its use as a detection signal in the development of biosensors (Carlini and Nadeau 2013, Orte, Alvarez-Pez et al. 2013). For example, intracellular pH can be monitored using pH-sensitive QD-MPA nanosensor. FLIM technology permits sensitive monitoring of pH changes within distinct cellular compartments and therefore provides a sensitive readout for the quantification of the intracellular pH. Changes in lifetime can be observed as the QDs are processed through the endosomal transport machinery in the cells, and are consistent with lifetime measurements made in bulk solution using buffers that correspond to different cellular regions (Carlini and Nadeau 2013).

5.5. Cellular excretion and clearance of nanoparticles

Although cellular internalization of nanoparticles is an important factor in toxicity, it is also important to consider clearance. Cellular elimination mechanisms of nanoparticles, though not yet routinely studied, deserve thorough investigation. Recent studies showed that QD elimination from the cell was mediated partially by microtubule-dependent transport (Jiang, Rocker et al. 2010). Results from these studies are consistent with findings from Chapter 3, which suggest the slow export of QDs into the extracellular media. The rate of endocytosis seems to be fastest for particles between 20—50 nm in size, while the rate of exocytosis decreases with increasing particle size (Chithrani and Chan 2007, Jin, Heller et al. 2009). An open question is also what happens to nanoparticles once they have been released from cells and whether or not they can be re-internalized. This topic requires further study.

Many research groups have focused on the development of biodegradable particles that are expected to be efficiently metabolized within endosomes/lysosome compartment. Such particles are commonly composed of polylactic acid and similar polymers, albumin particles or liposomes (Torchilin 2006, Vasir and Labhasetwar 2007). QDs on the other hand, are highly stable both *in vitro* and *in vivo* systems. Although well protected by the ZnS shell and capping layers, there is still the potential that the core will degrade over time. This is a concern considering the QD core contains heavy metal ions such as cadmium. Recent *in vivo* studies of fluorescent QDs revealed that they were still present two years after injection in mice (Fitzpatrick, Andreko et al. 2009). QDs were found to accumulate in the lymph nodes, bone marrow and intestinal contents, as well as the liver and spleen, suggesting eventual excretion of these nanoparticles through these organs with time (Choi, Ipe et al. 2009). Other studies showed that QDs were poorly metabolized and retained by cells of the MPS (Fischer, Liu et al. 2006, Choi, Liu et al. 2007). Taken together, these studies reveal that several requirements must be satisfied for efficient renal filtration and urinary elimination. The first and most important is particle size as a final hydrodynamic diameter greater than 5.5 nm hinders renal excretion, whereas nanoparticles smaller than 5.5 nm are effectively excreted in the urine. In addition, QD surfaces with zwitterionic charge are cleared more rapidly than positively and negatively charged surfaces, as QD interactions with plasma proteins and interactions with the MPS are enhanced.

5.6. Effect of sedimentation on uptake

In vitro experiments typically measure uptake by exposing cells at the bottom of a culture plate to a suspension of nanoparticles. As described earlier, this was the case for all plate based uptake experiments carried out in Chapters 3 and 4. It is generally assumed that nanoparticles suspended in cell culture media are well-dispersed. However, as we saw in Chapter 4, nanoparticles can sediment at the bottom of the well, especially those that tend to form aggregates.

A recent study investigated the effect of diffusion and sedimentation on the rate of nanoparticle internalization (Cho, Zhang et al. 2011). Cells were grown on a microscope slide

which was then suspended upside-down and exposed to gold nanoparticles of different sizes immersed within the cell media. Using this experimental setup, the cells can be inverted and are therefore not exposed to the nanoparticles which may have settled out to the bottom of the well, as is the case in traditional plate based uptake assays. Due to the sedimentation effect, the local nanoparticle concentration at the bottom of the plate is much higher compared to that of the entire well volume. As discussed previously, nanoparticle uptake is dependent on the local concentration at the plasma membrane (Zhang and Monteiro-Riviere 2009). Therefore more nanoparticles are internalized in the upright configuration than in the inverted one, and nanoparticles with faster sedimentation rates showed greater differences in uptake between the two configurations (Cho, Zhang et al. 2011). Taken together, these results suggest that sedimentation should be considered when performing *in vitro* studies for large or heavy nanoparticles, and especially those that tend to aggregate in the presence of biological media.

5.7. Effect of cell cycle on uptake

It has been recently shown that nanoparticle uptake can also be influenced by the cell cycle. Although cells in different phases of the cell cycle were found to internalize nanoparticles at a similar rate, after longer exposure the concentration of nanoparticles in the cells was greatest in the G2/M phase compared to the S phase and G0/G1 phase, respectively (Kim, Aberg et al. 2012). In addition, cell division could be perceived as nanoparticle clearance, as measured by a reduction in fluorescence intensity and/or intracellular cadmium content, due to the splitting of the cytosolic contents between mother and daughter cells when the parent cell divides. Care should be taken not to mistake this process for nanoparticle export.

In our studies, we did not directly account for the cell cycle in our uptake experiments. In Chapter 2 and 3, nanoparticle exposure studies were carried out in serum free media, to limit potential nanoparticle aggregation. It is well known that serum starvation synchronizes cells into the G0/G1 phase, while cells incubated in serum containing media readily cycle until reaching confluence (Khammanit, Chantakru et al. 2008). Therefore, it is

possible that we underrepresented nanoparticle uptake in serum free conditions. Several cycle inhibitors are commercially available and should have been considered as additional controls in our uptake studies for Chapter 2 and 3 (Besson, Dowdy et al. 2008). In Chapter 3, cells were incubated with QDs in serum free and serum containing media. We observed much higher QD uptake in serum free media compared to that with serum, primarily due to the reduced presence of aggregates. These results suggest that even if nanoparticle uptake was underreported in serum free conditions (Chapter 2 and 3), it does not change our interpretation of the results.

5.8. Alternatives to cadmium based quantum dots

Despite some of the toxicity issues associated with cadmium containing QDs described herein and by others, the superior photophysical properties arguably outweigh the potential risks when studying interactions at the nano-bio interface. For the sake of avoiding cadmium related toxicity, several cadmium free nanocrystals have recently been developed. QD cores based on indium arsenide (InAs) or indium gallium phosphide (InGaP) capped with a zinc selenide shell are highly stable and can be bioconjugated with other surface ligands for imaging applications (Zimmer, Kim et al. 2006, Kumar, Deep et al. 2012). The optical properties of these nanocrystals are comparable to their cadmium based equivalents, as is their subcellular localization, and are therefore considered to be a valuable alternative to CdTe and CdSe QDs (Behrendt, Sandros et al. 2009).

In addition to nanocrystals with metal semiconductor cores, new carbon based nanodots (C-dots) have been recently developed as useful luminescent markers. They offer the same benefits as conventional QDs such as wide excitation and narrow emission wavelengths, resistance to photobleaching and potential for surface functionalization, all without the risk of toxicity from the chemical composition or risk due to the scarcity of materials used. Unlike QDs, C-dots can be produced inexpensively and on a large scale. However, their optical properties are not quite as efficient as traditional quantum dots, with reduced quantum yield and emission in the visible spectrum, lacking the potential to reach the near infrared (Baker and Baker 2010).

Conclusions

This thesis work elucidates key interactions that take place between synthetic and biological materials at the nano-bio interface. Herein, we aimed to characterize the forces and consequences of nanoparticle-cell interactions, while providing insight into the underlying cellular mechanisms and biological implications.

In Chapter 2, we investigated the underlying mechanisms of the adaptive cell response following exposure to QDs. Our findings showed that short term incubation with uncapped QDs brings about a dynamic redistribution of intracellular glutathione by selectively killing cells with low GSH concentrations and sparing those with medium to high GSH concentrations. On the other hand, QDs that were bioconjugated with capping ligands, such as MPA or PEG were found to be non-toxic and did not elicit changes in intracellular glutathione. These findings emphasize the importance of nanoparticle composition when considering QDs for biological applications. This work led us to subsequently investigate the various mechanisms of nanoparticle uptake.

In Chapter 3, we investigated the role of surface charge on nanoparticle internalization using capped QDs with the same core, but varied surface functionalization. Four small ligands were non-covalently bound to the QD surface. These small ligands were of comparable size, but imparted varied surface properties. The contribution of specific modes of internalization towards the total QD uptake was investigated using pharmacological inhibitors. Results from these studies showed QDs were differentially internalized based on their surface ligand and charge. Our findings show a strong dependence between the properties of QD-associated small ligands and modes of uptake in human cells.

In Chapter 4, we characterized QD agglomeration states, tracked the agglomerates in a time and concentration dependent manner *in vitro* and measured the viability of predominantly agglomerated QDs against the finely dispersed QDs. These studies focused on investigating particle agglomeration induced by high concentrations of salts and proteins within increasingly complex physiological medium. We used asymmetric flow-field flow

fractionation as an essential approach for the determination of QD size and stability. This technique provided particle by particle size determination and dynamics of agglomerate formation. These findings highlight that serum proteins are differentially adsorbed to the particle surface, depending on their surface ligands. In addition, QD stability directs interactions at the cell membrane, driving particle uptake.

Given the wide range of engineered nanomaterials currently in production, the development of a robust and standardized characterization protocol is urgently required. Care should be paid not only to the usual criteria for valid toxicological studies (physical and chemical characterization) but also particle aggregation and solubility in the biological milieu to ensure exposure data is properly attributed to specific nanoparticle risks. We have summarized several techniques that can be used to characterize and investigate cellular uptake of nanoparticles, as well as the limitations of such studies. In particular, our results highlight the need for a suitable characterization technique for nanoparticles in complex biological media. Understanding particle stability in the biological microenvironment is essential to properly interpret cellular mechanistic studies and diagnostic assays.

The studies presented here make significant contributions to our limited understanding of how nanomaterials interact with the biological microenvironment. These results emphasize that nanoparticles play an active role in mediating biological effects and should not be considered as inert carriers for biomedical applications. In addition, we highlight key differences between the “synthetic” and “biological” identity of nanoparticles and their biological consequences, while in the presence of cell culture. The complexity of interactions at the nano-bio interface, make it clear that future nanoparticles research must be performed as a close collaboration between scientists with different but complementary backgrounds, such as physics, chemistry, biology and physiology. Only in this way will we prevent misleading/wrong interpretations and thus aid in the development of nanoparticles for clinical use.

References

Al-Hajaj, N. A., A. Moquin, K. D. Neibert, G. M. Soliman, F. M. Winnik and D. Maysinger (2011). "Short ligands affect modes of QD uptake and elimination in human cells." ACS Nano **5**(6): 4909-4918.

Anderson, R. E. and W. C. Chan (2008). "Systematic investigation of preparing biocompatible, single, and small ZnS-Capped CdSe quantum dots with amphiphilic polymers." ACS Nano **2**(7): 1341-1352.

Andreadi, C. K., L. M. Howells, P. A. Atherfold and M. M. Manson (2006). "Involvement of Nrf2, p38, B-Raf, and nuclear factor-kappaB, but not phosphatidylinositol 3-kinase, in induction of hemeoxygenase-1 by dietary polyphenols." Mol Pharmacol **69**(3): 1033-1040.

Arvizo, R. R., K. Giri, D. Moyano, O. R. Miranda, B. Madden, D. J. McCormick, R. Bhattacharya, V. M. Rotello, J. P. Kocher and P. Mukherjee (2012). "Identifying new therapeutic targets via modulation of protein corona formation by engineered nanoparticles." PLoS One **7**(3): e33650.

Aubin-Tam, M. E. and K. Hamad-Schifferli (2008). "Structure and function of nanoparticle-protein conjugates." Biomed Mater **3**(3): 034001.

Aurell, C. A. and A. O. Wistrom (1998). "Critical aggregation concentrations of gram-negative bacterial lipopolysaccharides (LPS)." Biochem Biophys Res Commun **253**(1): 119-123.

Baker, S. N. and G. A. Baker (2010). "Luminescent carbon nanodots: emergent nanolights." Angew Chem Int Ed Engl **49**(38): 6726-6744.

Behrendt, M., M. G. Sandros, R. A. McKinney, K. McDonald, E. Przybytkowski, M. Tabrizian and D. Maysinger (2009). "Imaging and organelle distribution of fluorescent InGaP/ZnS nanoparticles in glial cells." Nanomedicine (Lond) **4**(7): 747-761.

Besson, A., S. F. Dowdy and J. M. Roberts (2008). "CDK inhibitors: cell cycle regulators and beyond." Dev Cell **14**(2): 159-169.

Bouby, M., H. Geckeis and F. W. Geyer (2008). "Application of asymmetric flow field-flow fractionation (AsFlFFF) coupled to inductively coupled plasma mass spectrometry (ICPMS) to the quantitative characterization of natural colloids and synthetic nanoparticles." Anal Bioanal Chem **392**(7-8): 1447-1457.

Breus, V. V., C. D. Heyes and G. U. Nienhaus (2007). "Quenching of CdSe−ZnS Core−Shell Quantum Dot Luminescence by Water-Soluble Thiolated Ligands." The Journal of Physical Chemistry C **111**(50): 18589-18594.

Brown, G. C. and J. J. Neher (2012). "Eaten alive! Cell death by primary phagocytosis: 'phagoptosis'." Trends Biochem Sci **37**(8): 325-332.

Calzolai, L., D. Gilliland, C. P. Garcia and F. Rossi (2011). "Separation and characterization of gold nanoparticle mixtures by flow-field-flow fractionation." J Chromatogr A **1218**(27): 4234-4239.

Carlini, L. and J. L. Nadeau (2013). "Uptake and processing of semiconductor quantum dots in living cells studied by fluorescence lifetime imaging microscopy (FLIM)." Chem Commun (Camb) **49**(17): 1714-1716.

Casals, E., T. Pfaller, A. Duschl, G. J. Oostingh and V. Puntes (2010). "Time evolution of the nanoparticle protein corona." ACS Nano **4**(7): 3623-3632.

Cedervall, T., I. Lynch, M. Foy, T. Berggard, S. C. Donnelly, G. Cagney, S. Linse and K. A. Dawson (2007). "Detailed identification of plasma proteins adsorbed on copolymer nanoparticles." Angew Chem Int Ed Engl **46**(30): 5754-5756.
Cedervall, T., I. Lynch, S. Lindman, T. Berggard, E. Thulin, H. Nilsson, K. A. Dawson and S. Linse (2007). "Understanding the nanoparticle-protein corona using methods to quantify exchange rates and affinities of proteins for nanoparticles." Proceedings of the National Academy of Sciences of the United States of America **104**(7): 2050-2055.
Cedervall, T., I. Lynch, S. Lindman, T. Berggard, E. Thulin, H. Nilsson, K. A. Dawson and S. Linse (2007). "Understanding the nanoparticle-protein corona using methods to quantify exchange rates and affinities of proteins for nanoparticles." Proc Natl Acad Sci U S A **104**(7): 2050-2055.
Champion, J. A. and S. Mitragotri (2006). "Role of target geometry in phagocytosis." Proc Natl Acad Sci U S A **103**(13): 4930-4934.
Chan, W. C., D. J. Maxwell, X. Gao, R. E. Bailey, M. Han and S. Nie (2002). "Luminescent quantum dots for multiplexed biological detection and imaging." Curr Opin Biotechnol **13**(1): 40-46.
Chan, W. C. and S. Nie (1998). "Quantum dot bioconjugates for ultrasensitive nonisotopic detection." Science **281**(5385): 2016-2018.
Chang, Y. P., F. Pinaud, J. Antelman and S. Weiss (2008). "Tracking bio-molecules in live cells using quantum dots." J Biophotonics **1**(4): 287-298.
Chazotte, B. (2011). "Fluorescent labeling of membrane lipid rafts." Cold Spring Harb Protoc **2011**(5): pdb prot5625.
Chen, L., W. Zhao, Y. Jiao, X. He, J. Wang and Y. Zhang (2007). "Characterization of Ag/Pt core-shell nanoparticles by UV-vis absorption, resonance light-scattering techniques." Spectrochim Acta A Mol Biomol Spectrosc **68**(3): 484-490.
Cheng, J., B. A. Teply, I. Sherifi, J. Sung, G. Luther, F. X. Gu, E. Levy-Nissenbaum, A. F. Radovic-Moreno, R. Langer and O. C. Farokhzad (2007). "Formulation of functionalized PLGA-PEG nanoparticles for in vivo targeted drug delivery." Biomaterials **28**(5): 869-876.
Chithrani, B. D. and W. C. Chan (2007). "Elucidating the mechanism of cellular uptake and removal of protein-coated gold nanoparticles of different sizes and shapes." Nano Lett **7**(6): 1542-1550.
Chithrani, B. D., A. A. Ghazani and W. C. Chan (2006). "Determining the size and shape dependence of gold nanoparticle uptake into mammalian cells." Nano Lett **6**(4): 662-668.
Cho, E. C., Q. Zhang and Y. Xia (2011). "The effect of sedimentation and diffusion on cellular uptake of gold nanoparticles." Nat Nanotechnol **6**(6): 385-391.
Cho, E. J., H. Holback, K. C. Liu, S. A. Abouelmagd, J. Park and Y. Yeo (2013). "Nanoparticle characterization: state of the art, challenges, and emerging technologies." Mol Pharm **10**(6): 2093-2110.
Cho, S. J., D. Maysinger, M. Jain, B. Roder, S. Hackbarth and F. M. Winnik (2007). "Long-term exposure to CdTe quantum dots causes functional impairments in live cells." Langmuir **23**(4): 1974-1980.
Cho, T. J. and V. A. Hackley (2010). "Fractionation and characterization of gold nanoparticles in aqueous solution: asymmetric-flow field flow fractionation with MALS, DLS, and UV-Vis detection." Anal Bioanal Chem **398**(5): 2003-2018.

Choi, A. O., S. J. Cho, J. Desbarats, J. Lovric and D. Maysinger (2007). "Quantum dot-induced cell death involves Fas upregulation and lipid peroxidation in human neuroblastoma cells." J Nanobiotechnology **5**: 1.
Choi, H. S., B. I. Ipe, P. Misra, J. H. Lee, M. G. Bawendi and J. V. Frangioni (2009). "Tissue- and organ-selective biodistribution of NIR fluorescent quantum dots." Nano Lett **9**(6): 2354-2359.
Choi, H. S., W. Liu, P. Misra, E. Tanaka, J. P. Zimmer, B. Itty Ipe, M. G. Bawendi and J. V. Frangioni (2007). "Renal clearance of quantum dots." Nat Biotechnol **25**(10): 1165-1170.
Clapp, A. R., E. R. Goldman and H. Mattoussi (2006). "Capping of CdSe-ZnS quantum dots with DHLA and subsequent conjugation with proteins." Nat Protoc **1**(3): 1258-1266.
Clift, M. J., S. Bhattacharjee, D. M. Brown and V. Stone (2010). "The effects of serum on the toxicity of manufactured nanoparticles." Toxicol Lett **198**(3): 358-365.
Colvin, V. L. (2003). "The potential environmental impact of engineered nanomaterials." Nat Biotechnol **21**(10): 1166-1170.
Contreras, J., J. Xie, Y. J. Chen, H. Pei, G. Zhang, C. L. Fraser and S. F. Hamm-Alvarez (2010). "Intracellular uptake and trafficking of difluoroboron dibenzoylmethane-polylactide nanoparticles in HeLa cells." ACS Nano **4**(5): 2735-2747.
Crist, R. M., J. H. Grossman, A. K. Patri, S. T. Stern, M. A. Dobrovolskaia, P. P. Adiseshaiah, J. D. Clogston and S. E. McNeil (2013). "Common pitfalls in nanotechnology: lessons learned from NCI's Nanotechnology Characterization Laboratory." Integr Biol (Camb) **5**(1): 66-73.
Cui, B., C. Wu, L. Chen, A. Ramirez, E. L. Bearer, W. P. Li, W. C. Mobley and S. Chu (2007). "One at a time, live tracking of NGF axonal transport using quantum dots." Proc Natl Acad Sci U S A **104**(34): 13666-13671.
D'Autreaux, B. and M. B. Toledano (2007). "ROS as signalling molecules: mechanisms that generate specificity in ROS homeostasis." Nat Rev Mol Cell Biol **8**(10): 813-824.
Daou, T. J., L. Li, P. Reiss, V. Josserand and I. Texier (2009). "Effect of poly(ethylene glycol) length on the in vivo behavior of coated quantum dots." Langmuir **25**(5): 3040-3044.
Demento, S. L., S. C. Eisenbarth, H. G. Foellmer, C. Platt, M. J. Caplan, W. Mark Saltzman, I. Mellman, M. Ledizet, E. Fikrig, R. A. Flavell and T. M. Fahmy (2009). "Inflammasome-activating nanoparticles as modular systems for optimizing vaccine efficacy." Vaccine **27**(23): 3013-3021.
Dickinson, D. A., D. R. Moellering, K. E. Iles, R. P. Patel, A. L. Levonen, A. Wigley, V. M. Darley-Usmar and H. J. Forman (2003). "Cytoprotection against oxidative stress and the regulation of glutathione synthesis." Biol Chem **384**(4): 527-537.
Dobrovolskaia, M. A. and S. E. McNeil (2007). "Immunological properties of engineered nanomaterials." Nat Nanotechnol **2**(8): 469-478.
Dobrovolskaia, M. A., B. W. Neun, J. D. Clogston, H. Ding, J. Ljubimova and S. E. McNeil (2010). "Ambiguities in applying traditionalLimulusAmebocyte Lysate tests to quantify endotoxin in nanoparticle formulations." Nanomedicine **5**(4): 555-562.
Dominska, M. and D. M. Dykxhoorn (2010). "Breaking down the barriers: siRNA delivery and endosome escape." J Cell Sci **123**(Pt 8): 1183-1189.
Dorfs, D. and A. Eychmüller (2006). "Multishell Semiconductor Nanocrystals." Zeitschrift für Physikalische Chemie **220**(12): 1539-1552.

Doyle, S. E., R. M. O'Connell, G. A. Miranda, S. A. Vaidya, E. K. Chow, P. T. Liu, S. Suzuki, N. Suzuki, R. L. Modlin, W. C. Yeh, T. F. Lane and G. Cheng (2004). "Toll-like receptors induce a phagocytic gene program through p38." J Exp Med **199**(1): 81-90.
Dubertret, B., P. Skourides, D. J. Norris, V. Noireaux, A. H. Brivanlou and A. Libchaber (2002). "In vivo imaging of quantum dots encapsulated in phospholipid micelles." Science **298**(5599): 1759-1762.
Duncan, R. and S. C. Richardson (2012). "Endocytosis and intracellular trafficking as gateways for nanomedicine delivery: opportunities and challenges." Mol Pharm **9**(9): 2380-2402.
Durisic, N., A. G. Godin, D. Walters, P. Grutter, P. W. Wiseman and C. D. Heyes (2011). "Probing the "dark" fraction of core-shell quantum dots by ensemble and single particle pH-dependent spectroscopy." ACS Nano **5**(11): 9062-9073.
Ehrenberg, M. S., A. E. Friedman, J. N. Finkelstein, G. Oberdorster and J. L. McGrath (2009). "The influence of protein adsorption on nanoparticle association with cultured endothelial cells." Biomaterials **30**(4): 603-610.
Ehrlich, M., W. Boll, A. Van Oijen, R. Hariharan, K. Chandran, M. L. Nibert and T. Kirchhausen (2004). "Endocytosis by random initiation and stabilization of clathrin-coated pits." Cell **118**(5): 591-605.
Elsaesser, A., A. Taylor, G. S. de Yanes, G. McKerr, E. M. Kim, E. O'Hare and C. V. Howard (2010). "Quantification of nanoparticle uptake by cells using microscopical and analytical techniques." Nanomedicine (Lond) **5**(9): 1447-1457.
Erickson, B. E. (2012). "Mapping Nanotech Drugs' Landscape." Chemical & Engineering News Archive **90**(36): 46-48.
Ferreira, R., T. Santos, L. Cortes, S. Cochaud, F. Agasse, A. P. Silva, S. Xapelli and J. O. Malva (2012). "Neuropeptide Y inhibits interleukin-1 beta-induced microglia motility." J Neurochem **120**(1): 93-105.
Filipe, V., A. Hawe and W. Jiskoot (2010). "Critical evaluation of Nanoparticle Tracking Analysis (NTA) by NanoSight for the measurement of nanoparticles and protein aggregates." Pharm Res **27**(5): 796-810.
Fischer, H. C., L. Liu, K. S. Pang and W. C. W. Chan (2006). "Pharmacokinetics of Nanoscale Quantum Dots: In Vivo Distribution, Sequestration, and Clearance in the Rat." Advanced Functional Materials **16**(10): 1299-1305.
Fitzpatrick, J. A., S. K. Andreko, L. A. Ernst, A. S. Waggoner, B. Ballou and M. P. Bruchez (2009). "Long-term persistence and spectral blue shifting of quantum dots in vivo." Nano Lett **9**(7): 2736-2741.
Florence, A. T. (1997). "The oral absorption of micro- and nanoparticulates: neither exceptional nor unusual." Pharm Res **14**(3): 259-266.
Franca, A., P. Aggarwal, E. V. Barsov, S. V. Kozlov, M. A. Dobrovolskaia and A. Gonzalez-Fernandez (2011). "Macrophage scavenger receptor A mediates the uptake of gold colloids by macrophages in vitro." Nanomedicine (Lond) **6**(7): 1175-1188.
Fraunhofer, W. and G. Winter (2004). "The use of asymmetrical flow field-flow fractionation in pharmaceutics and biopharmaceutics." Eur J Pharm Biopharm **58**(2): 369-383.
Gao, H., W. Shi and L. B. Freund (2005). "Mechanics of receptor-mediated endocytosis." Proc Natl Acad Sci U S A **102**(27): 9469-9474.
Gao, X., L. Yang, J. A. Petros, F. F. Marshall, J. W. Simons and S. Nie (2005). "In vivo molecular and cellular imaging with quantum dots." Curr Opin Biotechnol **16**(1): 63-72.

Gaumet, M., A. Vargas, R. Gurny and F. Delie (2008). "Nanoparticles for drug delivery: the need for precision in reporting particle size parameters." Eur J Pharm Biopharm **69**(1): 1-9.
Gelperina, S., K. Kisich, M. D. Iseman and L. Heifets (2005). "The potential advantages of nanoparticle drug delivery systems in chemotherapy of tuberculosis." Am J Respir Crit Care Med **172**(12): 1487-1490.
Gerion, D., F. Pinaud, S. C. Williams, W. J. Parak, D. Zanchet, S. Weiss and A. P. Alivisatos (2001). "Synthesis and properties of biocompatible water-soluble silica-coated CdSe/ZnS semiconductor quantum dots." The Journal of Physical Chemistry B **105**(37): 8861-8871.
Goddette, D. W. and C. Frieden (1986). "Actin polymerization. The mechanism of action of cytochalasin D." J Biol Chem **261**(34): 15974-15980.
Goodman, C. M., C. D. McCusker, T. Yilmaz and V. M. Rotello (2004). "Toxicity of gold nanoparticles functionalized with cationic and anionic side chains." Bioconjug Chem **15**(4): 897-900.
Gottstein, C., G. Wu, B. J. Wong and J. A. Zasadzinski (2013). "Precise quantification of nanoparticle internalization." ACS Nano **7**(6): 4933-4945.
Grabolle, M., J. Ziegler, A. Merkulov, T. Nann and U. Resch-Genger (2008). "Stability and fluorescence quantum yield of CdSe-ZnS quantum dots--influence of the thickness of the ZnS shell." Ann N Y Acad Sci **1130**: 235-241.
Gratton, S. E., P. A. Ropp, P. D. Pohlhaus, J. C. Luft, V. J. Madden, M. E. Napier and J. M. DeSimone (2008). "The effect of particle design on cellular internalization pathways." Proc Natl Acad Sci U S A **105**(33): 11613-11618.
Grecco, H. E., K. A. Lidke, R. Heintzmann, D. S. Lidke, C. Spagnuolo, O. E. Martinez, E. A. Jares-Erijman and T. M. Jovin (2004). "Ensemble and single particle photophysical properties (two-photon excitation, anisotropy, FRET, lifetime, spectral conversion) of commercial quantum dots in solution and in live cells." Microsc Res Tech **65**(4-5): 169-179.
Guo, S., Y. Huang, Q. Jiang, Y. Sun, L. Deng, Z. Liang, Q. Du, J. Xing, Y. Zhao, P. C. Wang, A. Dong and X. J. Liang (2010). "Enhanced gene delivery and siRNA silencing by gold nanoparticles coated with charge-reversal polyelectrolyte." ACS Nano **4**(9): 5505-5511.
Gupta, S. C., B. Sung, S. Prasad, L. J. Webb and B. B. Aggarwal (2013). "Cancer drug discovery by repurposing: teaching new tricks to old dogs." Trends Pharmacol Sci **34**(9): 508-517.
Hagendorfer, H., R. Kaegi, M. Parlinska, B. Sinnet, C. Ludwig and A. Ulrich (2012). "Characterization of silver nanoparticle products using asymmetric flow field flow fractionation with a multidetector approach--a comparison to transmission electron microscopy and batch dynamic light scattering." Anal Chem **84**(6): 2678-2685.
Hassellov, M., J. W. Readman, J. F. Ranville and K. Tiede (2008). "Nanoparticle analysis and characterization methodologies in environmental risk assessment of engineered nanoparticles." Ecotoxicology **17**(5): 344-361.
Haustein, E. and P. Schwille (2007). "Fluorescence correlation spectroscopy: novel variations of an established technique." Annu Rev Biophys Biomol Struct **36**: 151-169.
Hendren, C. O., X. Mesnard, J. Droge and M. R. Wiesner (2011). "Estimating production data for five engineered nanomaterials as a basis for exposure assessment." Environ Sci Technol **45**(7): 2562-2569.
Herd, H., N. Daum, A. T. Jones, H. Huwer, H. Ghandehari and C.-M. Lehr (2013). "Nanoparticle Geometry and Surface Orientation Influence Mode of Cellular Uptake." ACS Nano.

Herd, H., N. Daum, A. T. Jones, H. Huwer, H. Ghandehari and C. M. Lehr (2013). "Nanoparticle geometry and surface orientation influence mode of cellular uptake." ACS Nano **7**(3): 1961-1973.
Hermanson, G. T. (2008). Bioconjugate techniques. Amsterdam [etc.], Elsevier.
Hill, H. D., J. E. Millstone, M. J. Banholzer and C. A. Mirkin (2009). "The role radius of curvature plays in thiolated oligonucleotide loading on gold nanoparticles." ACS Nano **3**(2): 418-424.
Holder, A. N., A. L. Ellis, J. Zou, N. Chen and J. J. Yang (2009). "Facilitating chromophore formation of engineered Ca2+ binding green fluorescent proteins." Archives of biochemistry and biophysics **486**(1): 27-34.
Hondow, N., R. Brydson, P. Wang, M. D. Holton, M. R. Brown, P. Rees, H. D. Summers and A. Brown (2012). "Quantitative characterization of nanoparticle agglomeration within biological media." Journal of Nanoparticle Research **14**(7): 1-15.
Hornung, V., F. Bauernfeind, A. Halle, E. O. Samstad, H. Kono, K. L. Rock, K. A. Fitzgerald and E. Latz (2008). "Silica crystals and aluminum salts activate the NALP3 inflammasome through phagosomal destabilization." Nat Immunol **9**(8): 847-856.
Hoshino, A., K. Fujioka, T. Oku, M. Suga, Y. F. Sasaki, T. Ohta, M. Yasuhara, K. Suzuki and K. Yamamoto (2004). "Physicochemical properties and cellular toxicity of nanocrystal quantum dots depend on their surface modification." Nano Letters **4**(11): 2163-2169.
Hotze, E. M., J. Y. Bottero and M. R. Wiesner (2010). "Theoretical framework for nanoparticle reactivity as a function of aggregation state." Langmuir **26**(13): 11170-11175.
Howes, M. T., S. Mayor and R. G. Parton (2010). "Molecules, mechanisms, and cellular roles of clathrin-independent endocytosis." Curr Opin Cell Biol **22**(4): 519-527.
Hu, J., L. Dong and C. E. Outten (2008). "The redox environment in the mitochondrial intermembrane space is maintained separately from the cytosol and matrix." J Biol Chem **283**(43): 29126-29134.
Hutter, E., S. Boridy, S. Labrecque, M. Lalancette-Hebert, J. Kriz, F. M. Winnik and D. Maysinger (2010). "Microglial response to gold nanoparticles." ACS Nano **4**(5): 2595-2606.
Idowu, M., E. Lamprecht and T. Nyokong (2008). "Interaction of water-soluble thiol capped CdTe quantum dots and bovine serum albumin." Journal of Photochemistry and Photobiology A: Chemistry **198**(1): 7-12.
Illum, L. (2000). "Transport of drugs from the nasal cavity to the central nervous system." Eur J Pharm Sci **11**(1): 1-18.
Ishizaki, T., M. Uehata, I. Tamechika, J. Keel, K. Nonomura, M. Maekawa and S. Narumiya (2000). "Pharmacological properties of Y-27632, a specific inhibitor of rho-associated kinases." Mol Pharmacol **57**(5): 976-983.
Iversen, T.-G., T. Skotland and K. Sandvig (2011). "Endocytosis and intracellular transport of nanoparticles: Present knowledge and need for future studies." Nano Today **6**(2): 176-185.
Iversen, T. G., N. Frerker and K. Sandvig (2012). "Uptake of ricinB-quantum dot nanoparticles by a macropinocytosis-like mechanism." J Nanobiotechnology **10**: 33.
Jain, M. P., A. O. Choi, K. D. Neibert and D. Maysinger (2009). "Probing and preventing quantum dot-induced cytotoxicity with multimodal alpha-lipoic acid in multiple dimensions of the peripheral nervous system." Nanomedicine (Lond) **4**(3): 277-290.
Jaiswal, J. K., H. Mattoussi, J. M. Mauro and S. M. Simon (2003). "Long-term multiple color imaging of live cells using quantum dot bioconjugates." Nat Biotechnol **21**(1): 47-51.

James, M. L. and S. S. Gambhir (2012). "A molecular imaging primer: modalities, imaging agents, and applications." Physiol Rev **92**(2): 897-965.
Jefferis, R. and D. S. Kumararatne (1990). "Selective IgG subclass deficiency: quantification and clinical relevance." Clin Exp Immunol **81**(3): 357-367.
Jiang, J., G. Oberdorster and P. Biswas (2009). "Characterization of size, surface charge, and agglomeration state of nanoparticle dispersions for toxicological studies." J. Nanopart. Res. **11**: 77-89.
Jiang, J., G. Oberdörster and P. Biswas (2009). "Characterization of size, surface charge, and agglomeration state of nanoparticle dispersions for toxicological studies." Journal of Nanoparticle Research **11**(1): 77-89.
Jiang, W., B. Y. Kim, J. T. Rutka and W. C. Chan (2008). "Nanoparticle-mediated cellular response is size-dependent." Nat Nanotechnol **3**(3): 145-150.
Jiang, X., C. Rocker, M. Hafner, S. Brandholt, R. M. Dorlich and G. U. Nienhaus (2010). "Endo- and exocytosis of zwitterionic quantum dot nanoparticles by live HeLa cells." ACS Nano **4**(11): 6787-6797.
Jin, H., D. A. Heller, R. Sharma and M. S. Strano (2009). "Size-dependent cellular uptake and expulsion of single-walled carbon nanotubes: single particle tracking and a generic uptake model for nanoparticles." ACS Nano **3**(1): 149-158.
Johnston, H. J., M. Semmler-Behnke, D. M. Brown, W. Kreyling, L. Tran and V. Stone (2010). "Evaluating the uptake and intracellular fate of polystyrene nanoparticles by primary and hepatocyte cell lines in vitro." Toxicol Appl Pharmacol **242**(1): 66-78.
Kah, J. C., J. Chen, A. Zubieta and K. Hamad-Schifferli (2012). "Exploiting the protein corona around gold nanorods for loading and triggered release." ACS Nano **6**(8): 6730-6740.
Kamaly, N., Z. Xiao, P. M. Valencia, A. F. Radovic-Moreno and O. C. Farokhzad (2012). "Targeted polymeric therapeutic nanoparticles: design, development and clinical translation." Chem Soc Rev **41**(7): 2971-3010.
Kaplan, D. R. (1998). "Studying signal transduction in neuronal cells: the Trk/NGF system." Prog Brain Res **117**: 35-46.
Kettenmann, H., U. K. Hanisch, M. Noda and A. Verkhratsky (2011). "Physiology of microglia." Physiol Rev **91**(2): 461-553.
Khatchadourian, A. and D. Maysinger (2009). "Lipid droplets: their role in nanoparticle-induced oxidative stress." Mol Pharm **6**(4): 1125-1137.
Kim, J. A., C. Aberg, A. Salvati and K. A. Dawson (2012). "Role of cell cycle on the cellular uptake and dilution of nanoparticles in a cell population." Nat Nanotechnol **7**(1): 62-68.
Kumar, P., A. Deep, S. C. Sharma and L. M. Bharadwaj (2012). "Bioconjugation of InGaP quantum dots for molecular sensing." Anal Biochem **421**(1): 285-290.
Kumari, S., S. Mg and S. Mayor (2010). "Endocytosis unplugged: multiple ways to enter the cell." Cell Res **20**(3): 256-275.
Lacerda, S. H., J. J. Park, C. Meuse, D. Pristinski, M. L. Becker, A. Karim and J. F. Douglas (2010). "Interaction of gold nanoparticles with common human blood proteins." ACS Nano **4**(1): 365-379.
Lambeth, J. D. (2004). "NOX enzymes and the biology of reactive oxygen." Nat Rev Immunol **4**(3): 181-189.
Lewinski, N., V. Colvin and R. Drezek (2008). "Cytotoxicity of nanoparticles." Small **4**(1): 26-49.

Li, W. and A. N. Kong (2009). "Molecular mechanisms of Nrf2-mediated antioxidant response." Mol Carcinog **48**(2): 91-104.
Linse, S., C. Cabaleiro-Lago, W. F. Xue, I. Lynch, S. Lindman, E. Thulin, S. E. Radford and K. A. Dawson (2007). "Nucleation of protein fibrillation by nanoparticles." Proc Natl Acad Sci U S A **104**(21): 8691-8696.
Lovric, J., S. J. Cho, F. M. Winnik and D. Maysinger (2005). "Unmodified cadmium telluride quantum dots induce reactive oxygen species formation leading to multiple organelle damage and cell death." Chem Biol **12**(11): 1227-1234.
Lundqvist, M., J. Stigler, T. Cedervall, T. Berggard, M. B. Flanagan, I. Lynch, G. Elia and K. Dawson (2011). "The evolution of the protein corona around nanoparticles: a test study." ACS Nano **5**(9): 7503-7509.
Lundqvist, M., J. Stigler, G. Elia, I. Lynch, T. Cedervall and K. A. Dawson (2008). "Nanoparticle size and surface properties determine the protein corona with possible implications for biological impacts." Proc Natl Acad Sci U S A **105**(38): 14265-14270.
Magalhaes, P. O., A. M. Lopes, P. G. Mazzola, C. Rangel-Yagui, T. C. Penna and A. Pessoa, Jr. (2007). "Methods of endotoxin removal from biological preparations: a review." J Pharm Pharm Sci **10**(3): 388-404.
Maiorano, G., S. Sabella, B. Sorce, V. Brunetti, M. A. Malvindi, R. Cingolani and P. P. Pompa (2010). "Effects of cell culture media on the dynamic formation of protein-nanoparticle complexes and influence on the cellular response." ACS Nano **4**(12): 7481-7491.
Marcu, L. (2012). "Fluorescence lifetime techniques in medical applications." Ann Biomed Eng **40**(2): 304-331.
Matheny, C. J., R. Y. Ali, X. Yang and G. M. Pollack (2004). "Effect of prototypical inducing agents on P-glycoprotein and CYP3A expression in mouse tissues." Drug Metab Dispos **32**(9): 1008-1014.
Mattoussi, H., J. M. Mauro, E. R. Goldman, G. P. Anderson, V. C. Sundar, F. V. Mikulec and M. G. Bawendi (2000). "Self-Assembly of CdSe−ZnS Quantum Dot Bioconjugates Using an Engineered Recombinant Protein." Journal of the American Chemical Society **122**(49): 12142-12150.
Maysinger, D. (2007). "Nanoparticles and cells: good companions and doomed partnerships." Org Biomol Chem **5**(15): 2335-2342.
McNeil, S. E. (2011). "Challenges for nanoparticle characterization." Methods Mol Biol **697**: 9-15.
Medintz, I. L., H. T. Uyeda, E. R. Goldman and H. Mattoussi (2005). "Quantum dot bioconjugates for imaging, labelling and sensing." Nat Mater **4**(6): 435-446.
Mei, B. C., K. Susumu, I. L. Medintz and H. Mattoussi (2009). "Polyethylene glycol-based bidentate ligands to enhance quantum dot and gold nanoparticle stability in biological media." Nat Protoc **4**(3): 412-423.
Meng, H., M. Liong, T. Xia, Z. Li, Z. Ji, J. I. Zink and A. E. Nel (2010). "Engineered design of mesoporous silica nanoparticles to deliver doxorubicin and P-glycoprotein siRNA to overcome drug resistance in a cancer cell line." ACS Nano **4**(8): 4539-4550.
Michalet, X., F. F. Pinaud, L. A. Bentolila, J. M. Tsay, S. Doose, J. J. Li, G. Sundaresan, A. M. Wu, S. S. Gambhir and S. Weiss (2005). "Quantum dots for live cells, in vivo imaging, and diagnostics." Science **307**(5709): 538-544.

Michaud, J. P., M. Halle, A. Lampron, P. Theriault, P. Prefontaine, M. Filali, P. Tribout-Jover, A. M. Lanteigne, R. Jodoin, C. Cluff, V. Brichard, R. Palmantier, A. Pilorget, D. Larocque and S. Rivest (2013). "Toll-like receptor 4 stimulation with the detoxified ligand monophosphoryl lipid A improves Alzheimer's disease-related pathology." Proc Natl Acad Sci U S A **110**(5): 1941-1946.
Mistry, A., S. Stolnik and L. Illum (2009). "Nanoparticles for direct nose-to-brain delivery of drugs." Int J Pharm **379**(1): 146-157.
Mitragotri, S. and J. Lahann (2009). "Physical approaches to biomaterial design." Nat Mater **8**(1): 15-23.
Mittal, R. and M. P. Bruchez (2009). "Calibration of Flow Cytometry for Quantitative Quantum Dot Measurements." Curr Protoc Cytom **Chapter 6**: Unit6 26.
Moghimi, S. M., A. C. Hunter and J. C. Murray (2001). "Long-circulating and target-specific nanoparticles: theory to practice." Pharmacol Rev **53**(2): 283-318.
Moquin, A., E. Hutter, A. O. Choi, A. Khatchadourian, A. Castonguay, F. M. Winnik and D. Maysinger (2013). "Caspase-1 activity in microglia stimulated by pro-inflammagen nanocrystals." ACS Nano **7**(11): 9585-9598.
Moquin, A. and F. Winnik (2012). The Use of Field-Flow Fractionation for the Analysis of Drug and Gene Delivery Systems. Field-Flow Fractionation in Biopolymer Analysis. S. K. R. Williams and K. D. Caldwell, Springer Vienna**:** 187-206.
Moquin, A., F. Winnik and D. Maysinger (2013). Separation Science: Principles and Applications for the Analysis of Bionanoparticles by Asymmetrical Flow Field-Flow Fractionation (AF4). Cellular and Subcellular Nanotechnology. V. Weissig, T. Elbayoumi and M. Olsen, Humana Press. **991:** 325-341.
Mullen, D. G., M. Fang, A. Desai, J. R. Baker, B. G. Orr and M. M. Banaszak Holl (2010). "A quantitative assessment of nanoparticle-ligand distributions: implications for targeted drug and imaging delivery in dendrimer conjugates." ACS Nano **4**(2): 657-670.
Murdock, R. C., L. Braydich-Stolle, A. M. Schrand, J. J. Schlager and S. M. Hussain (2008). "Characterization of nanomaterial dispersion in solution prior to In vitro exposure using dynamic light scattering technique." Toxicological Sciences **101**(2): 239-253.
Murdock, R. C., L. Braydich-Stolle, A. M. Schrand, J. J. Schlager and S. M. Hussain (2008). "Characterization of nanomaterial dispersion in solution prior to in vitro exposure using dynamic light scattering technique." Toxicol Sci **101**(2): 239-253.
Muro, E., A. Fragola, T. Pons, N. Lequeux, A. Ioannou, P. Skourides and B. Dubertret (2012). "Comparing intracellular stability and targeting of sulfobetaine quantum dots with other surface chemistries in live cells." Small **8**(7): 1029-1037.
Murray, C. B., D. J. Norris and M. G. Bawendi (1993). "Synthesis and characterization of nearly monodisperse CdE (E = sulfur, selenium, tellurium) semiconductor nanocrystallites." Journal of the American Chemical Society **115**(19): 8706-8715.
Nabiev, I., S. Mitchell, A. Davies, Y. Williams, D. Kelleher, R. Moore, Y. K. Gun'ko, S. Byrne, Y. P. Rakovich, J. F. Donegan, A. Sukhanova, J. Conroy, D. Cottell, N. Gaponik, A. Rogach and Y. Volkov (2007). "Nonfunctionalized nanocrystals can exploit a cell's active transport machinery delivering them to specific nuclear and cytoplasmic compartments." Nano Lett **7**(11): 3452-3461.
Nativo, P., I. A. Prior and M. Brust (2008). "Uptake and intracellular fate of surface-modified gold nanoparticles." ACS Nano **2**(8): 1639-1644.

Neher, J. J., U. Neniskyte and G. C. Brown (2012). "Primary phagocytosis of neurons by inflamed microglia: potential roles in neurodegeneration." Front Pharmacol **3**: 27.
Neibert, K. D. and D. Maysinger (2012). "Mechanisms of cellular adaptation to quantum dots--the role of glutathione and transcription factor EB." Nanotoxicology **6**(3): 249-262.
Nel, A. E., L. Madler, D. Velegol, T. Xia, E. M. Hoek, P. Somasundaran, F. Klaessig, V. Castranova and M. Thompson (2009). "Understanding biophysicochemical interactions at the nano-bio interface." Nat Mater **8**(7): 543-557.
Nel, A. E., L. Madler, D. Velegol, T. Xia, E. M. V. Hoek, P. Somasundaran, F. Klaessig, V. Castranova and M. Thompson (2009). "Understanding biophysicochemical interactions at the nano-bio interface." Nat Mater **8**(7): 543-557.
Nie, S., Y. Xing, G. J. Kim and J. W. Simons (2007). "Nanotechnology applications in cancer." Annu Rev Biomed Eng **9**: 257-288.
Nimmerjahn, A., F. Kirchhoff and F. Helmchen (2005). "Resting microglial cells are highly dynamic surveillants of brain parenchyma in vivo." Science **308**(5726): 1314-1318.
Orte, A., J. M. Alvarez-Pez and M. J. Ruedas-Rama (2013). "Fluorescence lifetime imaging microscopy for the detection of intracellular pH with quantum dot nanosensors." ACS Nano **7**(7): 6387-6395.
Panyam, J., W. Z. Zhou, S. Prabha, S. K. Sahoo and V. Labhasetwar (2002). "Rapid endo-lysosomal escape of poly(DL-lactide-co-glycolide) nanoparticles: implications for drug and gene delivery." FASEB J **16**(10): 1217-1226.
Parton, R. G. and K. Simons (2007). "The multiple faces of caveolae." Nat Rev Mol Cell Biol **8**(3): 185-194.
Pasricha, R. (2011). "HRTEM characterization in environmental risk assessment of engineered nanoparticles." J Biomed Nanotechnol **7**(1): 81-82.
Pettibone, J. M., J. Gigault and V. A. Hackley (2013). "Discriminating the states of matter in metallic nanoparticle transformations: what are we missing?" ACS Nano **7**(3): 2491-2499.
Piccirillo, S., G. Filomeni, B. Brune, G. Rotilio and M. R. Ciriolo (2009). "Redox mechanisms involved in the selective activation of Nrf2-mediated resistance versus p53-dependent apoptosis in adenocarcinoma cells." J Biol Chem **284**(40): 27721-27733.
Powers, K. W., M. Palazuelos, B. M. Moudgil and S. M. Roberts (2007). "Characterization of the size, shape, and state of dispersion of nanoparticles for toxicological studies." Nanotoxicology **1**(1): 42-51.
Prapainop, K., D. P. Witter and P. Wentworth, Jr. (2012). "A chemical approach for cell-specific targeting of nanomaterials: small-molecule-initiated misfolding of nanoparticle corona proteins." J Am Chem Soc **134**(9): 4100-4103.
Przybytkowski, E., M. Behrendt, D. Dubois and D. Maysinger (2009). "Nanoparticles can induce changes in the intracellular metabolism of lipids without compromising cellular viability." FEBS J **276**(21): 6204-6217.
Qiu, Y., Y. Liu, L. Wang, L. Xu, R. Bai, Y. Ji, X. Wu, Y. Zhao, Y. Li and C. Chen (2010). "Surface chemistry and aspect ratio mediated cellular uptake of Au nanorods." Biomaterials **31**(30): 7606-7619.
Rao, C. N. R., A. Müller and A. K. Cheetham (2006). The chemistry of nanomaterials, Wiley-VCH.
Reiss, P., M. Protiere and L. Li (2009). "Core/Shell semiconductor nanocrystals." Small **5**(2): 154-168.

Rodal, S. K., G. Skretting, O. Garred, F. Vilhardt, B. van Deurs and K. Sandvig (1999). "Extraction of cholesterol with methyl-beta-cyclodextrin perturbs formation of clathrin-coated endocytic vesicles." Mol Biol Cell **10**(4): 961-974.
Rogers, N. J., N. M. Franklin, S. C. Apte and G. E. Batley (2007). "The importance of physical and chemical characterization in nanoparticle toxicity studies." Integr Environ Assess Manag **3**(2): 303-304.
Rothen-Rutishauser, B. M., S. Schurch, B. Haenni, N. Kapp and P. Gehr (2006). "Interaction of fine particles and nanoparticles with red blood cells visualized with advanced microscopic techniques." Environ Sci Technol **40**(14): 4353-4359.
Ruffmann, R. and A. Wendel (1991). "GSH rescue by N-acetylcysteine." Klin Wochenschr **69**(18): 857-862.
Ryman-Rasmussen, J. P., J. E. Riviere and N. A. Monteiro-Riviere (2007). "Surface coatings determine cytotoxicity and irritation potential of quantum dot nanoparticles in epidermal keratinocytes." J Invest Dermatol **127**(1): 143-153.
Salvati, A., A. S. Pitek, M. P. Monopoli, K. Prapainop, F. B. Bombelli, D. R. Hristov, P. M. Kelly, C. Aberg, E. Mahon and K. A. Dawson (2013). "Transferrin-functionalized nanoparticles lose their targeting capabilities when a biomolecule corona adsorbs on the surface." Nat Nanotechnol **8**(2): 137-143.
Sathishkumar, K., X. Gao, A. C. Raghavamenon, S. N. Murthy, P. J. Kadowitz and R. M. Uppu (2010). "Determination of glutathione, mitochondrial transmembrane potential, and cytotoxicity in H9c2 cardiomyoblasts exposed to reactive oxygen and nitrogen species." Methods Mol Biol **610**: 51-61.
Savic, R., L. Luo, A. Eisenberg and D. Maysinger (2003). "Micellar nanocontainers distribute to defined cytoplasmic organelles." Science **300**(5619): 615-618.
Schimpf, M., K. Caldwell and J. C. Giddings (2000). "Field flow fractionation handbook."
Schmidt, B., K. Loeschner, N. Hadrup, A. Mortensen, J. J. Sloth, C. B. Koch and E. H. Larsen (2011). "Quantitative characterization of gold nanoparticles by field-flow fractionation coupled online with light scattering detection and inductively coupled plasma mass spectrometry." Anal Chem **83**(7): 2461-2468.
Sidorov, S. N., L. M. Bronstein, Y. A. Kabachii, P. M. Valetsky, P. L. Soo, D. Maysinger and A. Eisenberg (2004). "Influence of metalation on the morphologies of poly(ethylene oxide)-block-poly(4-vinylpyridine) block copolymer micelles." Langmuir **20**(9): 3543-3550.
Sierra, A., O. Abiega, A. Shahraz and H. Neumann (2013). "Janus-faced microglia: beneficial and detrimental consequences of microglial phagocytosis." Front Cell Neurosci **7**: 6.
Smith, A. M. and S. Nie (2009). "Next-generation quantum dots." Nat Biotechnol **27**(8): 732-733.
Smulders, S., J. P. Kaiser, S. Zuin, K. L. Van Landuyt, L. Golanski, J. Vanoirbeek, P. Wick and P. H. Hoet (2012). "Contamination of nanoparticles by endotoxin: evaluation of different test methods." Part Fibre Toxicol **9**: 41.
Soo, P. L., S. N. Sidorov, J. Mui, L. M. Bronstein, H. Vali, A. Eisenberg and D. Maysinger (2007). "Gold-labeled block copolymer micelles reveal gold aggregates at multiple subcellular sites." Langmuir **23**(9): 4830-4836.
Stansley, B., J. Post and K. Hensley (2012). "A comparative review of cell culture systems for the study of microglial biology in Alzheimer's disease." J Neuroinflammation **9**: 115.
Stern, S. T., P. P. Adiseshaiah and R. M. Crist (2012). "Autophagy and lysosomal dysfunction as emerging mechanisms of nanomaterial toxicity." Part Fibre Toxicol **9**: 20.

Stern, S. T., B. S. Zolnik, C. B. McLeland, J. Clogston, J. Zheng and S. E. McNeil (2008). "Induction of autophagy in porcine kidney cells by quantum dots: a common cellular response to nanomaterials?" Toxicol Sci **106**(1): 140-152.
Summers, H. D., M. R. Brown, M. D. Holton, J. A. Tonkin, N. Hondow, A. P. Brown, R. Brydson and P. Rees (2013). "Quantification of nanoparticle dose and vesicular inheritance in proliferating cells." ACS Nano **7**(7): 6129-6137.
Susumu, K., H. T. Uyeda, I. L. Medintz, T. Pons, J. B. Delehanty and H. Mattoussi (2007). "Enhancing the stability and biological functionalities of quantum dots via compact multifunctional ligands." J Am Chem Soc **129**(45): 13987-13996.
Tenzer, S., D. Docter, S. Rosfa, A. Wlodarski, J. Kuharev, A. Rekik, S. K. Knauer, C. Bantz, T. Nawroth, C. Bier, J. Sirirattanapan, W. Mann, L. Treuel, R. Zellner, M. Maskos, H. Schild and R. H. Stauber (2011). "Nanoparticle size is a critical physicochemical determinant of the human blood plasma corona: a comprehensive quantitative proteomic analysis." ACS Nano **5**(9): 7155-7167.
Torchilin, V. P. (2006). "Multifunctional nanocarriers." Adv Drug Deliv Rev **58**(14): 1532-1555.
Torchilin, V. P. (2007). "Targeted pharmaceutical nanocarriers for cancer therapy and imaging." AAPS J **9**(2): E128-147.
Treuel, L. and G. U. Nienhaus (2012). "Toward a molecular understanding of nanoparticle–protein interactions." Biophysical Reviews **4**(2): 137-147.
Tsukita, S. and H. Ishikawa (1980). "The movement of membranous organelles in axons. Electron microscopic identification of anterogradely and retrogradely transported organelles." J Cell Biol **84**(3): 513-530.
Vacha, R., F. J. Martinez-Veracoechea and D. Frenkel (2011). "Receptor-mediated endocytosis of nanoparticles of various shapes." Nano Lett **11**(12): 5391-5395.
Vallhov, H., J. Qin, S. M. Johansson, N. Ahlborg, M. A. Muhammed, A. Scheynius and S. Gabrielsson (2006). "The importance of an endotoxin-free environment during the production of nanoparticles used in medical applications." Nano Lett **6**(8): 1682-1686.
Variola, F., J. B. Brunski, G. Orsini, P. Tambasco de Oliveira, R. Wazen and A. Nanci (2011). "Nanoscale surface modifications of medically relevant metals: state-of-the art and perspectives." Nanoscale **3**(2): 335-353.
Vasir, J. K. and V. Labhasetwar (2007). "Biodegradable nanoparticles for cytosolic delivery of therapeutics." Adv Drug Deliv Rev **59**(8): 718-728.
Ventola, C. L. (2012). "The nanomedicine revolution: part 2: current and future clinical applications." P T **37**(10): 582-591.
Verma, A. and F. Stellacci (2010). "Effect of surface properties on nanoparticle-cell interactions." Small **6**(1): 12-21.
Verma, A., O. Uzun, Y. Hu, Y. Hu, H. S. Han, N. Watson, S. Chen, D. J. Irvine and F. Stellacci (2008). "Surface-structure-regulated cell-membrane penetration by monolayer-protected nanoparticles." Nat Mater **7**(7): 588-595.
von der Kammer, F., P. L. Ferguson, P. A. Holden, A. Masion, K. R. Rogers, S. J. Klaine, A. A. Koelmans, N. Horne and J. M. Unrine (2012). "Analysis of engineered nanomaterials in complex matrices (environment and biota): general considerations and conceptual case studies." Environ Toxicol Chem **31**(1): 32-49.
Walczyk, D., F. B. Bombelli, M. P. Monopoli, I. Lynch and K. A. Dawson (2010). "What the cell "sees" in bionanoscience." J Am Chem Soc **132**(16): 5761-5768.

Walczyk, D., F. B. Bombelli, M. P. Monopoli, I. Lynch and K. A. Dawson (2010). "What the Cell "Sees" in Bionanoscience." Journal of the American Chemical Society **132**(16): 5761-5768.
Walkey, C. D. and W. C. Chan (2012). "Understanding and controlling the interaction of nanomaterials with proteins in a physiological environment." Chem Soc Rev **41**(7): 2780-2799.
Walkey, C. D., J. B. Olsen, H. Guo, A. Emili and W. C. Chan (2012). "Nanoparticle size and surface chemistry determine serum protein adsorption and macrophage uptake." J Am Chem Soc **134**(4): 2139-2147.
Wang, C., X. Gao and X. Su (2010). "In vitro and in vivo imaging with quantum dots." Anal Bioanal Chem **397**(4): 1397-1415.
Wang, Q., X. Zhang, X. Zhou, T. Fang, P. Liu, P. Liu, X. Min and X. Li (2012). "Interaction of different thiol-capped CdTe quantum dots with bovine serum albumin." Journal of Luminescence **132**(7): 1695-1700.
Wang, T., J. Bai, X. Jiang and G. U. Nienhaus (2012). "Cellular uptake of nanoparticles by membrane penetration: a study combining confocal microscopy with FTIR spectroelectrochemistry." ACS Nano **6**(2): 1251-1259.
Warheit, D. B. (2008). "How meaningful are the results of nanotoxicity studies in the absence of adequate material characterization?" Toxicol Sci **101**(2): 183-185.
Webster, T. J. (2006). "Nanomedicine: what's in a definition?" Int J Nanomedicine **1**(2): 115-116.
West, A. P., I. E. Brodsky, C. Rahner, D. K. Woo, H. Erdjument-Bromage, P. Tempst, M. C. Walsh, Y. Choi, G. S. Shadel and S. Ghosh (2011). "TLR signalling augments macrophage bactericidal activity through mitochondrial ROS." Nature **472**(7344): 476-480.
Wright, M. (2012). "Nanoparticle tracking analysis for the multiparameter characterization and counting of nanoparticle suspensions." Methods Mol Biol **906**: 511-524.
Xia, T., M. Kovochich, M. Liong, J. I. Zink and A. E. Nel (2008). "Cationic polystyrene nanosphere toxicity depends on cell-specific endocytic and mitochondrial injury pathways." ACS Nano **2**(1): 85-96.
Xiao, Y., S. P. Forry, X. Gao, R. D. Holbrook, W. G. Telford and A. Tona (2010). "Dynamics and mechanisms of quantum dot nanoparticle cellular uptake." J Nanobiotechnology **8**: 13.
Yang, L., L. Shang and G. U. Nienhaus (2013). "Mechanistic aspects of fluorescent gold nanocluster internalization by live HeLa cells." Nanoscale **5**(4): 1537-1543.
Yang, P., S. Wang and N. Murase (2012). "Near-infrared emitting CdTe0.5Se0.5/Cd0.5Zn0.5S quantum dots: synthesis and bright luminescence." Nanoscale Res Lett **7**(1): 615.
Yohannes, G., M. Jussila, K. Hartonen and M. L. Riekkola (2011). "Asymmetrical flow field-flow fractionation technique for separation and characterization of biopolymers and bioparticles." J Chromatogr A **1218**(27): 4104-4116.
Yoo, J. W., N. Doshi and S. Mitragotri (2010). "Endocytosis and Intracellular Distribution of PLGA Particles in Endothelial Cells: Effect of Particle Geometry." Macromol Rapid Commun **31**(2): 142-148.
Yu, W. W., L. Qu, W. Guo and X. Peng (2003). "Experimental Determination of the Extinction Coefficient of CdTe, CdSe, and CdS Nanocrystals." Chemistry of Materials **15**(14): 2854-2860.

Zamborini, F. P., L. Bao and R. Dasari (2012). "Nanoparticles in measurement science." Anal Chem **84**(2): 541-576.
Zattoni, A., D. C. Rambaldi, P. Reschiglian, M. Melucci, S. Krol, A. M. Garcia, A. Sanz-Medel, D. Roessner and C. Johann (2009). "Asymmetrical flow field-flow fractionation with multi-angle light scattering detection for the analysis of structured nanoparticles." J Chromatogr A **1216**(52): 9106-9112.
Zhang, L. W. and N. A. Monteiro-Riviere (2009). "Mechanisms of quantum dot nanoparticle cellular uptake." Toxicol Sci **110**(1): 138-155.
Zhang, Y. and A. Clapp (2011). "Overview of stabilizing ligands for biocompatible quantum dot nanocrystals." Sensors (Basel) **11**(12): 11036-11055.
Zhang, Y., H. Pan, P. Zhang, N. Gao, Y. Lin, Z. Luo, P. Li, C. Wang, L. Liu, D. Pang, L. Cai and Y. Ma (2013). "Functionalized quantum dots induce proinflammatory responses in vitro: the role of terminal functional group-associated endocytic pathways." Nanoscale **5**(13): 5919-5929.
Zhao, F., Y. Zhao, Y. Liu, X. Chang, C. Chen and Y. Zhao (2011). "Cellular uptake, intracellular trafficking, and cytotoxicity of nanomaterials." Small **7**(10): 1322-1337.
Zhu, Z. J., T. Posati, D. F. Moyano, R. Tang, B. Yan, R. W. Vachet and V. M. Rotello (2012). "The interplay of monolayer structure and serum protein interactions on the cellular uptake of gold nanoparticles." Small **8**(17): 2659-2663.
Zhu, Z. J., Y. C. Yeh, R. Tang, B. Yan, J. Tamayo, R. W. Vachet and V. M. Rotello (2011). "Stability of quantum dots in live cells." Nat Chem **3**(12): 963-968.
Zimmer, J. P., S. W. Kim, S. Ohnishi, E. Tanaka, J. V. Frangioni and M. G. Bawendi (2006). "Size series of small indium arsenide-zinc selenide core-shell nanocrystals and their application to in vivo imaging." J Am Chem Soc **128**(8): 2526-2527.